ADDIS ABABA UNIVERSITY

ADDIS ABABA INSTITUTE OF TECHNOLOGY

SCHOOL OF CIVIL AND ENVIRONMENTAL ENGINEERING

Nonlinear Behavior of Slender Reinforced Concrete Columns Subjected to Short Term Loading

A Thesis in Structural Engineering

By Dawit Negasi

July 15, 2021

A Thesis

Submitted in Partial Fulfillment of the Requirements for the Degree of Master of Science

The undersigned have examined the thesis entitled '**Nonlinear behavior of slender reinforced concrete columns subjected to short term loading**' presented by **Dawit Negasi**, a candidate for the degree of **Master of Science** and hereby certify that it is worthy of acceptance.

Prof. Girma Zerayohannes	____________________	____________
Advisor	Signature	Date
Dr. Ing. Adil Zekaria	____________________	____________
Internal Examiner	Signature	Date
Dr. Esayas G/yohannes	____________________	____________
External Examiner	Signature	Date
Dr. Mebruk Mohammed	____________________	____________
Chairperson	Signature	Date

UNDERTAKING

I certify that research work titled "**Nonlinear behavior of slender reinforced concrete columns subjected to short term loading**" is my own work. The work has not been presented elsewhere for assessment. Where material has been used from other sources it has been properly acknowledged/ referred.

Dawit Negasi

ABSTRACT

When a stress is beyond elastic limit or cracking occurs in reinforced concrete section subjected to axial force and uniaxial bending, the principal axes of the cross section may translate. Because of this phenomenon, axial force applied at the centroid of gross section may have an effect on curvature and bending moment may also have an effect on axial strain at the sectional centroid.

In this study, nonlinear second-order analysis is implemented in MATLAB R2019a program to predict the response of reinforced concrete column subjected to axial load and uniaxial bending moment under monotonic short term loadings which takes into account material nonlinearity including tension stiffening and geometric nonlinearity.

There has been a lot of research for the nonlinear analysis of slender reinforced concrete columns by adopting analytical methods which assume the deflection curve of a column as a sine wave and then solve the governing differential equations. However, as the load is increased beyond the elastic limit, the post peak deflected response of the reinforced concrete column differs from the deflection curve which is assumed in the analytical method. To overcome these short comings of the analytical methods, the geometrically nonlinear finite element and materially layered cross-section model was adopted in this study. The iterative secant stiffness algorithm is adopted under displacement control.

According the results, the application of the analytical method is almost impossible when the columns are existing as a part of a complex structure. The increment of the ultimate load due to the increase of concrete compressive strength was decreased with the increase in the slenderness ratio. The possibility of stability failure for the slender column was increased with increasing concrete strength. The increase of longitudinal steel ratio on the increase of ultimate load of column was more effective for slender columns than for short ones. The effect of tension stiffening on the increases of ultimate load of column was more evident for short columns than slender columns. An increase in the initial eccentricity ratio resulted in a decrease in the ultimate load and an increase in the column deflection at failure.

Keywords: uniaxial bending, concrete compressive strength, longitudinal steel ratio, slenderness ratio, layered cross-section model, tension stiffening.

ACKNOWLEDGMENTS

First of all, I would like to thank the almighty God, who gave me the commitment and tolerance to pass the various obstacles and come up to the accomplishment of this thesis.

This thesis work becomes successful with the help and encouragement of many people and my appreciation goes to all of them, leaving their long list. Specially, I would like to express my deepest gratitude to my advisor, Prof. Girma Zerayohannes for his continues valuable professional guidance, experience, immense knowledge and constant encouragement throughout the work.

I am deeply indebted to acknowledge Dr. Esayas G/yohannes for his direction, constructive discussions, sharing his great knowledge and experience at all phase of my work.

I would like to express my deepest appreciation to Dr. Ing. Adil Zekaria, for his incredible support, valuable advice, providing and suggesting valuable materials from the very beginning to finish of this work.

I would like to kindly acknowledge Ethiopian Road Authority (ERA) research and training department for giving me the scholarship to pursue the study.

I would like to express my deepest gratitude to my parents for their boundless patience, continual encouragement throughout the duration of the study and especial thanks goes to Kidanemariam Zeru, for his support, encouragement and being with me in all ups and downs.

TABLE OF CONTENTS

LIST OF TABLES

LIST OF FIGURES

CHAPTER 1 INTRODUCTION

1.1 Background

A reinforced concrete column, which is primary structural member, is subjected to the axial force and bending moment which may be due to end restraint arising from the monotonic placement of floor beams and columns or due to eccentricity from imperfect alignment.

The inherent characteristic of quasi-brittle materials such as concrete creates cracking when the material is applied with external loading. Therefore, the failure mechanism of a concrete column with multiple loading conditions changes from uncracked to cracked condition. In the uncracked condition, the axial force and bending moment applied to the column will have no coupling effects. However, in the cracked condition, as shown in axial force applied at the centroid of gross section may have an effect on curvature and bending moment about principal axis of gross section may also have an effect on axial strain at the sectional centroid, Kim and Lee (2000). This is mainly due to the translation of principal axes of the cross-section after cracking, as shown on Fig. 1.1. In this case, the axial force and bending moment are coupled.

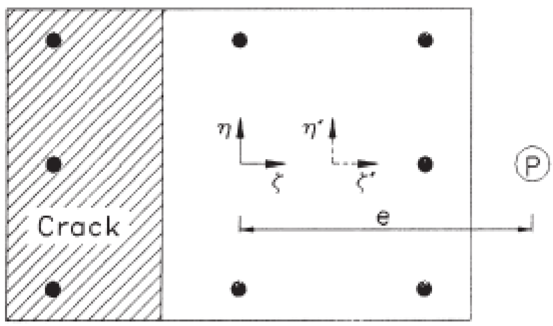

Figure 1-1: Principal axes of cross-section after cracking

In recent years, high strength concrete (HSC) columns have been widely used in major construction projects, especially, in high-rise buildings, Kwak and Kim (2006). The use of high strength concrete (HSC) in the field of construction has been increasing, and it is being highly accepted by practitioners. The introduction of high-strength concrete in high-rise building has made it possible to design slender columns and, thereby, facilitate not only new architectural ideas but also economic benefits as it provides considerable savings associated with material costs by allowing smaller cross-sections, permit more rentable floor space and reduction of dead loads. However, the stability of reinforced concrete column made of high-strength concrete has recently become a major concern for design engineers because there is great likeliness to reach a limit state. Moreover, slender reinforced concrete column may fail due to not only material failure in a section but also instability of a structure, they require more rigorous numerical analyses which consider second-order $P - \delta$ effect and creep deformation of concrete in order to reserve their ultimate resisting capacity and serviceability, Kwak and Kim(2006).

1.2 Problem Statement

There has been a lot of research on the behavior and design of slender reinforced concrete columns. Lloyd and Rangan (1996); Chuang and Kong (1998), for the strength analysis of slender columns were generally based on a simplified nonlinear analysis that approximates the column deflection to a sine wave function with constant wavelength. This assumption of constant wavelength is an unnecessarily simplification. Other researcher, Bazant *et al.* (1991 and 1997), on the basis of the force equilibrium equation and the strain compatibility condition at a section, analytically calculated the resisting capacity of slender reinforced concrete columns that assume the deflection curve of the column as a sine wave function with variable wavelength (effective length of the column).

Kim and Yang (1995) proposed that, as the load is increased beyond the elastic limit, the deflection shape of the reinforced concrete column gradually differs from the deflection curve, which is assumed in the analytical method, and the application of the analytical method is almost impossible when the columns are a part of a complex structure. This indicates, further investigation is required for better understanding of nonlinear second-order behavior of slender reinforced concrete columns.

Bazant and Xiang (1997), proposed an improved method of analysis of reinforced concrete columns in braced (no-sway) frames. In their investigation, the tensile resistance of the cracked concrete was neglected. This is known to give a very good approximation of the column strength, but, as far as curvatures are concerned, the actual behavior is appreciably stiffer, because of the phenomenon known as tension stiffening (consisting of the tensile resistance of concrete between the cracks). Nevertheless, in buckling, this phenomenon probably is much weaker than in bending of beams, and at the same time there are insufficient data for the role of tension stiffening in buckling. Kim and Yang (1995), Kwak and Kim (2006) have included the un-cracked and cracked (post-peak softening) tensile stress-strain relation of concrete in their numerical and analytical analysis, respectively. However, they hadn't discussed its role on the column behavior. Therefore, in the present analysis of layered cross-section model, the tension stiffening is included as the properties of concrete to examine its contribution on the load-deflection response of the reinforced concrete column.

1.3 Objective of the Study

1.3.1 General Objective

The ultimate aim of this work was to develop nonlinear second-order finite element analysis program using MATLAB R2019a programming code to predict the response of reinforced concrete columns subjected to axial load and uniaxial bending moment which takes into account both material nonlinearity including tension stiffening and geometric nonlinearity under displacement control.

1.3.2 Specific Objective

The specific objectives are as follows:

- To investigate the deflected curve of a reinforced concrete column beyond elastic limit.
- To obtain the maximum load,P_{max}, carried by the reinforced concrete column as well as the entire axial force-lateral deflection curve including the post peak nonlinear softening behavior.
- To investigate the effect of concrete strength, longitudinal steel reinforcement ratio, slenderness ratio and initial eccentricity on the ultimate load carrying capacity.
- To examine the role of tension stiffening on buckling of reinforced concrete columns

1.4 Methodology

i. Conduct a deep literature review on various layered models and iteration techniques of reinforced concrete beams, columns and frames.
ii. Implement the geometrically nonlinear finite element code and materially nonlinear layered cross-section model in MATLAB R2019a program and verify with the experimental test results.

1.5 Scope of the Study

The primary concern of this paper was investigating the nonlinear second-order behavior of uniaxial bending of reinforced high strength concrete slender columns under static short-term loading. The long-term loading effect (time-dependent deformations such as creep) and cyclic loading are not included. Although these are potentially important in an overall assessment of a concrete structure, they are beyond the scope of this thesis.

1.6 Importance of the Study

This study is used as starting point of programming code to investigate the material and geometric nonlinear behavior of reinforced concrete column subjected to axial load and uniaxial bending under short term monotonic loading condition. Developing such like tool used for students, instructors and structural engineers to grasp deep knowledge and skill on the entire detail analysis process of structures rather than using developed commercial structural engineering software's, as their source code is black source, not accessible to users. Along with this, the independent development of such a program enabled computer source codes to be created for subsequent modification to include second-order nonlinear behavior of reinforced concrete columns subjected to axial load and biaxial bending under short and long term time dependent effect (or creep effect).

CHAPTER 2 LITRATURE REVIEW

In this chapter, general overview of slender reinforced concrete columns and review of different researchers on material nonlinearity including the tension stiffening of the cracked concrete and geometric nonlinearity of reinforced concrete column and frame will be discussed. In addition to this, different nonlinear analysis iteration techniques will be presented.

2.1 Slender Reinforced Concrete Column

A slender reinforced concrete column is defined as a long column that has a significant reduction in its axial-load capacity due to moments resulting from lateral deflections of the column. A long reinforced concrete column of length deflects laterally when subjected to an eccentric axial load and is therefore subjected to additional bending moment along its height. This additional bending moment is negligible for columns having small slenderness ratio. The second-order moment at mid-height caused by the axial load acting through additional eccentricity due to mid-height lateral deflection, however, becomes significant in slender columns and the maximum moment acting on the column. An eccentrically loaded, pin-ended column is shown in Fig.2.1a. The moments at the ends of the column are

$$M_e = Pe \qquad \textbf{(2.1)}$$

When the loads P are applied, the column deflects laterally by an amount, δ. For equilibrium, the internal moment at mid-height is (Fig.2.1b)

$$M_e = P(e + \delta) \qquad \textbf{(2.2)}$$

The deflection increases the moments for which the column must be designed. In the symmetrical column shown here, the maximum moment occurs at mid-height, where the maximum deflection occurs.

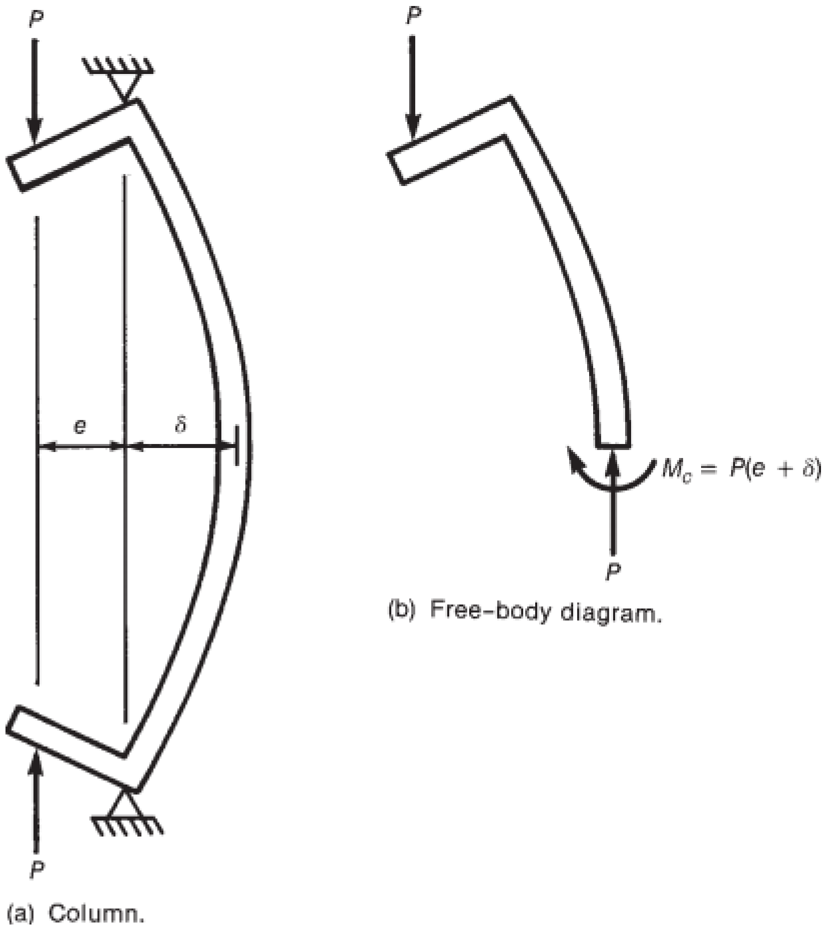

Figure 2-1: Forces in a deflected column (MacGregor and Wight, 2009)

2.2 Material Non-linearity

The nonlinear response of reinforced concrete structures under monotonic loading at each load or displacement increment is caused by two major effects, Kwak and Filippou (1997), namely, cracking of concrete in tension, yielding of reinforcement in tension and compression or crushing or pinching of a layer or a number of layers. Nonlinearities also arise from the interaction of the constituents of reinforced concrete, aggregate interlock at a crack and dowel action of the reinforcing steel crossing a crack. The time-dependent effects of creep, shrinkage, and temperature variations also contribute to the nonlinear behavior. Furthermore, the stress-strain relation of concrete is not only nonlinear, but is different in tension than in compression and the mechanical properties are dependent on concrete age at loading and on environmental conditions, such as ambient temperature and humidity. The material properties of concrete and steel are also strain-rate dependent to a different extent. For long-term loading, time-dependent material effects such as creep and shrinkage of concrete columns also contribute to the non-linear behavior. However, these are not included in the present study

El-Metwally and Chen (1989) used the stiffness matrix given by Equation 2.3 to investigate the nonlinear load-deflection relationship of reinforced concrete frame under gravity and/or lateral loads . The member stiffness matrix K_m, is modified by the stiffness functions $\emptyset_1$, $\emptyset_2$, $\emptyset_3$ and $\emptyset_4$, which modify the flexural stiffness terms. These stability functions, or coefficients, are in fact a modification to the first order matrix, to take into account the $P-\delta$ effect. Stiffness terms are updated by performing section analyses. A tangent stiffness method under load control approach was adopted and hence this method was only giving results up to the peak load.

$$K_m = \begin{bmatrix} \frac{EA}{L} & 0 & 0 & -\frac{EA}{L} & 0 & 0 \\ 0 & \frac{12EI\emptyset_1}{L^3} & \frac{6EI\emptyset_2}{L^2} & 0 & -\frac{12EI\emptyset_1}{L^3} & \frac{6EI\emptyset_2}{L^2} \\ 0 & \frac{6EI\emptyset_2}{L^2} & \frac{4EI\emptyset_4}{L} & 0 & -\frac{6EI\emptyset_2}{L^2} & \frac{2EI\emptyset_3}{L} \\ -\frac{EA}{L} & 0 & 0 & \frac{EA}{L} & 0 & 0 \\ 0 & -\frac{12EI\emptyset_1}{L^3} & -\frac{6EI\emptyset_2}{L^2} & 0 & \frac{12EI\emptyset_1}{L^3} & -\frac{6EI\emptyset_2}{L^2} \\ 0 & \frac{6EI\emptyset_2}{L^2} & \frac{2EI\emptyset_3}{L} & 0 & -\frac{6EI\emptyset_2}{L^2} & \frac{6EI\emptyset_4}{L} \end{bmatrix} \qquad \textbf{(2.3)}$$

When loaded to destruction, reinforced concrete frames may exhibit a softening response in which the load, after reaching its peak value, does not follow a constant-load yield plateau but gradually declines with increasing displacement, Bazant *et al* (1987) because of the limited ductility and strain softening behavior of typical reinforced concrete sections. Due to the absence of yield plateau, the condition of plastic limit analysis is not satisfied, which means that the ultimate load of statically indeterminate beam or frame is not correctly predicted from a plastic hinge mechanism. Generally, the maximum load is less, since one plastic hinge may already soften before another hinge reaches its maximum bending moment. For this reason, many researchers attempted nonlinear analyses of reinforced concrete structure problem by the load or displacement control with different incremental-iterative methods, which makes it possible to follow the response up to the snapback point, if such a point exists.

Kim and Lee (1992) studied material nonlinearity of reinforced concrete beam with softening using nonlayered (modified stiffness) method by employing line elements. Tangent stiffness iteration method under displacement control solution procedure was used. The stiffness of an element is normally assumed to be uniform within its length and is determined from the behavior of a section at mid-length. Based on the moment-curvature relations of this section, tangent stiffness of each element, and hence of the global stiffness matrix, is updated at each incremental controlled displacement and iteration.

Alternative approach for modelling nonlinear behavior of reinforced concrete structures is to use properties of layered elements directly in the formation of the element stiffness matrix. In this approach, section analyses to obtain moment-curvature axial load relations are not required. The layers are used to model the behavior of steel reinforcement and concrete within the elements. This approach was used by Bazant *et al.* (1987), Kim and Lee (1993), Kim and Yang (1995) and Kwak and Kim (2006) for the nonlinear analysis of reinforced concrete frames and columns. Except Kwak and Kim (2006), they have been used secant stiffness method of iteration technique under displacement control solution procedure. However, in Bazant *et al.* (1987) and Kim and Lee (1993), the full geometric nonlinearity effects caused by the deflection of the joints of the frames ($P - \Delta$) and that caused by the deflection of the members away from the centerline joining the ends of the member ($P - \delta$) were not considered. Kim and Yang (1995) introduced a numerical method taking into account material and geometric nonlinearity of reinforced concrete column under short term loading and carried out an experimental study to verify the exactness of the algorithm they developed. For both short and medium slender reinforced concrete columns they adopted displacement control test set-up and capture the post peak nonlinear softening behavior. However, the test result of the slender reinforced concrete columns was up to the peak load as they were tested by load control test set-up.

Kwak and Kim (2006) introduced analytical model to simulate nonlinear behavior of slender reinforced concrete columns. The material nonlinearity including cracking and creep deformation of concrete was taken into consideration. The geometric nonlinearity due to $P - \delta$ effect was taken in to account by using the initial stress matrix. In this paper tangent stiffness matrix combined with constant stiffness matrix iteration technique under load control solution procedure used. Hence, their analysis was only up to peak load.

For the nonlinear analysis of reinforced concrete structures in the finite element method, both the nonlayered (modified stiffness) and the layered methods have been developed and have been widely used in recent years. The layered method, made up of a series of layers idealized as being in a state of plane stress, leads to success, Kim and Lee (1993).

In the nonlayered method, the result of analysis is speedily obtained by using the models or the integral forms for the sectional behaviors such as moment-curvature relation of all elements. The nonlayed method, however, cannot be considered the effect of the loading history, thus only limited success or sometimes an incorrect result is achieved. Consequently, the result of analysis on the inelastic range (i.e., a different results depends on the loading history) is not reliable. Therefore, in this study, the reinforced concrete columns are discretized in to finite element along the length and layered cross-section model were used for all element cross-section. Material stiffness matrix have been used to simulate material nonlinearity due to cracking of concrete in tension, tension and compression yielding of reinforcement and compression crushing of concrete or pinching of a layer or a number of layers. The geometric nonlinearity due to axial load-lateral deflection interaction is taken in to account using second-order geometric stiffness matrix. In addition to this, due to the significance influence of bulking on the loading state provided by an eccentric axial load, the lateral deflection is added to the applied initial eccentricity at each iteration for the simulation of second-order $P - \delta$ moment.

In Bazant *et al.* (1997), unloading is taken as a straight line parallel to the initial tangent of the stress-strain curve. During loading at constant axial load, unloading typically occurs as the neutral axis moves into the previously compressed portion of the cross-section. This effect, however, was seen to be negligible, at least up to the peak point of the column response. The reason is that the loading-unloading reversal occurs near the neutral axis where stress has little effect on bending moment. Furthermore, it occurs at low strain levels at which the stress-strain diagram for loading is close to that for unloading. Therefore, in this paper, unloading-reloading curve were neglected for both tension and compression of reinforcing steel and concrete.

2.3 Tension Stiffening Models

Essential to any tension stiffening model is an estimate of the tensile strength of concrete in uniaxial tension and the post-peak softening response. Although this strength is only 10-15%

of the value for compressive strength, it is an important parameter in any tension stiffening model because it determines the load level at which the flexural crack forms. The different approaches that have been used for approximating tension stiffening are described in the following sessions.

2.3.1 Scanlon and Murray Model

The concept of tension stiffening (strain softening branch of tension stress-strain curve of concrete) was first introduced by Scanlon and Murray (1974) to account the tensile stiffening effect of concrete between cracks. This concept is simple yet powerful, hence it has been used extensively since its inception. They assumed that after concrete reaches its ultimate tensile strength, a primary crack will form, but the cracked concrete carries some tensile stresses perpendicular to the crack direction. As the load increases, more cracks will form, but the amount of tensile stresses carried by the concrete gradually decreases. Further, it is suggested that the gradual decrease in stress can be modelled as stepwise reduction in stress. Figure 2.2 gives the details of the model.

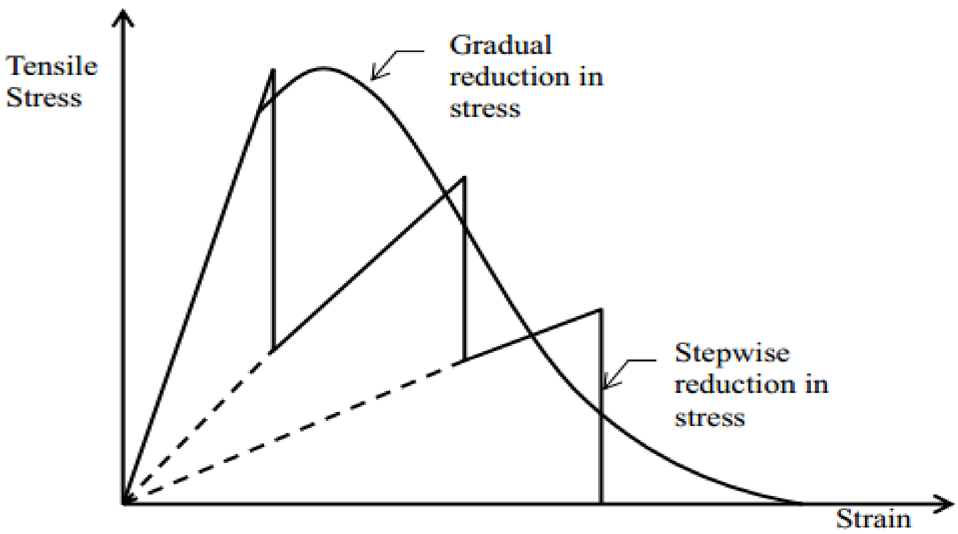

Figure 2-2: Scanlon and Murray Model (1974)

2.3.2 Lin and Scordelis Model

Lin and Scordelis (1975) have described the tension stiffening effect by the linear descending branch of the stress-strain curve. The cracking occurs at the stress f_{ct} and the corresponding strain at that point is ε_{ct}, as shown in figure 2.3. After the section has cracked, the tensile resistance decreases till the strain value is $\alpha\varepsilon_{ct}$. When the strain in the section reaches $\alpha\varepsilon_{ct}$, the tensile resistance of concrete is assumed to be zero.

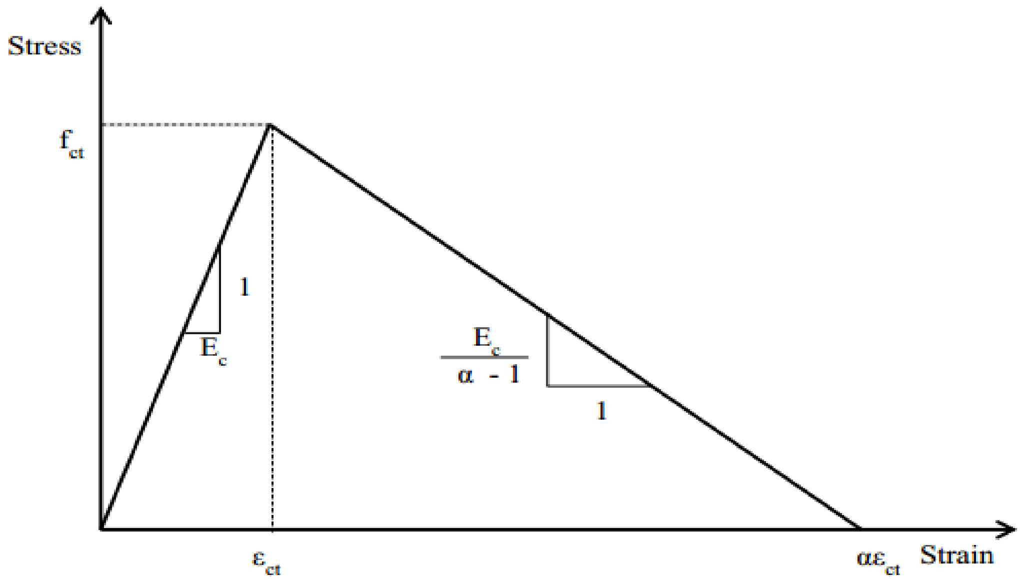

Figure 2-3: Lin and Scordelis model (1975)

2.3.3 Vebo and Ghali's model

Regarding the material model for concrete in tension, this is assumed to be a trilinear stress-strain relationship. A linear ascending branch of the stress-strain relationship was assumed for uncracked concrete with a gradient equal to 75% of the initial elastic modulus of concrete in compression ($0.75E_c$), whereas a bilinear deceasing softening branch was used to account for the cracked concrete with 50% and 5% of E_c, the Young's modulus for concrete in compression , as shown in Figure 2.4.

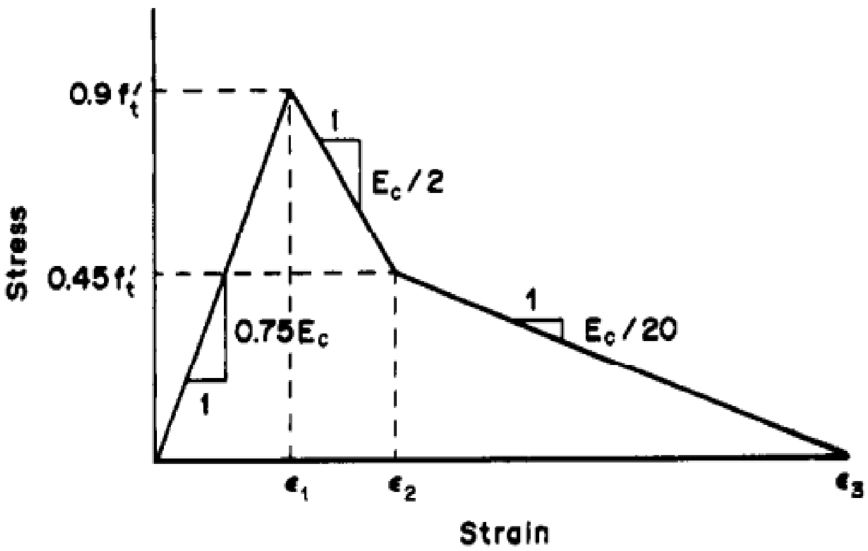

Figure 2-4: Vebo and Ghali (1977)

2.3.4 Gilbert and Warner Model

Gilbert and Warner (1978) were used two techniques to represent tension stiffening. The first method is, to assume an average tensile stress to act over an effective area of concrete surrounding the reinforcing steel in the tension zone. Based on this method three stress-strain relationships used for the concrete in the tension zone. The first relationship, shown in Figure 2.5(a), has stepped diagrams similar to that proposed by Scanlon and Murray (1974), but the number and magnitude of the steps have been reduced in the once-removed and twice-removed layers. The second relationship, shown in Figure 2.5(b), has unloading curves similar to that of Lin and Scordelis, but as in the earlier case, the shapes of the unloading curves have been adjusted to reflect the position of the layer relative to the reinforcement. The third relationship, shown in Figure 2.5(c), has piece-wise linear diagrams with a discontinuity at the initial cracking stress. Gilbert and Warner also proposed a second method to account for the tension stiffening indirectly. To include the tension stiffening in the surrounding concrete, this assumed that the retention of stresses after the development of a crack is represented by increasing/or modifying the steel stresses as illustrated in the modified stress-strain curves shown in Figure 2.6. In this case, the cracked concrete is assumed not to carry any load but an additional stress is carried by the steel. The additional force acting on the steel represents the total internal force carried by the concrete between the cracks. Gilbert and Warner suggested using the second techniques as it required considerably less computing time and yet produced good results when compared with the first technique. Gilbert and Warner also showed that the load-deflection curves obtained using tension stiffening or the modified approach for steel gave much better results than with no tension stiffening.

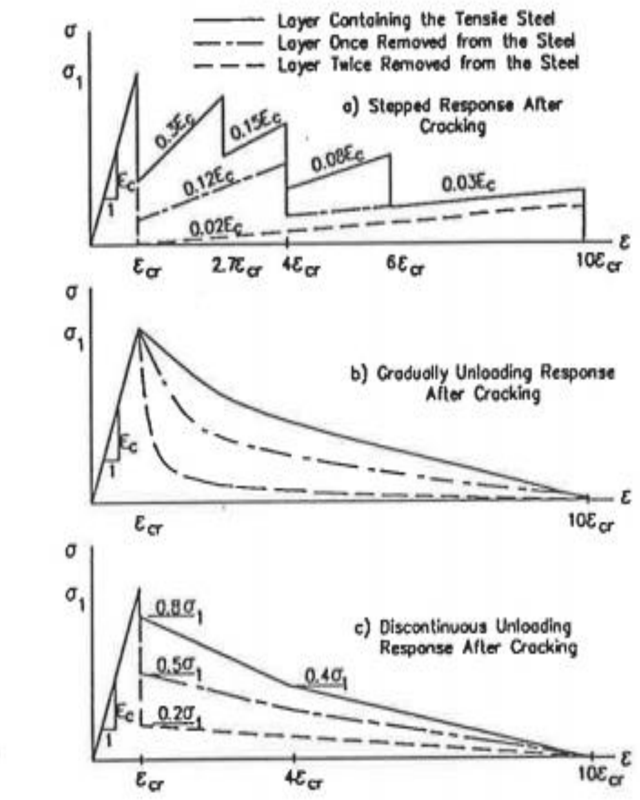

Figure 2-5: Stress-strain diagram for concrete in tension (Gilbert and Warner, 1978b)

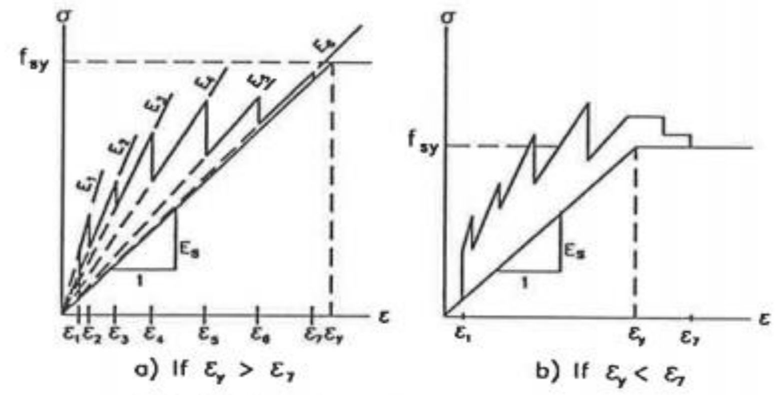

Material Modelling Law:

ε_1	ε_2	ε_3	ε_4	ε_5	ε_6	ε_7
ε_{cr}	$1.5\varepsilon_{cr}$	$3.0\varepsilon_{cr}$	$5.0\varepsilon_{cr}$	$8.0\varepsilon_{cr}$	$11.0\varepsilon_{cr}$	$14.0\varepsilon_{cr}$

E_1	E_2	E_3	E_4	E_5	E_6
$4.0E_s$	$2.7E_s$	$2.0E_s$	$1.6E_s$	$1.15E_s$	$1.05E_s$

Figure 2-6: Modified stress-strain relation for tension steel after cracking (Gilbert and Warner, 1978b)

2.3.5 Cope *et al.* Model

The model show in Figure 2.7, assumes that

For $\alpha_1\varepsilon_{cr} > \varepsilon \geq \varepsilon_{cr}$

$$\sigma = \frac{\alpha_2 f_t' \left(\alpha_1 - \frac{\varepsilon}{\varepsilon_{cr}}\right)}{(\alpha_1 - 1)}$$

For $\varepsilon \geq \alpha_1\varepsilon_{cr}$

$$\sigma = 0$$

Where f_t'-the tensile strength of concrete, ε_{cr}-the cracking strain, σ and ε- strain and stress normal to the crack directions, and α_1 and α_2-material constants.

The parameters α_1 and α_2 are usually difficult to select in practice because of the lack of experimental data for calibrating them. These parameters are related to the fracture energy of the concrete. This at least reduces the dependency of the model on the mesh size, because the fracture energy of the opening crack can be related to a characteristic length associated with the crack, which in turn can be related to the volume represented by a sampling point of element.

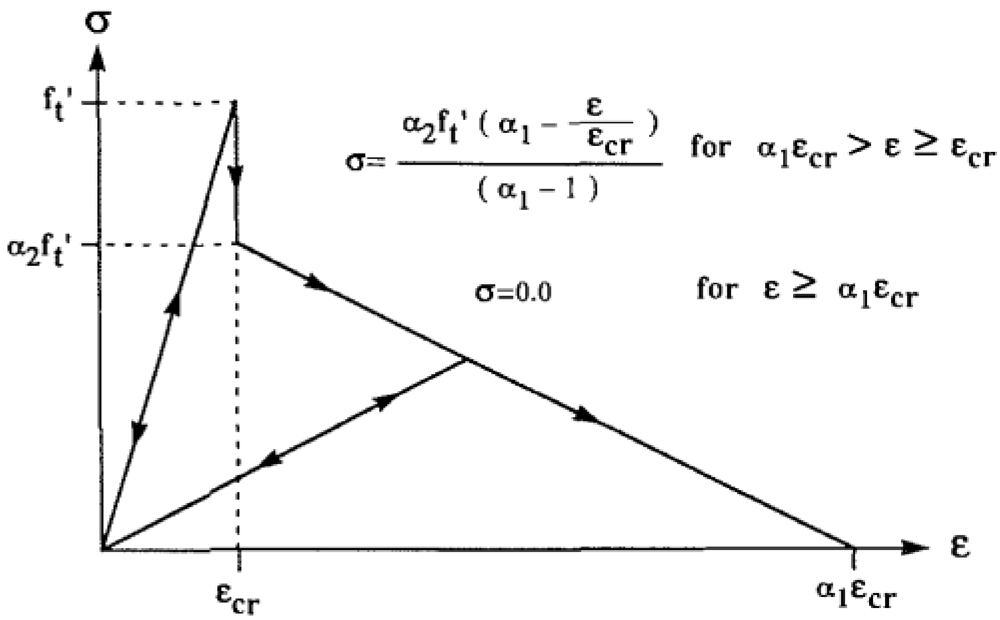

Figure 2-7: Tension stiffening model (Cope *et al.*, 1979)

2.4 Geometric Non-Linearity

A second type of nonlinearity which influences column behavior is due to geometric effects. As a column deforms under increasing load, changes in geometry may induce additional second order moments within members. These changes in geometry may be due to the movement at the ends of the columns and also lateral deflections within the length of columns. Non-linear geometric effects in a slender column may lead to a stability failure which can occur well before material strength has been reached.

2.4.1 $\boldsymbol{P-\delta}$ Moments and $\boldsymbol{P-\Delta}$ Moments

First-order linear analysis is an analysis assuming the deflection and stress are proportional to load. It does not consider buckling nor material yielding which is then considered in the design stage using codes. Second-order $P-\Delta$ analysis used to plot the bending moment and force diagram based on the deformed nodal coordinates. It does not consider member curvature or the $P-\delta$ effect. Second-order analysis determines the two types of second order effects, being $P-\Delta$ and $P-\delta$ moments.

$\boldsymbol{P-\delta}$ moments (member stability): second-order effect due to member curvature and change of member stiffness under load. These result from deflections, δ of the axis of the bent column away from the chord joining the ends of the column, as shown in Fig. 2.8. The slenderness effects in pin-ended columns and in non-sway frames result from $P-\delta$ effects.

$\boldsymbol{P-\Delta}$ moments (structural stability): second order effect due to change of geometry of the structure. It is relative deflection of one end of column to the other end of column, which is common in sway frames. These result from lateral deflection, Δ of the beam-column joints from their original un-deflected locations, as shown in Fig.2.8. The slenderness effects in sway frames result from $P-\Delta$ moments

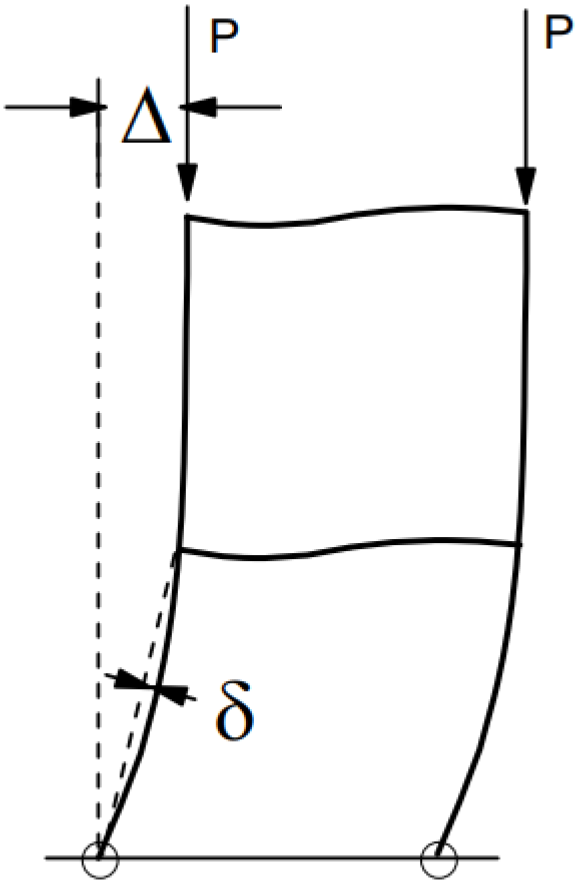

Figure 2-8: 2D Frame including both $P-\Delta$ and $P-\delta$ moments

El-Metwally and Chen (1986), were considered two different aspects of geometric nonlinearity for the study of nonlinear behavior of reinforced concrete frames. These are the stability analysis considering the $P-\delta$ effect of the member and the overall structural stability considering the $P-\Delta$ effect. The axial deformation of a member due to geometric deformations of a member was found to be insignificant in reinforced concrete members because of their deep sections.

Kim and Yang (1995) and Kwak and Kim (2006), the second-order effect due to axial load-lateral deflection interaction of the slender reinforced concrete column had accounted by adding the initial stress matrix to the material stiffness matrix.

2.5 Load Control and Displacement Control Methods

The load control method is that the global applied incremental load vector $\{\Delta F\}$ is given, then the corresponding global unknown incremental displacement vector $\{\Delta U\}$ can be solved by the iteration scheme. In the displacement control method, mean-while, the load vector and the displacement terms except the control point can be obtained iteration procedure. If the c^{th} incremental displacement $\{\Delta U\}$, is controlled as a certain known value, the applied incremental load vector $\{\Delta F\}$ and displacements which are not controlled are unknowns. In particular, two primary DO LOOPS are necessary to iterate the solution until convergence of the solution occurs and to increment the applied loading.

2.6 Basic Numerical Iterative Solution Techniques for Non-Linear Problems

The use of finite element discretization in a large class of non-linear problems results in a system of simultaneous equations of the form

$$KU + F = 0 \tag{2.4}$$

in which U is the vector of the basic unknowns, F is the vector of applied loads and $K$is the assembles stiffness matrix. If the coefficients of the matrix K depend on the unknowns U, the problem is clearly became non-linear. In this case, direct solution of equation system (2.4) is generally impossible and an iterative scheme must be adopted and discussed as follows.

The non-linear analysis of reinforced concrete column can be made either by simulating a load control and displacement control test set-up. In the latter approach, a set of displacements is incremented to the structure and the corresponding set of loads is calculated. In an analysis for load control, a load pattern is incremented to the structure up to peak value. It should be noted that analysis beyond the peak load can only be made by employing additional techniques. Usually, iterative procedures are requiring to achieve convergence for the load-displacement relationships. There are four basic numerical iterative solution techniques for non-linear analysis. These are the secant stiffness method (direct iteration method), the tangent stiffness method (also referred to as the Newton-Raphson method), the initial stiffness method (also referred to as the modified Newton-Raphson method) and combination of initial stiffness and tangent stiffness method (mixed-modified Newton Raphson method).

2.6.1 Secant Stiffness Method (Direct Iteration Method)

In this approach successive solutions are performed, in each of which the previous solution for the unknowns U is used to predict the current value of the coefficient matrix $K(U)$, Owen and Hinton (1980). Rewriting Eq. 2.4 as

$$U = -[K(U)]^{-1}F \tag{2.5}$$

Then the iterative process yields $(i+1)^{th}$approximation to be

$$U^{(i+1)} = -\left[K\left(U^{i}\right)\right]^{-1}F \tag{2.6}$$

It is seen from Eq. 2.6 that it is necessary to recalculate the stiffness matrix K for each iteration. To commence the process, an initial gross cross-section material and geometric properties are required in order to calculate K. For the direct iteration method, the problem is completely reanalyzed for every iteration and therefore the vector of the prescribed unknown must be introduced unchanged into the solution subroutines at every stage. In this method, the evaluation of the residual forces is not required.

As the name suggests, the secant stiffness method makes use of the secant structural stiffness (secant flexural and axial stiffnesses) and it requires to be updated with each iterative cycle of the load step throughout the analysis, shown in Fig. 2.9, Chajes and Churchill (1986). This method requires updating of secant structural stiffness matrix (to reflect the most recent state of the structure, including the nonlinear effects) at the begging of each increment and iteration. This method differs to the tangent and initial stiffness methods by applying a total load at each step. The set of forces $F_{1,2\,.\,.\,.A}$ correspond to direct values for displacements $D_{1,2\,.\,.\,.A}$.

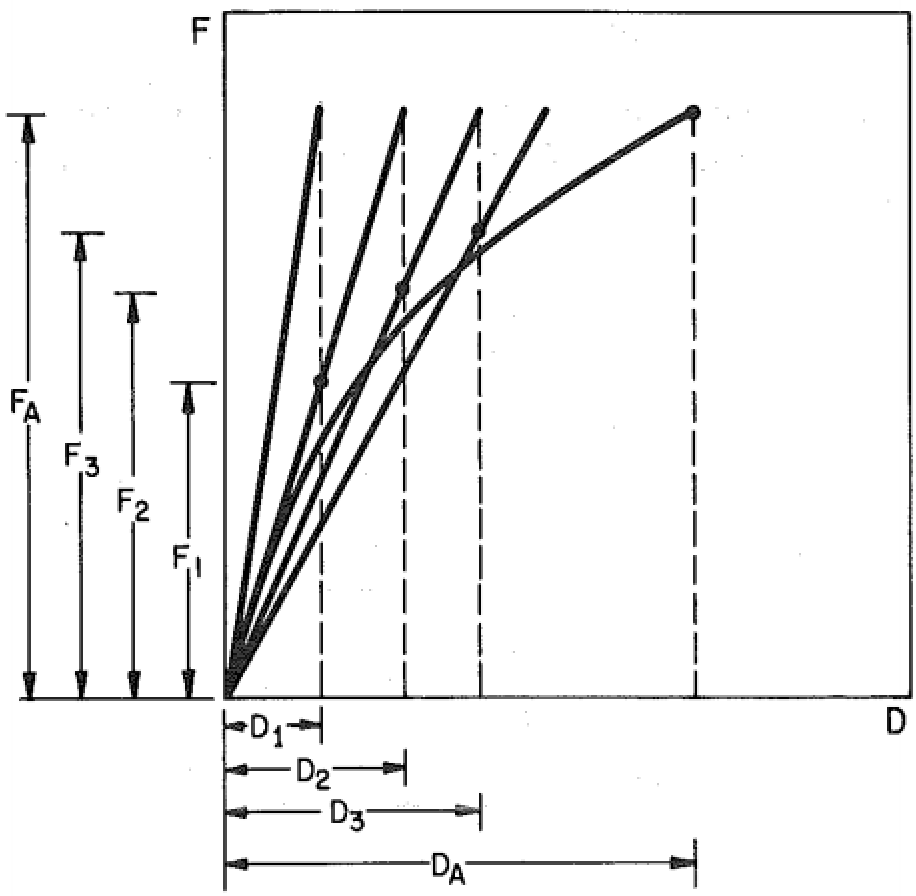

Figure 2-9: Secant stiffness method

2.6.2 Tangent Stiffness Method (Newton-Raphson Method)

During any step of an iterative process of solution, Eq. (2.4) will not be satisfied unless convergence has occurred, Owen and Hinton (1980). A system of residual forces can be assumed to exist, so that

$$\psi = KU + F \neq 0 \qquad \textbf{(2.7)}$$

These residual forces ψ can be interpreted as a measure of the departure of (2.4) from equilibrium. Since K is a function of U and possibly its derivatives, then at any stage of the process, $\psi = \psi(U)$. In this method, the stiffnesses must be reformulated for every iteration.

A typical load step in the tangent stiffness method is illustrated in Fig.2.10, Kenyon (1993). At the start of the load step, element stiffnesses are set to the values from the ends of the previous step. For commencement of the initial load step, element stiffness must have assembled values. These are usually based on gross-sectional values. The incremental load vector ΔP is applied to the structure and the global displacements $[\Delta D_1]$ are found by solving the following equation:

$$[K_o]|\Delta D_1| = |\Delta P| \quad \textbf{(2.8)}$$

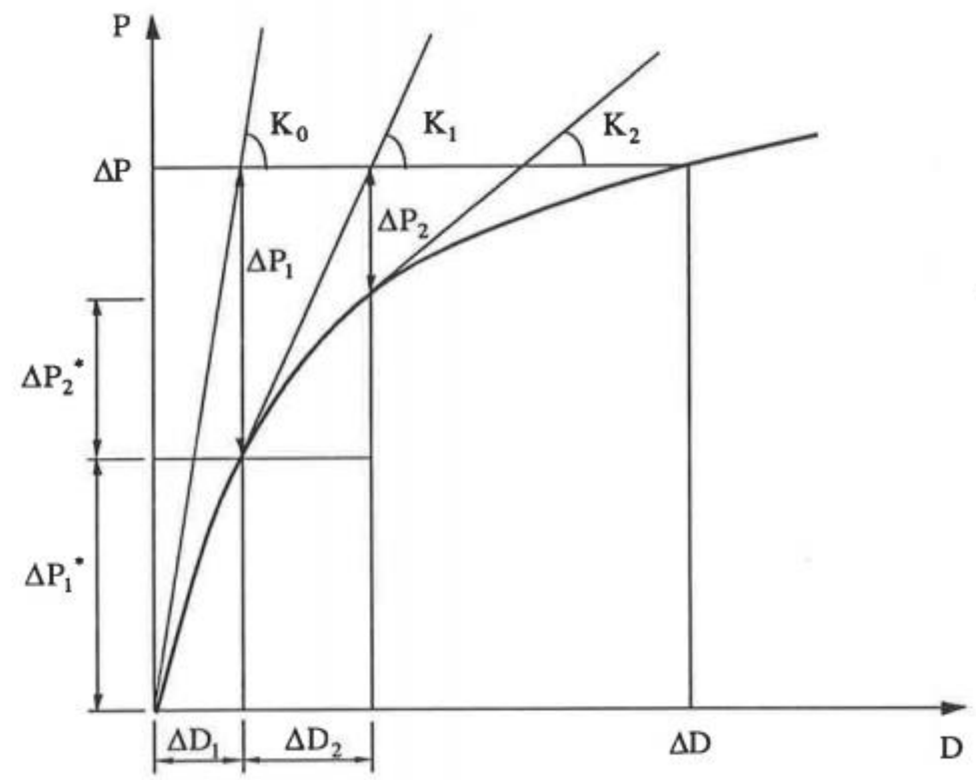

Figure 2-10: Tangent stiffness method

From the current deformed state of the structure, the nodal load vector, ΔP^*, is calculated. By considering existing nonlinear effects a new tangent stiffness matrix, K_1 is assembled. The out-of-balance load vector ΔP_1 is calculated, which is difference between the load vector at the start of the first iterative cycle and the system of loads from the current deformed configuration. This difference vector is given by:

$$\Delta P_1 = \Delta P - \Delta P_1^* \quad \textbf{(2.9)}$$

A second iterative cycle commences by applying the out-of balance loads, ΔP_1, to the structure and the incremental displacements, ΔD_2, are found by solving equation 2.11.

$$[K_1]|\Delta D_2| = |\Delta P_1| \quad \textbf{(2.10)}$$

A new tangent stiffness matrix K_2 is assembled and the out-of balance load vector is given by:

$$\Delta P_2 = \Delta P_1 - \Delta P_2^* \qquad \textbf{(2.11)}$$

At the end of the second and subsequent cycles, a check is made to see if the out-of balance loads are within an acceptable tolerance. When convergence has been achieved after n cycles, the set of total displacements, which correspond to the total load increment ΔP, is given by:

$$\Delta D = \sum_{i=1}^{n} \Delta D_i \qquad \textbf{(2.12)}$$

The value of ΔP and ΔD are added to existing quantities to give the total amount of load and displacement in the structure. Structural analysis is carried out by incrementing a system loads up to a maximum load level, where the tangent stiffness becomes zero. To analyse the structure beyond the limit point, additional procedures must be adopted, Kenyon (1993) and discussed in section 2.7. Generally, this method requires updating of structural stiffness matrix (to reflect the most recent state of the structure, including the nonlinear effects) at the begging of each increment and iteration.

2.6.3 The Initial Stiffness Method (Newton-Raphson's Modified Method)

The initial stiffness method, which is also referred to as Newton-Raphson's modified method, is shown in Figure 2.11, Kenyon (1993). Two cycles are shown, where ΔP_1 and ΔP_2 are the out-of balance forces at the end of these cycles. Structural stiffness K_o is held constant for the load step.

Calculation procedure for the initial stiffness method are the same as for the tangent stiffness method, except the stiffnesses for the first cycle are held constant for each iterative cycle of that particular load step. This reduces the amount of computational time required to assemble each element stiffness matrix into a global stiffness matrix. However, the number of iterative cycles required for convergence may be greater than for the tangent stiffness method and has an additional disadvantage that the solution may be less accurate.

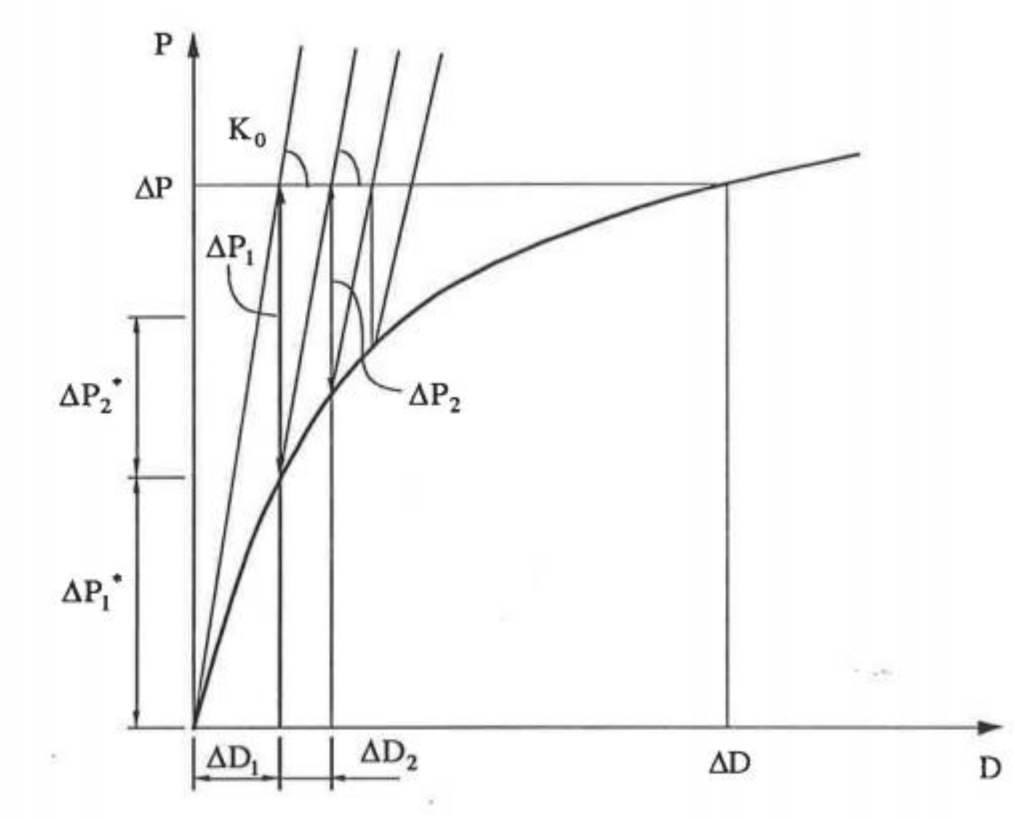

Figure 2-11: Initial stiffness method

This method can be shown to be unconditionally convergent and can even employed in situations where the material exhibits negative stiffness. Since, the initial stiffness method uses the initial stiffness throughout the analysis, thereby eliminating the considerable effort required to update the stiffness matrix. That is, the stiffness is calculated once and for all at the beginning of the computation and this value is then used throughout. This method is suitable for structures with stiffnesses that do not change much with loading and is therefore not suitable for highly nonlinear structures.

2.6.4 Combination of Initial Stiffness and Tangent Stiffness Method

A number of investigators have proposed mixed-modified Newton Raphson methods of analysis, Owen and Hinton (1980) and Kwak and Filippou (1997). In this type of approach, the initial stiffness and tangent stiffness methods are combine to improve the rate of convergence while maintaining accuracy of solution.

In the method proposed by Owen and Hinton (1980), the stiffnesses are recalculated only for the first iteration of any load increment and kept constant thereafter until convergence of solution under that particular loading is achieved. Alternatively, the element stiffnesses may be recomputed at the beginning of the second iteration. If the element stiffnesses are recalculated on the first iteration, the elements which have now yielded may have been elastic at the end of the previous load increment and consequently the reformulated stiffness will be based on elastic behavior. This can reduce the convergence rate of the process. Hence the tangential stiffness calculated grossly overestimates the true material response. This problem can be alleviated by reformulating the element stiffnesses during the second iteration of a load increment rather than the first, since the plastic strain evaluated on the first iteration will indicate yielding to have initiated. In addition to this, the nonlinear solution scheme selected in Kwak and Filippou (1997), uses the tangent stiffness matrix at the begging of the load step in combination of a constant stiffness matrix during the subsequent correction phase. The tangent stiffness method, initial stiffness method and combined initial and tangent stiffness method require to calculate the residual force vector, but secant stiffness method does not require.

2.7 Techniques for Traversing Limit Points and Post Peak Analysis

Wong (1989) reported that, tangent stiffness approach, secant stiffness approach and initial stiffness approach are suitable iterative solution techniques for nonlinear analysis problem up to the peak load, they generally fail to give a satisfactory solution beyond this point. This is due to:

i. The tangent stiffness of the frame being zero at the peak load;
ii. The multiple stable solutions available for a single value of load;
iii. Snap back instabilities in softening structures caused by some parts of the structures either unloading as a result of strain-softening or strain-reversal.

Limit points exist in a structure at peak strength (where ${dP}/{d\Delta} = 0$) or at local ultimate deflection (where ${dP}/{d\Delta} = -\infty$). Typical limit points are illustrated in Fig. 2.12 for a one degree of freedom structure. In Fig.2.12, point A represents a limit point for a structure under load control, while points B and C represent limit points for a structure under displacement control. Behavior that gives rise to both point B and C is referred to as snapback instability. For a structure with the behavior shown in Fig. 2.12, a load control procedure using monotonically increasing load can only follow the behavior up to approach point A, unless special techniques are devised as discussed below. If the displacement D is to be prescribed as the displacement control parameter, and this displacement is monotonically increased, the limit point A can be traced and the softening range AB can be traced. However, such a procedure would fail at a point approaching limit point B. for a one degree of freedom structure, the ability to trace the behavior up to this point is normally sufficient to give an indication of the peak load. For structures with many degrees of freedom of movement, a wrong choice of the displacement control parameter can result in premature termination of the analysis before reaching the peak load. Such termination will occur if the chosen parameter is not monotonically increasing, i.e., there is a reduction in the value of the control parameter as the global structural load continues to either increases or decreases. This would amount to forcing the control parameter to take on a value larger than its peak value which will result in non-convergence of the solution procedure. To overcome such premature termination does not occur during the analysis, Crisfield (1980, 1981 and 1986) numerical strategies have been developed to traverse limit points.

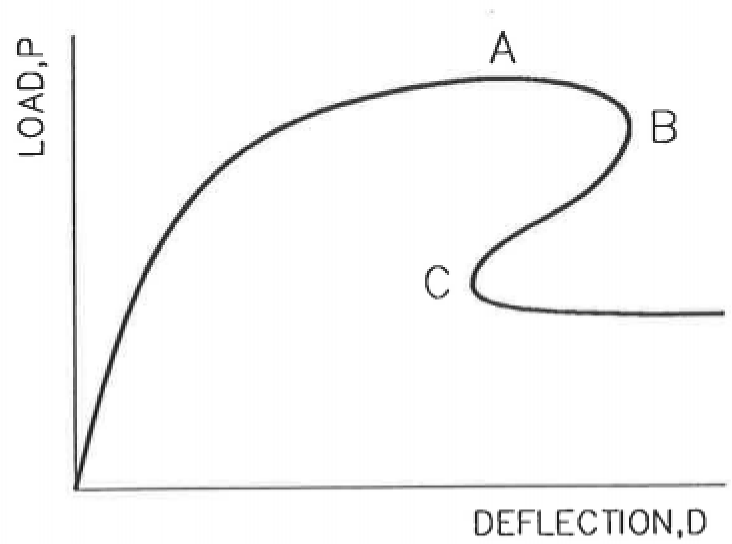

Figure 2-12: Limit points

CHAPTER 3 NUMERICAL ANALYSIS MODEL

In this paper, a two dimensional finite element method is employed for the nonlinear second-order behavior of reinforced concrete columns to formulate the load-deflection relationships. The finite element method is used for the discretization of the column into a sufficient number of equally spaced elements along its length, as well as the division of the cross-section into layered finite element. The finite element analysis of a continuum consists of three steps: firstly, structural idealization as an assemblage of discrete elements. Secondly, derivation of the element stiffness matrix resulting from the choice of a specific shape function and consequently, formation of the global stiffness matrix. Thirdly, structural analysis of the idealized assemblage of discrete elements.

3.1 Fundamental Assumptions

In order to formulate the constitutive relationships in a layer sections of reinforced concrete column, the following basic assumptions have been made in the calculations for theoretical load-deflection relations:

- Plane sections remain plane to represent the strain distribution across the depth of a cross-section is linear at any section and at any loading.
- The constitutive materials are assumed to carry uniaxial stress only.
- A perfect bond between the concrete matrix and reinforcing bars is assumed
- The confinement of concrete provided by lateral ties is included in the stress-strain relationship of material.
- The strain hardening of steel is neglected.
- Creep and shrinkage effects are neglected
- In addition, the shear deformation is not taken into account in the formulation because the shear effect is expected to be very small in slender reinforced concrete columns.

3.2 Modelling of Slender Reinforced Concrete Columns

The columns considered in this investigation are square reinforced concrete column having pin support at the bottom and roller support at the top which are subjected to axial load and uniaxial bending moment. The isolated two-dimensional pin-ended reinforced concrete columns are discretized into N identical column finite elements along the length as shown below in Figure 3.1. In this particular discretization, the length of the column is divided into 10 equally spaced elements having 11 nodes. There are three degrees of freedom per node, that is at each node of i of the element there are axial displacement, u_i, transverse displacement, v_i and rotational displacement, θ_i degrees of freedom corresponding to axial force,P, shear or transverse force,V and a bending moment,M, respectively.

Any nonlinear structural problems must obey the basic laws of continuum mechanics, that is, equilibrium, compatibility, and the constitutive relationship of materials.

a. The nodal Equilibrium equations: these states that at each node the external load must equal the sum of the nodal loads acting on the elements which meet there.
b. Strain-displacement relation: this is referring to the nodal strain or deformation compatibility equations. These equate the appropriate nodal displacements of those elements which have a common node.
c. The Stress-strain relationship of materials: this refer to material constitute laws. The nonlinear terms appear when the strains exceed the proportional limit of the material.

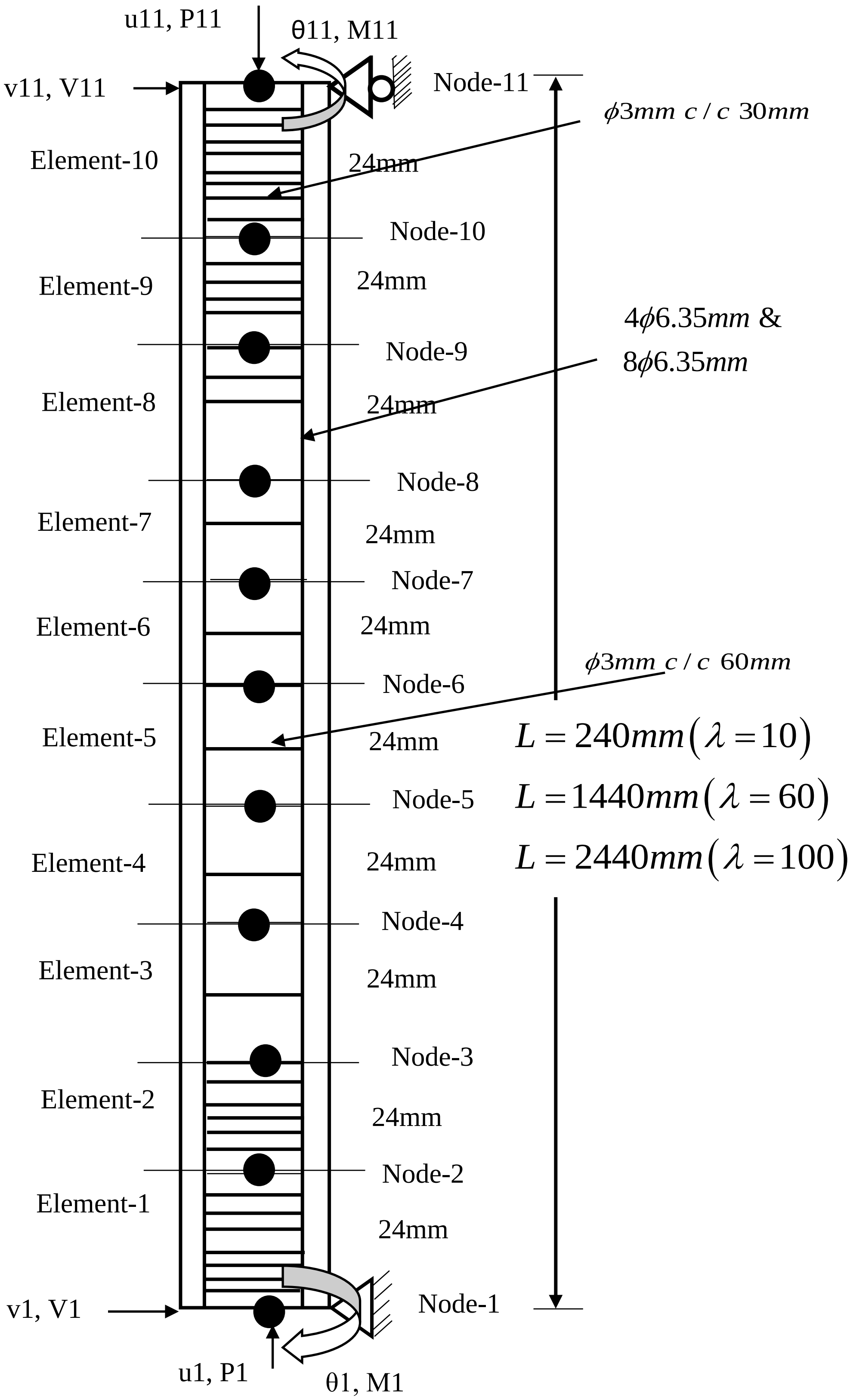

Figure 3-1: Discretization of reinforced concrete column into finite elements

3.2.1 Beam-Column Element

Consider a typical beam-column element from Fig. 3.1, which is in equilibrium under the external forces. The beam-column will be assumed to lie in the $x - y$ plane both before and after deformation takes place. Each column element has two nodes. The size of the element stiffness matrix for a two-dimensional beam element is 6x6 because of the three degrees of freedom associated with each node, Kim and Yang (19995).

The column matrices of the element nodal displacements and forces are $U = \{u_i, v_i, \theta_i, u_j, v_j, \theta_j\}^T$ and $F = \{P_i, V_i, M_i, P_j, V_j, M_j\}^T$, T denotes matrix transpose, u is axial displacement, v is transverse deflection, θ is bending rotation of cross section, and subscripts i and j refer to the adjacent cross-section at the ends of element, as shown in Fig.3.2.

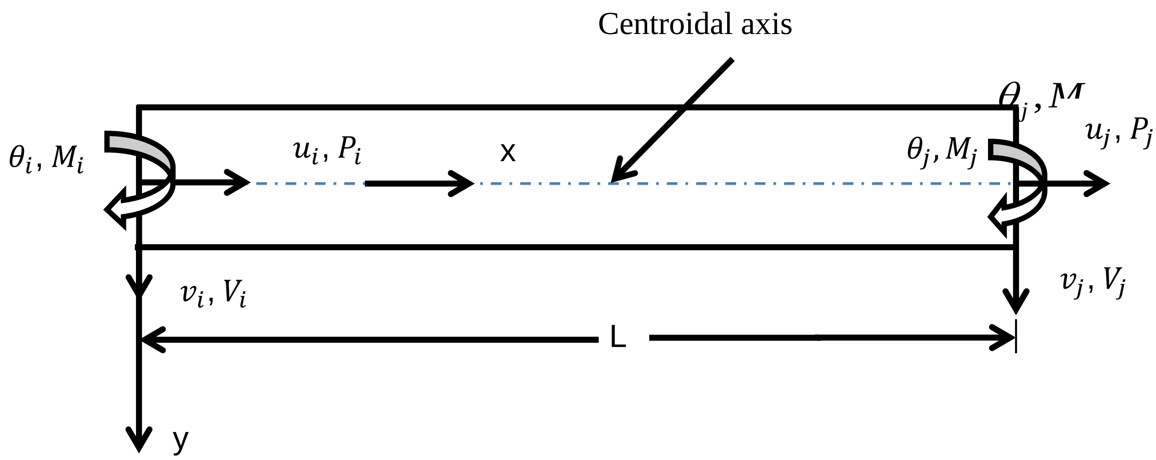

Figure 3-2: Beam-column nodal forces and displacements

3.2.2 Layered Cross-Section

Since the section is only subjected to uniaxial bending, it is subdivided into layers, rather than fibers and y and z are principal axes of the beam-column cross-section, as shown in Fig 3.3. Each column cross-section is divided in to N layers, some of which represent the reinforcing steel bars, so as to adopt the layering techniques. The steel reinforcement is represented by a separate steel layer. That is, the reinforcement bars are treated as additional layers with the properties of steel, having the same cross section as the steel reinforcement and it is assumed that the stresses and strains at the center of the layer are representative of the state of the entire layer. As the number of layers is increased, this model provides a more realistic representation of the gradual spread of cracks over the column cross-section.

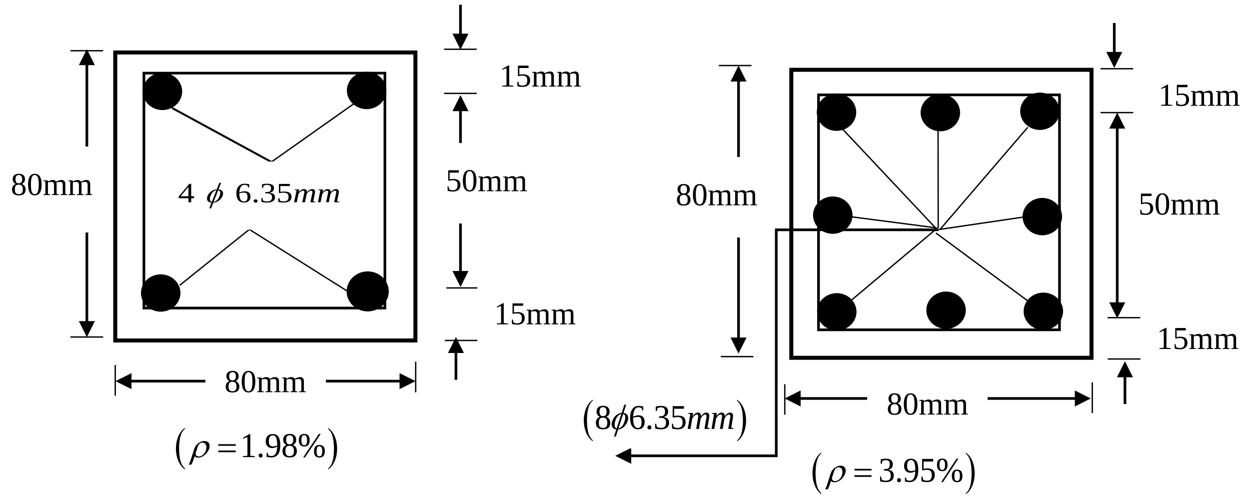

a) actual cross-section

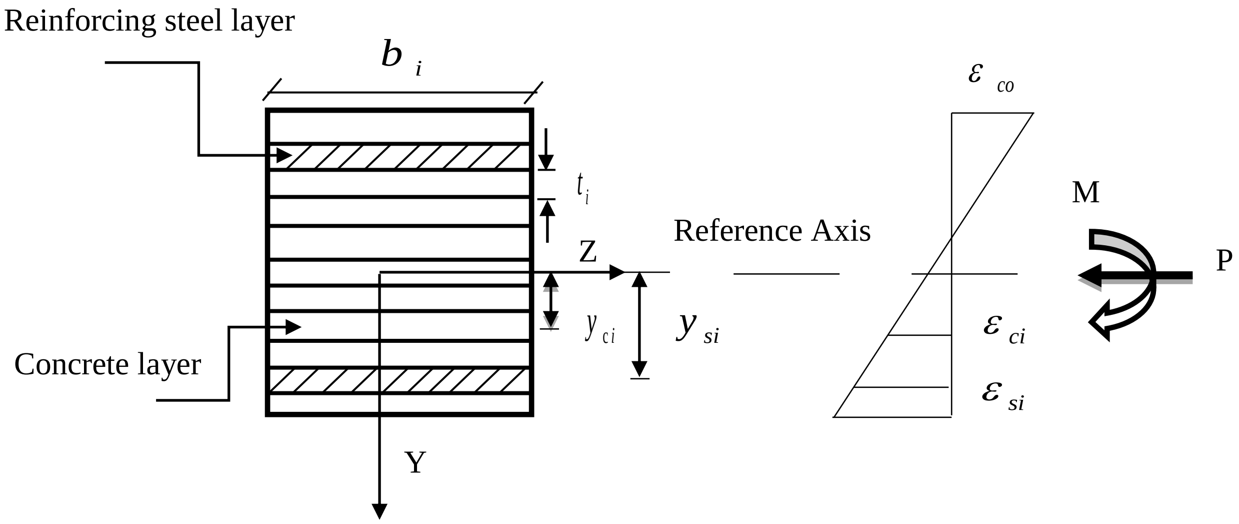

b) Idealized cross-section

Figure 3-3: Layered cross-section model

In this case, the length of each column is divided in to ten equally spaced elements along the length with eleven nodes and taking section at each node and divide it into N finite layers with $(N-2)$ concrete layers and two reinforcing steel layers. The distance of each concrete and steel layer are determined from geometric center of cross-section to the midpoint of each layer for all nodal cross-sections. The distance of each concrete layer, y_{ci} is positive above geometric center and negative below the geometric center of the cross-section and the same is true for reinforcing steel layers, y_{si}.

The thickness of each concrete and steel layer, t_i are determined as follows.

$$t_i = \frac{h}{N} \quad \textbf{(3.1)}$$

Area of each concrete layer:

$$A_{ci} = b_i t_i \tag{3.2}$$

Area of each longitudinal reinforcing steel layer:

$$A_{si} = \frac{\pi \phi_l^2}{4} \tag{3.3}$$

3.2.3 Shape Function of Beam-Column Element

A shape function defines the variations of the field variable, and its derivatives, through an element in terms of its values at the node. The displacement shape functions relate the displacements everywhere inside one element to the displacements at its nodes only. Often, although polynomials are selected as shape functions because they are relatively easy to manipulate mathematically, particularly with regard to integration and differentiation. However, the degree of polynomial chosen will clearly depend on the number of nodes and the degrees of freedom associated with the element, Al-Manaseer (1983). The standard shape functions along the elements are assumed to be a linear function for the axial displacement, $u(x)$ bar element as shown in Figure 3.4. This is consistent with the assumption of uniform member having a constant average axial strain along its length. In the case of transverse displacement, $v(x)$, it require a cubic function, Chajes and Churchill (1987). Hence, the following displacement functions for the beam-column element are assumed:

$$u(x) = a_o + a_1 x \tag{3.4}$$

$$v(x) = b_o + b_1 x + b_2 x^2 + b_3 x^3 \tag{3.5}$$

From Eqs.(3.4) and (3.5)

$$\frac{du}{dx} = a_1$$

$$\frac{dv}{dx} = b_1 + 2b_2 x + 3b_3 x^2$$

$$\frac{d^2 v}{dx^2} = 2b_2 + 6b_3 x$$

Applying the boundary condition at the ends of the element and using eq. (3.4) and (3.5)

$$u_i = u(x = 0) = a_o$$

$$u_j = u(x = L) = a_o + a_1 L$$

$$v_i = v(x = 0) = b_o$$

$$v_j = v(x = L) = b_o + b_1 L + b_2 L^2 + b_3 L^3$$

$$\theta_i = \left.\frac{dv}{dx}\right|_{x=0} = b_1$$

$$\theta_j = \left.\frac{dv}{dx}\right|_{x=L} = b_1 + 2b_2 L + 3b_3 L^2$$

The six equations can now be solved for the constants $a_o, a_1, b_o, b_1, b_2, b_3$ in terms of nodal displacements. Doing this yields

$$a_o = u_i \qquad\qquad a_1 = \frac{u_j - u_i}{L}$$

$$b_o = v_i \qquad\qquad b_1 = \theta_i$$

$$b_2 = \frac{3}{L^2}(v_j - v_i) - \frac{1}{L}(2\theta_i + \theta_j)$$

$$b_3 = \frac{2}{L^3}(v_i - v_j) + \frac{1}{L^2}(\theta_i + \theta_j)$$

Also from Eqs.(3.4) and (3.5) the displacement functions can be written as follows:

$$u = \left(1 - \frac{x}{L}\right) u_i + \left(\frac{x}{L}\right) u_j \qquad \textbf{(3.6)}$$

$$v = \left(1 - \frac{3x^2}{L^2} + \frac{2x^3}{L^3}\right) v_i + \left(\frac{3x^2}{L^2} - \frac{2x^3}{L^3}\right) v_j + \left(-\frac{2x^2}{L} + x + \frac{x^3}{L^2}\right)\theta_i + \left(-\frac{x^2}{L} + \frac{x^3}{L^2}\right)\theta_j \qquad \textbf{(3.7)}$$

In matrix form Eq. (3.7), can be written as: $v = [N]\{d\}$, Where $\{d\} = \begin{Bmatrix} v_i \\ v_j \\ \theta_i \\ \theta_j \end{Bmatrix}$ and $[N] = [N_1 \ \ N_2 \ \ N_3 \ \ N_4]$ are cubic shape function of a beam element and can represent graphically as shown in Fig. 3.5.

$$N_1 = \left(1 - \frac{x}{L}\right)$$

$$N_2 = \frac{x}{L}$$

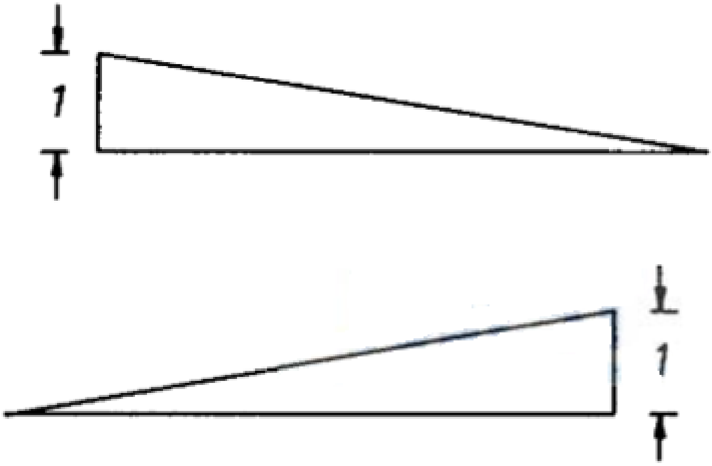

Figure 3-4: Linear shape function of bar element

$$N_1 = 1 - \frac{3x^2}{L^2} + \frac{2x^3}{L^3}$$

$$N_2 = \frac{3x^2}{L^2} - \frac{2x^3}{L^3}$$

$$N_3 = -\frac{2x^2}{L} + x + \frac{x^3}{L^2}$$

$$N_4 = -\frac{x^2}{L} + \frac{x^3}{L^2}$$

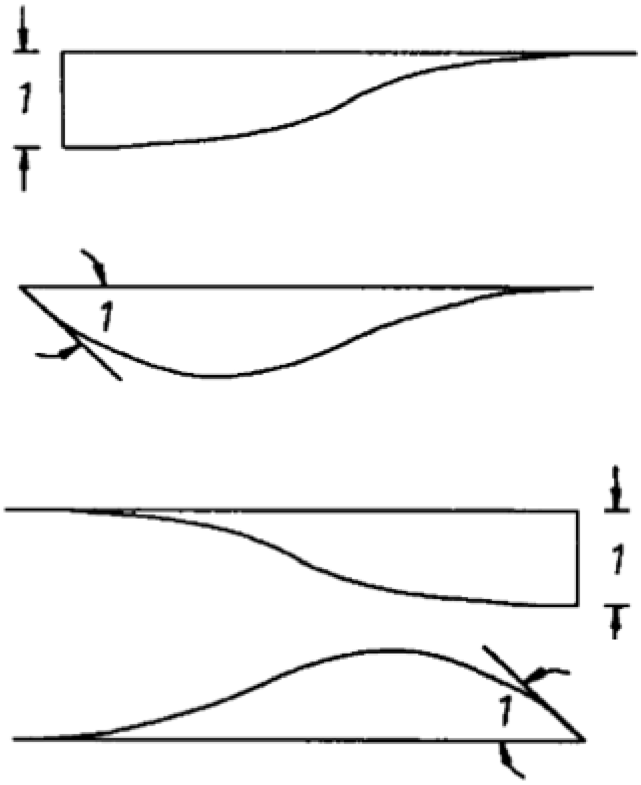

Figure 3-5: Cubic shape function of beam element

3.2.4 Strain-Displacement Relationships

The governing differential equations for a second-order analysis are formulated through the principle of virtual work, introducing the usual beam assumptions. This is mainly because the equilibrium equations consistent with the compatibility equations can be easily derived by purely mathematical manipulations, Goto and Chen (1987).

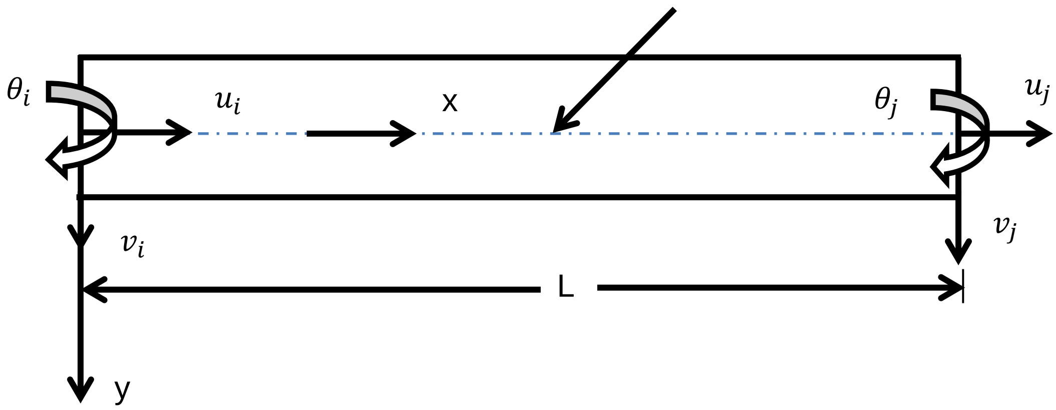

Figure 3-6: Displacement components in a beam element

By using the displacement components defined in eq. (3.6) and (3.7), the nonlinear Greens strain tensor ε_{jj} for plane problems is given by

$$\varepsilon_{xx} = \frac{\partial u}{\partial x} + \frac{1}{2}\left[\left(\frac{\partial u}{\partial x}\right)^2 + \left(\frac{\partial v}{\partial x}\right)^2\right] \quad \textbf{(3.8)}$$

$$\varepsilon_{yy} = \frac{\partial v}{\partial y} + \frac{1}{2}\left[\left(\frac{\partial u}{\partial y}\right)^2 + \left(\frac{\partial v}{\partial y}\right)^2\right] \quad \textbf{(3.9)}$$

$$\varepsilon_{xy} = +\frac{1}{2}\left(\frac{\partial v}{\partial x} + \frac{\partial u}{\partial y} + \frac{\partial u}{\partial x}\frac{\partial u}{\partial y} + \frac{\partial v}{\partial x}\frac{\partial v}{\partial y}\right) \quad \textbf{(3.10)}$$

If the derivative of axial displacement is negligibly small compared with those of deflection, the following conditions hold:

$$\frac{\partial u}{\partial x}, \frac{\partial u}{\partial y} \ll \frac{\partial v}{\partial x}, \frac{\partial v}{\partial y} \quad \textbf{(3.11)}$$

Considering the condition of Eq. (3.8),(3.9) , (3.10) and (3.11) gives as follows:

$$\varepsilon_{xx} = \frac{\partial u}{\partial x} + \frac{1}{2}\left(\frac{\partial v}{\partial x}\right)^2 \quad \textbf{(3.12)}$$

$$\varepsilon_{yy} = \frac{\partial v}{\partial y} + \frac{1}{2}\left(\frac{\partial v}{\partial y}\right)^2 \quad \textbf{(3.13)}$$

$$\varepsilon_{xy} = \frac{1}{2}\left(\frac{\partial v}{\partial x} + \frac{\partial u}{\partial y} + \frac{\partial v}{\partial x}\frac{\partial v}{\partial y}\right) \quad \textbf{(3.14)}$$

Here, introducing the usual beam assumptions, that is, the assumptions of no change of cross-sectional shapes and the Bernoulli-Euler hypothesis where the transverse plane is assumed to be plane and normal to the beam axis throughout deformation. These assumptions are mathematically expressed in terms of the strain tensor as

$$\varepsilon_{yy} = 0 \qquad \textbf{(3.15)}$$

$$\varepsilon_{xy} = 0 \qquad \textbf{(3.16)}$$

Assuming that the independent axial displacement in the axial direction, $u(x,0)$ varies linearly with x, and that the small rotation θ_i at each node can be calculated by derivation of the vertical displacement, v_i with respect to x, the displacements, $u(x,0)$ and $v(x)$ at any point within the element, can be represented by:

$$u(x,0) = \left[1-\frac{x}{L}, \frac{x}{L}\right]\begin{Bmatrix} u_i \\ u_j \end{Bmatrix}$$

$$v(x) = \left[\left(\left(1-\frac{3x^2}{L^2}+\frac{2x^3}{L^3}\right), \left(\frac{3x^2}{L^2}-\frac{2x^3}{L^3}\right), \left(x-\frac{2x^2}{L} + \frac{x^3}{L^2}\right), \left(-\frac{x^2}{L}+\frac{x^3}{L^2}\right)\right)\right]^T \begin{Bmatrix} v_i \\ v_j \\ \theta_i \\ \theta_j \end{Bmatrix} \qquad \textbf{(3.17)}$$

Then by adopting the plane section hypothesis and using the displacement components $\big(u(x,0), v(x)\big)$ on the centroidal axis, the x displacement field $u(x,y)$ at any point that satisfies Eq. 3.15 and 3.16 can be given by

$$u(x,y) = u(x,0) - y\frac{dv}{dx} \qquad \textbf{(3.18)}$$

Hence, the x displacement $u(x,y)$ and y displacement $v(x,y)$ may be expressed in terms of the nodal displacement of an element as follows.

$$u(x,y) = \left[1-\frac{x}{L}, \frac{x}{L}\right]\begin{Bmatrix} u_i \\ u_j \end{Bmatrix} - y\left[\left(\frac{6x}{L^2}+\frac{6x^2}{L^3}\right), \left(\frac{6x}{L^2}-\frac{6x^2}{L^3}\right), \left(1-\frac{4x}{L}+\frac{3x^2}{L^2}\right), \left(\frac{-2x}{L}+\frac{3x^2}{L^2}\right)\right]\begin{Bmatrix} v_i \\ v_j \\ \theta_i \\ \theta_j \end{Bmatrix} \qquad \textbf{(3.19)}$$

$$v(x,0) = \left[\left(\left(1-\frac{3x^2}{L^2}+\frac{2x^3}{L^3}\right), \left(\frac{3x^2}{L^2}-\frac{2x^3}{L^3}\right), \left(x-\frac{2x^2}{L}+\frac{x^3}{L^2}\right), \left(-\frac{x^2}{L}+\frac{x^3}{L^2}\right)\right)\right]^T \begin{Bmatrix} v_i \\ v_j \\ \theta_i \\ \theta_j \end{Bmatrix} \qquad \textbf{(3.20)}$$

Where, the terms inside the parenthesis represents displacement shape functions or interpolation functions which relates the displacements everywhere inside one element to the displacements at its nodes only, x is the position along the axis of the column element and L is length of column element.

Substituting Eq. 3.19 and 3.20 into Eq.3.12 the nonzero component of the strain tensor is expressed by the displacement components on the centriodal axis:

$$\varepsilon_{xx} = \varepsilon(x, y_i) = \frac{du(x,0)}{dx} - y_i \frac{d^2 v}{dx^2} + \frac{1}{2}\left(\frac{dv}{dx}\right)^2 \qquad \textbf{(3.21)}$$

Therefore, the nonlinear strain-displacement equation for the strain $\varepsilon(x, y)$ at level y_i for the i^{th} layer in the cross section in an axially loaded and uniaxial bending moment two dimensional element can be defined by:

$$\varepsilon(x, y_i) = -\frac{u_i}{L} + \frac{u_j}{L} - y_i \begin{bmatrix} \left(-\frac{6}{L^2} + \frac{12x}{L^3}\right) v_i + \left(\frac{6}{L^2} - \frac{12x}{L^3}\right) v_j + \\ \left(-\frac{4}{L} + \frac{6x}{L^2}\right) \theta_i + \left(-\frac{2}{L} + \frac{6x}{L^2}\right) \theta_j \end{bmatrix} + \frac{1}{2} \begin{bmatrix} \left(-\frac{6x}{L^2} + \frac{6x^2}{L^3}\right) v_i + \left(\frac{6x}{L^2} - \frac{6x^2}{L^3}\right) v_j + \\ \left(1 - \frac{4x}{L} + \frac{3x^2}{L^2}\right) \theta_i + \left(-\frac{2x}{L} + \frac{3x^2}{L^2}\right) \theta_j \end{bmatrix}^2 \qquad \textbf{(3.22)}$$

The terms on the right-hand side of Eq.(3.22) admit the following geometric interpretations: the first term defines the normal strain (axial strain) induced by axial deformations of the reference axis; the second term represents the elementary bending strain (strain produced by curvature); and the third term represents the contribution of bending of the reference axis to the normal strain (nonlinear part of the axial strain), that is, it accounts for the coupling of axial and flexural distortions. Generally, the first two terms represent linear effect, while the third squared term represents the nonlinear displacement effect. u and v are displacement components in the x and y directions, respectively.

3.2.5 Material and Geometric Element Stiffness Matrix

Making use of Hook's Law, the stress at any layer in the section is expressed as:

$$\sigma = E\varepsilon = E\left[\frac{du(x,0)}{dx} - y_i\frac{d^2v}{dx^2} + \frac{1}{2}\left(\frac{dv}{dx}\right)^2\right] \quad \textbf{(3.23)}$$

In which E is modulus of elasticity

Recalling that

$$dV = dA\,dx, \int_A dA = A, \ \int_A ydA = 0, \ \int_A y^2dA = I \text{ and } \int_A E\frac{du}{dx}dA = P$$

Where P is the axial force, negative in compression

Applying the law of virtual work in the beam element as shown in Fig.3.2, leads the strain energy to be written:

$$U_e = \int_0^l \int_A \sigma\delta\varepsilon dAdx \ = M_i\frac{\delta dv_i}{dx} + M_j\frac{\delta dv_j}{dx} + P_i\delta u_i + P_j\delta u_j + \ V_i\delta v_i + V_j\delta v_j \quad \textbf{(3.24)}$$

Substituting equation (3.21) and (3.23) in to the first expression of equation (3.24) the following relational expressions can be obtained:

$$U_e = \int_0^l \int_A \left(\frac{\delta du}{dx}E\frac{du}{dx} + \frac{\delta d^2v}{dx^2}Ey^2\frac{d^2v}{dx^2} + \frac{\delta dv}{dx}E\frac{du}{dx}\frac{dv}{dx}\right)dAdx - \int_0^l \int_A \left(\frac{\delta du}{dx}Ey\frac{d^2v}{dx^2} + \frac{\delta d^2v}{dx^2}Ey\frac{du}{dx}\right)dAdx \quad \textbf{(3.25)}$$

Here, the higher-order term is ignored and $P = \int_A \sigma dA = \int_A E\frac{du}{dx}dA$

As shown in Fig.3.4 and 3.5, those are interpolation functions of the beam-column element which are used for displacement in the x direction and displacement in the y direction, respectively.

$$u = B_a(x)\{U\} \quad \textbf{(3.26)}$$

$$v = B_b(x)\{U\} \quad \textbf{(3.27)}$$

Here, the strain-displacement matrix of the beam-column element is expressed as follows:

$$B_a(x) = \left[\left(1-\frac{x}{L}\right), 0,0, \frac{x}{L}, 0,0\right]$$

$$B_b(x) = \left[0, \left(1-\frac{3x^2}{L^2}+\frac{2x^3}{L^3}\right), \left(x-\frac{2x^2}{L}+\frac{x^3}{L^2}\right), 0, \left(\frac{3x^2}{L^2}-\frac{2x^3}{L^3}\right), \left(-\frac{x^2}{L}+\frac{x^3}{L^2}\right)\right]$$

$$\{U\} = \{u_i, v_i, \theta_i, u_j, v_j, \theta_j\}^T$$

Substituting equations (3.26) and (3.27) in to equation (3.25) leads to

$$([k_M] + P[k_G])\{U\} = [F] \qquad \textbf{(3.28)}$$

Here,

$$[k_M] = \begin{bmatrix} \frac{EA}{L} & 0 & -\frac{ER}{L} & -\frac{EA}{L} & 0 & \frac{ER}{L} \\ 0 & \frac{12EI}{L^3} & \frac{6EI}{L^2} & 0 & -\frac{12EI}{L^3} & \frac{6EI}{L^2} \\ -\frac{ER}{L} & \frac{6EI}{L^2} & \frac{4EI}{L} & \frac{ER}{L} & -\frac{6EI}{L^2} & \frac{2EI}{L} \\ -\frac{EA}{L} & 0 & \frac{ER}{L} & \frac{EA}{L} & 0 & -\frac{ER}{L} \\ 0 & -\frac{12EI}{L^3} & -\frac{6EI}{L^2} & 0 & \frac{12EI}{L^3} & -\frac{6EI}{L^2} \\ \frac{ER}{L} & \frac{6EI}{L^2} & \frac{2EI}{L} & -\frac{ER}{L} & -\frac{6EI}{L^2} & \frac{4EI}{L} \end{bmatrix} \qquad \textbf{(3.29)}$$

$$[k_G] = \begin{bmatrix} 0 & 0 & 0 & 0 & 0 & 0 \\ 0 & \frac{6P}{5L} & \frac{P}{10} & 0 & -\frac{6P}{5L} & \frac{P}{10} \\ 0 & \frac{P}{10} & \frac{2PL}{15} & 0 & -\frac{P}{10} & -\frac{PL}{30} \\ 0 & 0 & 0 & 0 & 0 & 0 \\ 0 & -\frac{6P}{5L} & -\frac{P}{10} & 0 & \frac{6P}{5L} & -\frac{P}{10} \\ 0 & \frac{P}{10} & -\frac{PL}{30} & 0 & -\frac{P}{10} & \frac{2PL}{15} \end{bmatrix} \qquad \textbf{(3.30)}$$

3.2.6 Element Equilibrium Matrix

Applying the virtual work principle for Eq.(3.24), the force-displacement relation, which acts at each node of the beam-column element shown in Fig 3.2, is determined as follows.

$$([k_M] + [k_G])\{U\} = \{F\} \qquad \textbf{(3.31)}$$

$$\{U\} = \{u_i \;\; v_i \;\; \theta_i \;\; u_j \;\; v_j \;\; \theta_j\}^T$$

$$\{F\} = \{P_i \;\; V_i \;\; M_i \;\; P_j \;\; V_j \;\; M_j\}^T$$

As the global coordinate system and the local coordinate system are identical, there is no need for coordinate transformation.

Where: T is matrix transpose

u_i and u_j -axial displacements;

v_i and v_j - transverse /lateral displacements;

θ_i and θ_j-bending rotations; and

subscripts i and j refer to the cross section i and j at the ends of the element.

$[k_M]$ is the linear-elastic material stiffness matrix of the element,

$[k_G]$ is the nonlinear geometric stiffness matrix of the element,

U is all nodal displacements of the element, and

$\{F\}$ is all nodal loads of the element

3.2.7 Formulation of Elastic Stiffness of a Column Cross-Section

In the layered cross-section model, each square cross-section is discretized into, N finite layers, with N_c number of concrete layers and N_s represents reinforcing steel layers as shown in Fig 3.3. Each of these layer is assumed to be under uniaxial strain. Where each concrete layer has width,b_i ,thickness,t_i and the centroidal coordinate of each layer, y_{ci} is measured from the geometric center of the cross section and each reinforced steel layer has the area of longitudinal steel, A_{si} and their centriodal coordinate is y_{si} from the geometric center. The cross-section at the end of the element is assumed to be representative of sections along the element when forming the element stiffness matrix.

Accordingly, the elastic section stiffness (elastic axial stiffness,EA, elastic combined axial and flexural stiffness,ER, and elastic flexural stiffness,EI) in each cross-sections are calculated approximately by a sum over the layers as follows.

i. Axial Stiffness

$$EA = \int_A E dA = \sum_{i=1}^{n} E_i A_i = \sum_{i=1}^{n_{ci}} E_{ci} A_{ci} + \sum_{j=1}^{n_{sj}} E_{sj} A_{sj} \qquad \textbf{(3.32)}$$

ii. Flexural Stiffness

$$EI = \int_A E y^2 dA = \sum_{i=1}^{n} E_i\, y_i^2 A_i + \sum_{i=1}^{n} EI_o$$
$$= \sum_{i=1}^{n_{ci}} E_{ci} y_{ci}^2 A_{ci} + \sum_{j=1}^{n_{ci}} E_{cj} I_{ocj} + \sum_{j=1}^{n_{sj}} E_{sj} y_j^2 A_{sj} + \sum_{j=1}^{n_{sj}} E_{sj} I_{osj}$$
$$= \sum_{i=1}^{n_{ci}} E_{ci} y_{ci}^2 A_{ci} + \sum_{i=1}^{n_{ci}} E_{ci} \frac{1}{12} b_i t_i^3 + \sum_{j=1}^{n_{sj}} E_{sj} y_j^2 A_{sj} + \sum_{j=1}^{n_{sj}} E_{sj} \frac{\pi r^4}{4} \qquad \textbf{(3.33)}$$

iii. Combined axial and flexural stiffness

A lot of researchers such as Bazant *et al.* (1987), Kim and Yang (1995), Kim and Lee (1993, 2000) additional stiffness terms are included and introduced in the off-diagonal positions which take into account the shift or change in the position of centroidal axis. These terms are given by, ER, where E is the young's modulus and R is the first moment of area of the section and this is given by:

$$ER = -\int_A E y dA = -\sum_{i=1}^{n} E_i y_i A_i = -\sum_{i=1}^{n_{ci}} E_{ci} y_{ci} A_{ci} - \sum_{j=1}^{n_{sj}} E_{sj} y_{sj} A_{sj} \qquad \textbf{(3.34)}$$

Where:

EA and EI are the axial and flexural stiffness, respectively;

ER is the combined axial and flexural stiffness;

$I_o = \frac{1}{12} b_i t_i^3$- a layered centroidal moment of inertia;

$I = I_o + A_i y_i^2 = \frac{1}{12} b_i t_i^3 + A_i y_i^2$-moment of inertia (parallel axis theorem);

E_{ci} and E_{si} are the material modulus for concrete and steel layer, respectively;

Notice that, EA , ER and EI are sometimes referred as zero, first and second stiffness terms respectively and are given by Eq.(3.32), (3.33) and (3.34). The combined axial and flexural stiffness ER which replace the zero stiffness component on the linear-elastic material stiffness matrix.

For a member with symmetric section which is composed of elastic material, ER is zero. Thus, Eq. (3.29) is the usual linear stiffness matrix because of uncoupled characteristics between the axial force action and bending moment action. However, reinforced concrete members are composed of nonlinear and inelastic materials, Kim and Lee (2000). When a stress is beyond elastic limit or cracking occurs in reinforced concrete section subjected to axial force and uniaxial bending, the principal axes of the cross section may translate. Because of this phenomenon, axial force applied at the centroid of gross section may have an effect on curvature and bending moment may also have an effect on axial strain at the sectional centroid. In this case, the axial force and the bending moments are coupled and ER is not a zero matrix. In other words, the ER terms define the increase in curvature caused by an increment of axial load and the increase in centroidal strain caused by an increment of bending moment.

3.2.8 Elastic Material Element Stiffness Matrix

This material stiffness is generated from the un-deformed configuration of the column and the initial properties (modulus of elasticity of concrete and reinforcing steel, cross-sectional area, and moment of inertia of each layer) of the cross section and are the same throughout for any section along the length of the columns. This leads to the same linear-elastic material stiffness matrix for all elements of the column. Along with this, while calculating the global elastic material stiffness matrix of the column, K_M , the value of elastic modulus E for each layer is assumed to be held constant throughout the column length. However, the combined axial and flexural stiffness has no contribution on the stiffness of the column until the elastic limit because of the same material properties for each layer of the cross-section. The material stiffness matrix of each finite element of the column is determined by repeating Eq.(3.29) and assemble them to obtain the structural material stiffness matrix of the column.

3.2.9 Geometric Element Stiffness Matrix

In order to allow geometric nonlinearities, the equilibrium equation have to be formed for the deformed column. This results in nonlinear relationships between loads and displacements. Geometric nonlinearity within the elements, caused by the interaction of axial forces with lateral deflections, is accounted for by the addition of a non-linear geometric stiffness matrix k_G to the first order elastic stiffness matrix, k_M.

The applied axial force P is usually not known in advance to evaluate the geometric stiffness matrix of each element of the column, and an iteration procedure must be used. When the controlled axial displacement is applied at the top roller support of the column, the axial load required to maintain equilibrium is unknown and can only be obtain by iteration. In the first iteration (first-order elastic analysis) the applied axial force is chosen equal to zero then the first order forces are calculated. Next, axial force which was obtained in the first iteration is used for the second iteration. Note that, the nonlinear geometric stiffness matrix of each finite element are calculate by repeating Eq. (3.30) and assemble them to obtain the structural nonlinear geometric stiffness matrix of the column.

3.3 Conversion into the Displacement Control

For loading in which the load is controlled, structures fail (become unstable) at their maximum load, while structural elements that are loaded under imposed displacement control or through displacement-controlled elastic devices fail in their post-peak strain-softening range. Hence, to analyse the post peak behavior, the columns were analysed by the displacement control method. Prescribed controlled axial displacement in the direction of axial displacement degree of freedom at the top roller support of the column is incrementally applied. This controlled displacement parameter act as a monitor for the stiffness degradation of the column at all stages of loading, irrespective of where in the structure this degradation occurs.

When the c^{th} incremental displacement U_c at which the c^{th}applied load F_c exists, is controlled, as a certain known value, the applied load vector F_i and the displacements which are not controlled are unknowns. Since each load which acts on a structure, can be expressed in terms of a certain load, F_c, the global incremental load vector, F_i can be written as the following expression.

$$\begin{bmatrix} F_1 \\ F_2 \\ . \\ . \\ . \\ F_c \\ . \\ . \\ . \\ F_n \end{bmatrix} = \begin{bmatrix} a_1 \\ a_2 \\ . \\ . \\ . \\ 1 \\ . \\ . \\ . \\ a_n \end{bmatrix} F_c \qquad \textbf{(3.35)}$$

Therefore, the resultant simultaneous equations in the displacement control method is written by:

$$\begin{bmatrix} K_{11} & K_{12} & . & . & . & -a_1 & . & . & . & K_{1n} \\ K_{21} & K_{22} & . & . & . & -a_2 & . & . & . & K_{1n} \\ . & . & . & . & . & . & . & . & . & . \\ . & . & . & . & . & . & . & . & . & . \\ . & . & . & . & . & . & . & . & . & . \\ K_{c1} & K_{c2} & . & . & . & -1 & . & . & . & K_{cn} \\ . & . & . & . & . & . & . & . & . & . \\ . & . & . & . & . & . & . & . & . & . \\ . & . & . & . & . & . & . & . & . & . \\ K_{n1} & K_{n2} & . & . & . & -a_n & . & . & . & K_{nn} \end{bmatrix} \begin{bmatrix} U_1 \\ U_2 \\ . \\ . \\ . \\ F_c \\ . \\ . \\ . \\ U_n \end{bmatrix} = \begin{bmatrix} -K_{1c} \\ -K_{2c} \\ . \\ . \\ . \\ -K_{cc} \\ . \\ . \\ . \\ -K_{nc} \end{bmatrix} U_c \qquad \textbf{(3.36)}$$

Where,$a_1, a_2, \dots\dots\dots\dots\dots\dots\dots., a_n$ are proportional constants of F_c.

3.3.1 Proportional Constants of the Controlled Force, $\boldsymbol{F_c}$

In this particular modeling, the column is divided in to ten elements with eleven nodes. Each element has six degree of freedom (three per node) corresponding to these degrees of freedom there are six unknown nodal loads (axial force, shear force and bending moment). Now, the value of each proportional constants is given as follows for each nodal force. These proportional constants are one for axial force, zero for shear force and axial load eccentricities which are equal and of the same sign for bending moment applied at the pin-roller support of the column.

$$\begin{bmatrix} Node_1 \\ . \\ . \\ Node_2 \\ . \\ . \\ Node_3 \\ . \\ . \\ Node_4 \\ . \\ . \\ Node_5 \\ . \\ . \\ Node_6 \\ . \\ . \\ Node_7 \\ . \\ . \\ Node_8 \\ . \\ . \\ Node_9 \\ . \\ . \\ Node_{10} \\ . \\ . \\ Node_{11} \\ . \\ . \end{bmatrix} = \begin{bmatrix} N_1 \\ V_1 \\ M_1 \\ N_2 \\ V_2 \\ M_2 \\ N_3 \\ V_3 \\ M_3 \\ N_4 \\ V_4 \\ M_4 \\ N_5 \\ V_5 \\ M_5 \\ N_6 \\ V_6 \\ M_6 \\ N_7 \\ V_7 \\ M_7 \\ N_8 \\ V_8 \\ M_8 \\ N_9 \\ V_9 \\ M_9 \\ N_{10} \\ V_{10} \\ M_{10} \\ N_{11} \\ V_{11} \\ M_{11} \end{bmatrix} = \begin{bmatrix} F_1 \\ F_2 \\ F_3 \\ F_4 \\ F_5 \\ F_6 \\ F_7 \\ F_8 \\ F_9 \\ F_{10} \\ F_{11} \\ F_{12} \\ F_{13} \\ F_{14} \\ F_{15} \\ F_{16} \\ F_{17} \\ F_{18} \\ F_{19} \\ F_{20} \\ F_{21} \\ F_{22} \\ F_{23} \\ F_{24} \\ F_{25} \\ F_{26} \\ F_{27} \\ F_{28} \\ F_{29} \\ F_{30} \\ F_{31} \\ F_{32} \\ F_{33} \end{bmatrix} = \begin{bmatrix} a_1F_{31} \\ a_2F_{31} \\ a_3F_{31} \\ a_4F_{31} \\ a_5F_{31} \\ a_6F_{31} \\ a_7F_{31} \\ a_8F_{31} \\ a_9F_{31} \\ a_{10}F_{31} \\ a_{11}F_{31} \\ a_{12}F_{31} \\ a_{13}F_{31} \\ a_{14}F_{31} \\ a_{15}F_{31} \\ a_{16}F_{31} \\ a_{17}F_{31} \\ a_{18}F_{31} \\ a_{19}F_{31} \\ a_{20}F_{31} \\ a_{21}F_{31} \\ a_{22}F_{31} \\ a_{23}F_{31} \\ a_{24}F_{31} \\ a_{25}F_{31} \\ a_{26}F_{31} \\ a_{27}F_{31} \\ a_{28}F_{31} \\ a_{29}F_{31} \\ a_{30}F_{31} \\ a_{31}F_{31} \\ a_{32}F_{31} \\ a_{33}F_{31} \end{bmatrix} = \begin{bmatrix} a_1 \\ a_2 \\ a_3 \\ a_4 \\ a_5 \\ a_6 \\ a_7 \\ a_8 \\ a_9 \\ a_{10} \\ a_{11} \\ a_{12} \\ a_{13} \\ a_{14} \\ a_{15} \\ a_{16} \\ a_{17} \\ a_{18} \\ a_{19} \\ a_{20} \\ a_{21} \\ a_{22} \\ a_{23} \\ a_{24} \\ a_{25} \\ a_{26} \\ a_{27} \\ a_{28} \\ a_{29} \\ a_{30} \\ a_{31} \\ a_{32} \\ a_{33} \end{bmatrix} * F_{31} = \begin{bmatrix} 1 \\ 0 \\ (e+\delta_i) \\ 0 \\ 0 \\ 0 \\ 0 \\ 0 \\ 0 \\ 0 \\ 0 \\ 0 \\ 0 \\ 0 \\ 0 \\ 0 \\ 0 \\ 0 \\ 0 \\ 0 \\ 0 \\ 0 \\ 0 \\ 0 \\ 0 \\ 0 \\ 0 \\ 0 \\ 0 \\ 0 \\ 1 \\ 0 \\ -(e+\delta_i) \end{bmatrix} * F_{31} \quad \textbf{(3.37)}$$

Where, e is axial load eccentricities of the column and δ_i is maximum lateral deflection at each iteration and incremental axial displacement.

3.3.2 Modified Nodal Forces

The numerical model adopted in this method is based on the incremental controlled axial displacement, where a controlled axial displacement is specified and prescribed at the top roller support in axial direction (parallel to the longitudinal axis of the column). Let the 31^{th} displacement (axial displacement) located at the 31^{th} node which is at the top roller support corresponding to the 31^{th} applied axial force,F_{31} exists, is controlled then the applied axial force, F_{31} and the displacements which are not controlled are unknowns. Visualize clearly, the vectors of the unknown nodal displacements of the column elements are given as follows:

$$\begin{bmatrix} \text{Node 11} \\ . \\ . \\ \text{Node 10} \\ . \\ . \\ \text{Node 9} \\ . \\ . \\ \text{Node 8} \\ . \\ . \\ \text{Node 7} \\ . \\ . \\ \text{Node 6} \\ . \\ . \\ \text{Node 5} \\ . \\ . \\ \text{Node 4} \\ . \\ . \\ \text{Node 3} \\ . \\ . \\ \text{Node 2} \\ . \\ . \\ \text{Node 1} \\ . \\ . \end{bmatrix} = \begin{bmatrix} u_{11} \\ v_{11} \\ \theta_{11} \\ u_{10} \\ v_{10} \\ \theta_{10} \\ u_9 \\ v_9 \\ \theta_9 \\ u_8 \\ v_8 \\ \theta_8 \\ u_7 \\ v_7 \\ \theta_7 \\ u_6 \\ v_6 \\ \theta_6 \\ u_5 \\ v_5 \\ \theta_5 \\ u_4 \\ v_4 \\ \theta_8 \\ u_3 \\ v_3 \\ \theta_3 \\ u_2 \\ v_2 \\ \theta_2 \\ u_1 \\ v_1 \\ \theta_1 \end{bmatrix}$$

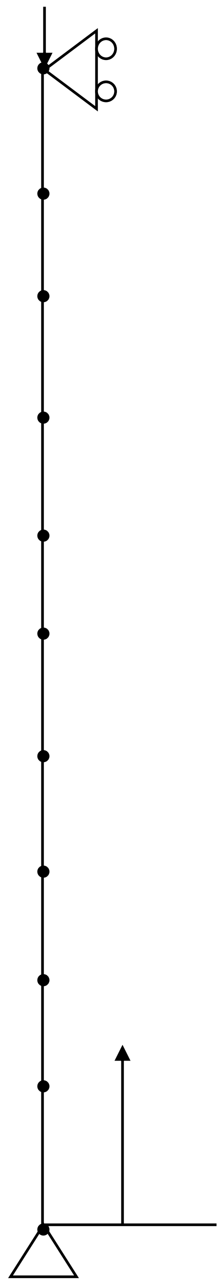

In this case as shown in equation(3.38), the nodal loads of the column are modified and replaced by multiplying the stiffness matrix corresponding to the controlled displacement by the incremental controlled axial displacement and clearly explained in Eq. (3.38) and Eq. (3.39).

$$F^{(i+1)} = -K_{ic}^{(i)} . U_c^{(i+1)} \qquad \textbf{(3.38)}$$

$$\left(-K_{jc}.U_c\right)=\begin{bmatrix}-K_{1c}\\-K_{2c}\\.\\.\\.\\-K_{cc}\\.\\.\\.\\-K_{nc}\end{bmatrix}.U_c=\begin{bmatrix}-K_{1c}\\-K_{2c}\\.\\.\\.\\.\\.\\.\\.\\:\\.\\-K_{cc}\\.\\-K_{nc}\end{bmatrix}.U_c=\begin{bmatrix}-K_{(1,31)}\\-K_{(2,31)}\\-K_{(3,31)}\\-K_{(4,31)}\\-K_{(5,31)}\\-K_{(6,31)}\\-K_{(7,31)}\\-K_{(8,31)}\\-K_{(9,31)}\\-K_{(10,31)}\\-K_{(11,31)}\\-K_{(12,31)}\\-K_{(13,31)}\\-K_{(14,31)}\\-K_{(15,31)}\\-K_{(16,31)}\\-K_{(17,31)}\\-K_{(18,31)}\\-K_{(19,31)}\\-K_{(20,31)}\\-K_{(21,31)}\\-K_{(22,31)}\\-K_{(23,31)}\\-K_{(24,31)}\\-K_{(25,31)}\\-K_{(26,31)}\\-K_{(27,31)}\\-K_{(28,31)}\\-K_{(29,31)}\\-K_{(30,31)}\\-K_{(31,31)}\\-K_{(32,31)}\\-K_{(33,31)}\end{bmatrix}.U_c \qquad \textbf{(3.39)}$$

3.4 Constitutive Laws for Materials

To take into account of material non-linearity of concrete and steel both compression and tension stress-strain relationships are considered.

3.4.1 Compression Stress-Strain Relationship of Concrete

The stress-strain relationship of concrete in uniaxial compressive had been proposed by many researchers. Most of the models, however, were based on the test results obtained from their experiments. Therefore, the results of the models can be subject to great variation according to the test method and test conditions.

A common representation of stress-strain curve for concrete is established by Hognestad (1951). Kim and Lee (1993) proposed a uniaxial compressive stress-strain relationship for concrete including the confinement effect represented by Eq. (3.46) and (3.48) in which the variables in Hognestad's model for ascending, and in Fafitis and Shah's model for descending, respectively, were recalculated properly by regression analysis with test data to obtain a modified model for high strength concrete.

In modeling the behavior of the post-peak softening part, unlike Fafitis and Shah's model, two values, B and C are used, so that the lateral reinforcement effect is increased according to the difference strength level. Several test data by other researchers were gathered and then the regression analysis was performed to determine the parameters A, B and C in Eq. (3.40), (3.41) and (3.42). This model makes a superior prediction for the uniaxial compressive stress-strain behavior regardless of the concrete strength.

Parameter A: the value of this parameter depends on the values of peak stress, peak strain and the secant modulus of elasticity(E_c).

$$A = \frac{E_c \varepsilon_o}{f_o} \qquad \textbf{(3.40)}$$

Parameter B: a constant to be determined so as to fit the experimental data of the descending part.

$$B = \left(260 + \frac{100}{f_c'}\right) exp\left(-30\frac{f_{cl}}{f_c'}\right) \qquad \textbf{(3.41)}$$

The expression for the parameter C is given by:

$$C = 1.2 - 0.006 f_c' \qquad \textbf{(3.42)}$$

Under a compressive load, the concrete in the square tied column shortens longitudinally under the stress f_o and so, to satisfy the Poisson's ratio, it expands laterally and for equilibrium, the concrete is subjected to lateral compressive stresses, f_{cl}. An element taken from within the core is subjected to tri-axial compression stress. That is, axial stress in the longitudinal direction and lateral stresses due to confinement in both directions. Thus, the ultimate compressive strength of confined concrete, $f_o(MPa)$ and the corresponding strain, ε_o is computed as follows:

$$f_o = f_c' + 4.2 f_{cl} \quad \textbf{(3.43)}$$

$$\varepsilon_o = 7 * 10^{-4} \sqrt[3]{f_c'} + 0.06 \frac{f_{cl}}{f_c'} \quad \textbf{(3.44)}$$

Where, f_c' is the cylinder compressive strength of concrete (MPa).

The confinement stress which takes into account for the strength increase due to confinement of ties (lateral reinforcing steel) is computed as:

$$f_{cl} = \frac{\rho_s f_{ys}}{2}\left(1 - \sqrt{\frac{s}{d_c}}\right) \quad \textbf{(3.45)}$$

Where, f_{cl} is the confining stress (MPa), f_{ys} is the yield strength of confining reinforcement (MPa), ρ_s is the ratio of the volume of tie reinforcement to the volume of concrete core, d_c and s are the depth of the concrete core measured to the outside of ties (mm) and the center to center spacing of tie (mm), respectively.

Ascending (pre-peak) part: for $0 \leq \varepsilon_c \leq \varepsilon_o$

$$\sigma_c = f_o \left[A\left(\frac{\varepsilon_c}{\varepsilon_0}\right) - (A-1)\left(\frac{\varepsilon_c}{\varepsilon_o}\right)^{\frac{A}{(A-1)}} \right] \quad \textbf{(3.46)}$$

$$E_{sec} = \frac{\sigma_c}{\varepsilon_c} (in\ MPa) \quad \textbf{(3.47)}$$

Descending (post-peak) part: for $\varepsilon_c > \varepsilon_o$

$$\sigma_c = f_o exp[-B(\varepsilon_c - \varepsilon_o)^C] \quad \textbf{(3.48)}$$

$$E_{sec} = -\frac{\sigma_c}{\varepsilon_c} (in\ MPa) \quad \textbf{(3.49)}$$

Where, σ_c and ε_c are the stress (MPa) and the corresponding strain of concrete at any point.

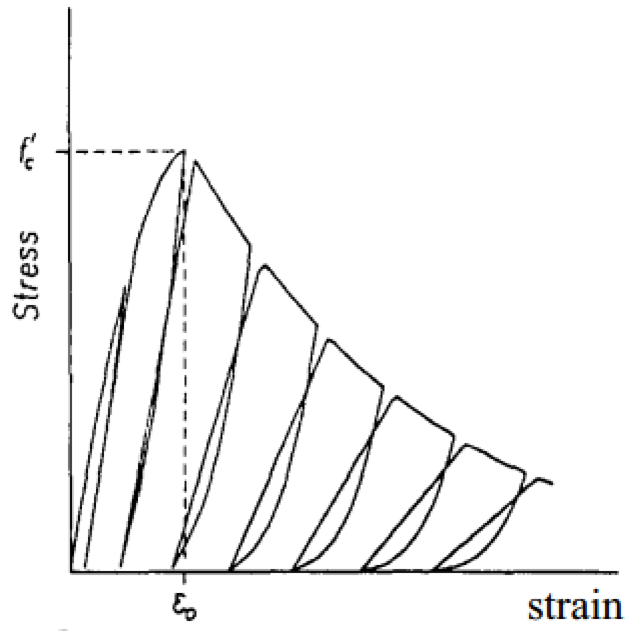

Figure 3-7: Uniaxial compression stress-strain relationships of concrete

3.4.1.1 Volumetric Ratio, ρ_s

Considering a square reinforced concrete column as shown in Fig.3.8, for single square hoops without crossties, the total cross-sectional area A_{sh} is defined as twice the area of a single hoop.

$$A_{sh} = 2\, A_{s,bar} \quad \textbf{(3.50)}$$

The volumetric transverse reinforcement ratio is defined as the volume of transverse reinforcement divided by the volume of the concrete core per spacing length.

$$\rho_{volume} = \frac{volume\ of\ transverse\ steel}{volume\ of\ concrete\ core} = \frac{C_{perimeter} \, . A_{s,bar}}{b_{core}. \, h_{core}. \, s} \quad \textbf{(3.51)}$$

Where, $C_{perimeter}$ is perimeter of tie, b_{core} and h_{core} are the concrete core dimensions measured to outside diameter of ties, and s is the center to center spacing of ties.

Expressing the volume of transverse steel as the steel area of the hoop multiplied by its perimeter $(2b_c + 2h_c)$ and the volume of concrete core as product of core width, b_c and height, h_c multiplied by the spacing leads to the following equation.

$$\rho_{Vol.} = \frac{2(b_c + h_c). A_{s,bar}}{b_c. h_c. s} \quad \textbf{(3.52)}$$

Considering only square column cross-sections, where core height and width are assumed to be equal, and then Eq. (3.52) is further simplified as follows.

$$\rho_{Vol.} = \frac{4h_c . A_{s,bar}}{h_c^2 . s} = \frac{4A_{s,bar}}{h_c . s} \quad \textbf{(3.53)}$$

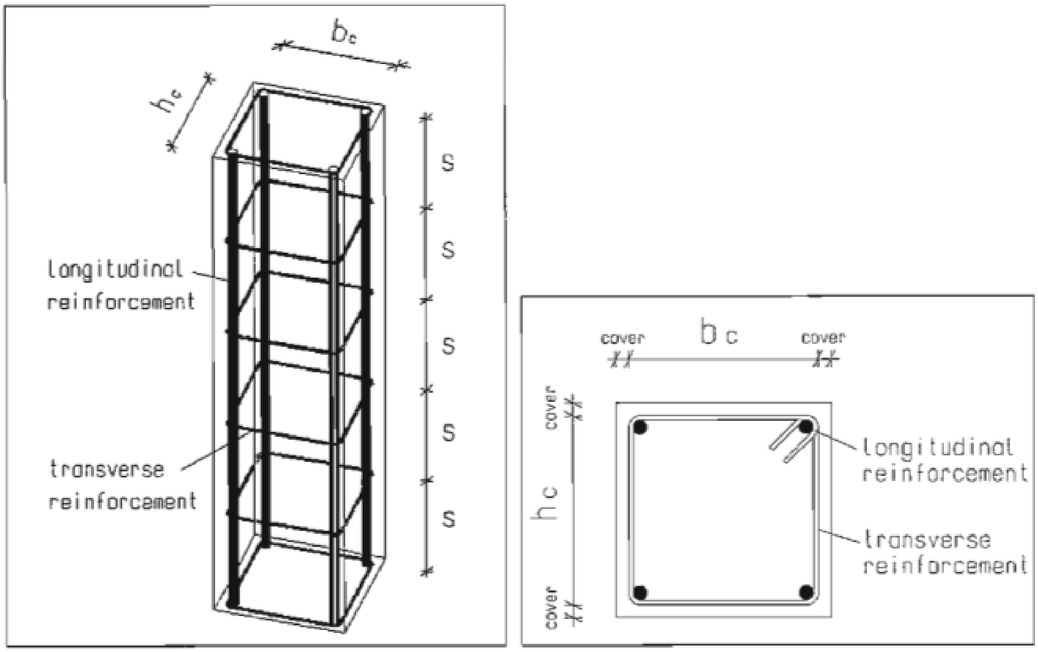

Figure 3-8: 3D View Cross-Section of a Square Column

3.4.1.2 Modulus of elasticity of concrete, E_c

For normal-weight concrete with a density of about 2300kg/m3, ACI 363-92 approximate the modulus of elasticity as:

$$E_c = 4500\sqrt{f_c'}(in\ MPa) \quad \textbf{(3.54)}$$

However, Eq. (3.54) ignore the type of aggregate that causes a significant error and this expression overestimates the modulus of elasticity for concretes with compressive strengths 41MPa and above. ACI Committee 363-92 proposed a correlation between the modulus of elasticity, E_c and the compressive strength f_c' for normal and high-strength compressive strength of concrete is expressed as follows:

$$E_c = 3320\sqrt{f_c'} + 6900\ (in\ MPa) \quad \textbf{(3.55)}$$

Therefore, in this study, equation (3.55) was used to analyse the column with the proposed analysis method and this equation can more accurately predict the modulus of elasticity, E_c according to the increase of compressive strength of concrete, f_c'.

3.4.2 Stress-Strain Relationship of Concrete under Tension

Even after the formation of cracks, it is possible for the tensile concrete to continue to carry some forces between the cracks. For concrete in tension, the stress-strain relationship including the tension stiffening effect as shown in Fig. 3.9 was used. The term ‘’tension stiffening’’ refers to the contribution of concrete between cracks to the overall stiffness of a member due to bond between concrete and steel reinforcement. In the present study, Cope *et al.* (1979) tension stiffening model is used to simulate the cracking of concrete and to describe the tension stiffening effect including the tension strain softening. A linear tensile stress-strain relationship is used with a slope of concrete modulus of elasticity,E_c until the concrete tensile principal stress, reaches the concrete tensile strength, f_t' corresponding to the cracked strain, ε_{cr}, and can be estimated from Eq. (3.56) and (3.57), respectively. The maximum tensile strain ε_{ut} which is $\alpha_1\varepsilon_{cr}$ as shown in Fig.3.9 can be determined by Eq. (3.58).

$$f_t' = -0.62\sqrt{f_c'}\ (in\ MPa) \quad \textbf{(3.56)}$$

$$\varepsilon_{cr} = \frac{f_t'}{E_c} \quad \textbf{(3.57)}$$

$$\varepsilon_{ut} = \alpha_1\varepsilon_{cr} = 10\ \varepsilon_{cr} \quad \textbf{(3.58)}$$

Ascending part: for $\varepsilon_{ct} \leq \varepsilon_{cr}$

$$\sigma_{ct} = f_t' \quad \textbf{(3.59)}$$

$$E_{sec} = E_c \quad \textbf{(3.60)}$$

Descending part-1: for $\varepsilon_{cr} < \varepsilon_{ct} < \alpha_1\varepsilon_{cr}$

$$\sigma_{ct} = \frac{\alpha_2\, f_t'\left(\alpha_1 - \frac{\varepsilon_{ct}}{\varepsilon_{cr}}\right)}{(\alpha_1 - 1)} \quad \textbf{(3.61)}$$

$$E_{sec} = \frac{\sigma_{ct}}{\varepsilon_{ct}} (in\ MPa) \qquad \textbf{(3.62)}$$

Descending part-2: for $\varepsilon_{ct} \geq \alpha_1 \varepsilon_{cr}$, the tensile stress becomes zero

$$\sigma_{ct} = 0, \quad E_{sec} = 0 \qquad \textbf{(3.63)}$$

Where, f_t' and ε_{cr} are the tensile strength of concrete in MPa and the corresponding cracking strain, ε_{cr}; ε_{ut} is the ultimate tensile strain of concrete., ε and σ strain and stress normal to the crack directions, and $\alpha_1 = 10$ and $\alpha_2 = 0.3$ are material constants. The parameters α_1 and α_2 are usually difficult to select in practice because of lack of experimental data for calibrating them. α_1 was chosen equal to 10 since this approximately represents a strain at which steel starts to yield. In this study, the unloading-reloading curve of concrete for tension was not taken in to account.

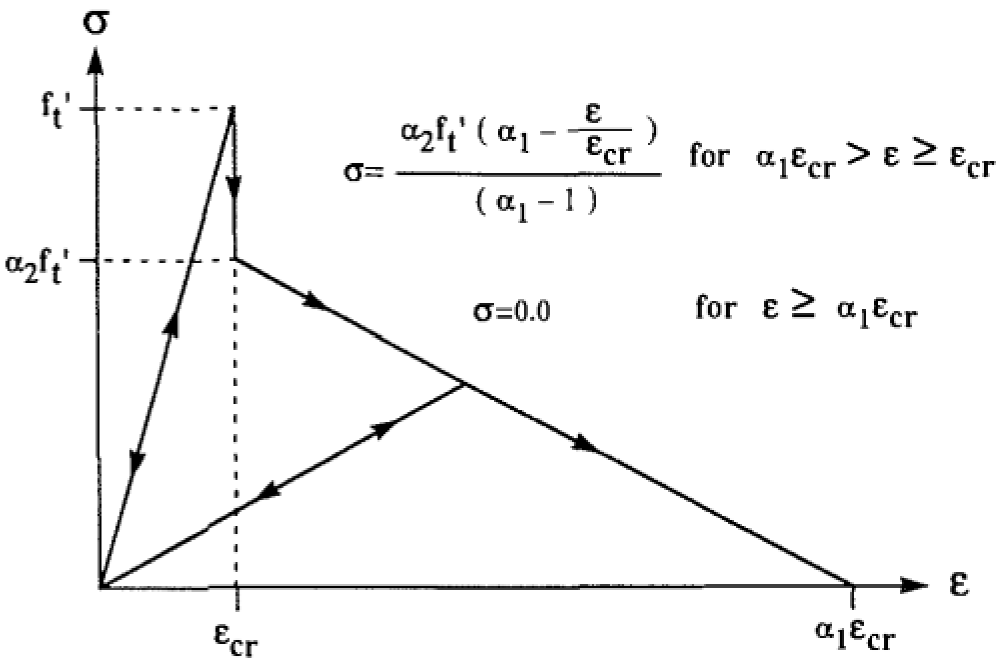

Figure 3-9: Tension stiffening model

3.4.3 Stress - Strain Relationship of Reinforcement Steel

For the reinforcing steel, an elastic-perfectly plastic stress-strain relationship identical in tension and compression as shown in Figure 3.10, is adopted in this analysis. The stress of the reinforcement below f_y shall be taken as E_s times steel strain. For strains greater than that corresponding to f_y, stress in reinforcement shall be considered independent of strain and equal to f_y. The secant modulus for the steel in tension or compression below the steel yield strain is equal to the modulus of elasticity, E_s, of the steel or the ratio of current stress to the current strain. However, the secant modulus beyond the yield strain will decrease with the strain attained.

Before yielding of steel reinforcement: for $\varepsilon_s \leq \varepsilon_{yd} = \frac{f_y}{E_s}$

$$\sigma_s = E_s \varepsilon_s, \qquad E_{sec} = \frac{\sigma_s}{\varepsilon_s} \tag{3.64}$$

After yielding of steel reinforcement: for $\varepsilon_s > \varepsilon_{yd} = \frac{f_y}{E_s}$

$$\sigma_s = f_y, \qquad E_{sec} = \frac{f_y}{\varepsilon_s} \tag{3.65}$$

Where, σ_s and ε_s are the stress in steel reinforcement and the corresponding strain, f_y and ε_y are the yield stress of reinforcing steel and the corresponding yield strain and E_s is elastic modulus of steel.

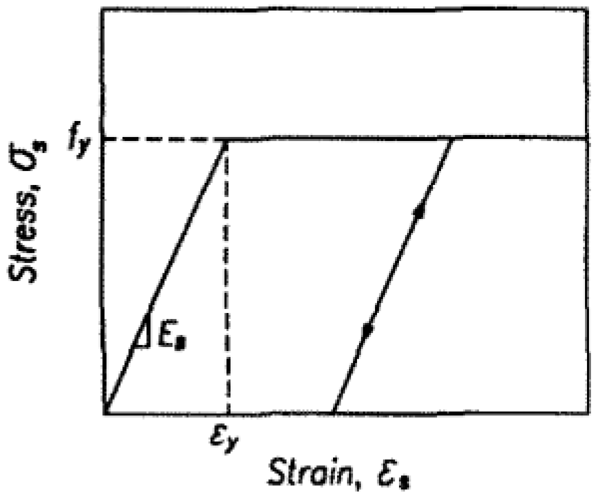

Figure 3-10: Stress-strain curve for reinforcing steel

3.5 Linear Elastic Analysis

This analysis provides an estimate of the nodal displacements and applied axial force that is required for the next iterative nonlinear second-order analysis. The procedures are states as follows:

Step-1: Insert the geometric and material parameters of the reinforced concrete column.

a) Geometry of the structure
- Square column cross section, $b = 80$mm and $h = 80$mm
- Lengths of column, $L = 240$mm, $L = 1440$mm and $L = 2400$mm

b) Material properties of the constituent materials

i. Concrete
- Cylinder compressive strength of concrete, $f_c' = 25.5$MPa, 63.5MPa and 86.2MPa
- Initial modulus of elasticity of concrete,$E_c = 3320\sqrt{f_c'}$+6900 (in MPa)
- Thickness of concrete cover from extreme concrete fiber to centroid of reinforcement, 15mm

ii. Reinforcing steel bar
- Yield strength of longitudinal steel reinforcement, $f_{yk} = 387$MPa
- Yield strength of ties, $f_{sy} = 250$MPa
- Modulus of elasticity of reinforcing steel, $E_s = 210$GPa
- Longitudinal reinforcement ratio $\rho_l = 1.98\%$ (4Ø6.35mm) and 3.98%(8Ø6.35mm)
- Area of longitudinal steel bars, $A_s = \rho bh = 1.98\% * (80 * 80) = 126.72\text{mm}^2$
- Diameter of longitudinal deformed steel bars-$\emptyset_l = 6.35$mm
- Diameter of plain steel bars for ties, Ø3mm
- Center to center spacing of ties is 60mm, but the spacing reduced to 30mm near support.

Step-2: Discretization of reinforced concrete column in to finite element

In this case, the column length is discretized in to ten finite elements and each cross-sectional node of the column is discretized in to four thousand ninety-six layers.

Step-3: Increment of the controlled axial displacement, U_c, (nodal point at which the value of the unknown is prescribed).

Step-4: Calculate the linear-elastic material section stiffness (axial stiffness,EA and flexural stiffness,EI) of each layer based on the initial material properties of concrete and steel reinforcement.

Step-5: Determine linear - elastic material stiffness matrix of each element, $[k_M]$ using Eq (3.29).

Note that, while calculating the linear-elastic material stiffness, k_M, the value of E at each layer is assumed to be held constant along the element length. This results the value of EA and EI for all nodal layered cross-sections of all elements are the same.

Step-6: Compute the nonlinear geometric stiffness matrix of each elements of the column, $[k_G]$ using Eq. (3.30).

Step-7: Develop the combination of linear-elastic material and geometric stiffness matrix of each element of the column. $[k] = [k_M] + [k_G]$

Step-8: Assemble the structural stiffness matrix of the column, $[K] = [K_M] + [K_G]$

Step-9: Assemble the element loads to give the global load vector.

Step-10: Construct the resultant simultaneous equilibrium equation based on the force-displacement relationship, $([K_M] + P[K_G])\{U\} = \{F\}$.

Step-11: Apply boundary conditions

The boundary conditions at the ends are pin support at the bottom end and roller support at the top end. This leads, axial and transverse displacements at the pin support and transverse displacement at the roller support are zero but the rotational displacements at both supports are differ from zero. Generally, the boundary conditions for simply supported columns are given by

$$\text{At } x = 0\text{: } u_i = 0,\ v_i = 0 \text{ and } \theta_i \neq 0$$

$$\text{At } x = L\text{: } v_j = 0 \text{ and } \theta_j \neq 0$$

For the particular case of a zero prescribed displacement value due to a pinned support, an alternative approach is to delete the row and column corresponding to the zero displacement from the equilibrium equation system. The column can be deleted since it always multiplies a zero quantity and the row is removed since it only relates to equilibrium at the supported node. Thus, according to the above boundary conditions, the resultant equilibrium simultaneous equation of the column is reduced by deleting the rows and columns corresponding to these zero displacements.

Step-12: Conversion into displacement control of the resultant simultaneous equilibrium equation Eq. (3.36) and obtain F_c and U_i except U_c. The assembled stiffness matrix of the column is modified by applying boundary conditions and the incremental controlled axial displacement.

Step-13: Solve the modified (conversion into displacement control) simultaneous equation using inverse of matrix to obtain new controlled axial force as a reaction, F_c corresponding to the controlled axial displacement and new nodal displacements of each element (axial displacements, lateral deflections and rotational displacements of the nodal cross sections),U_i except controlled displacement, U_c.

Step-14: Solve the original (load control) simultaneous equilibrium equations based on the latest nodal displacements in order to determine internal forces or all nodal forces (axial force, shear forces and bending moments) for each finite element.

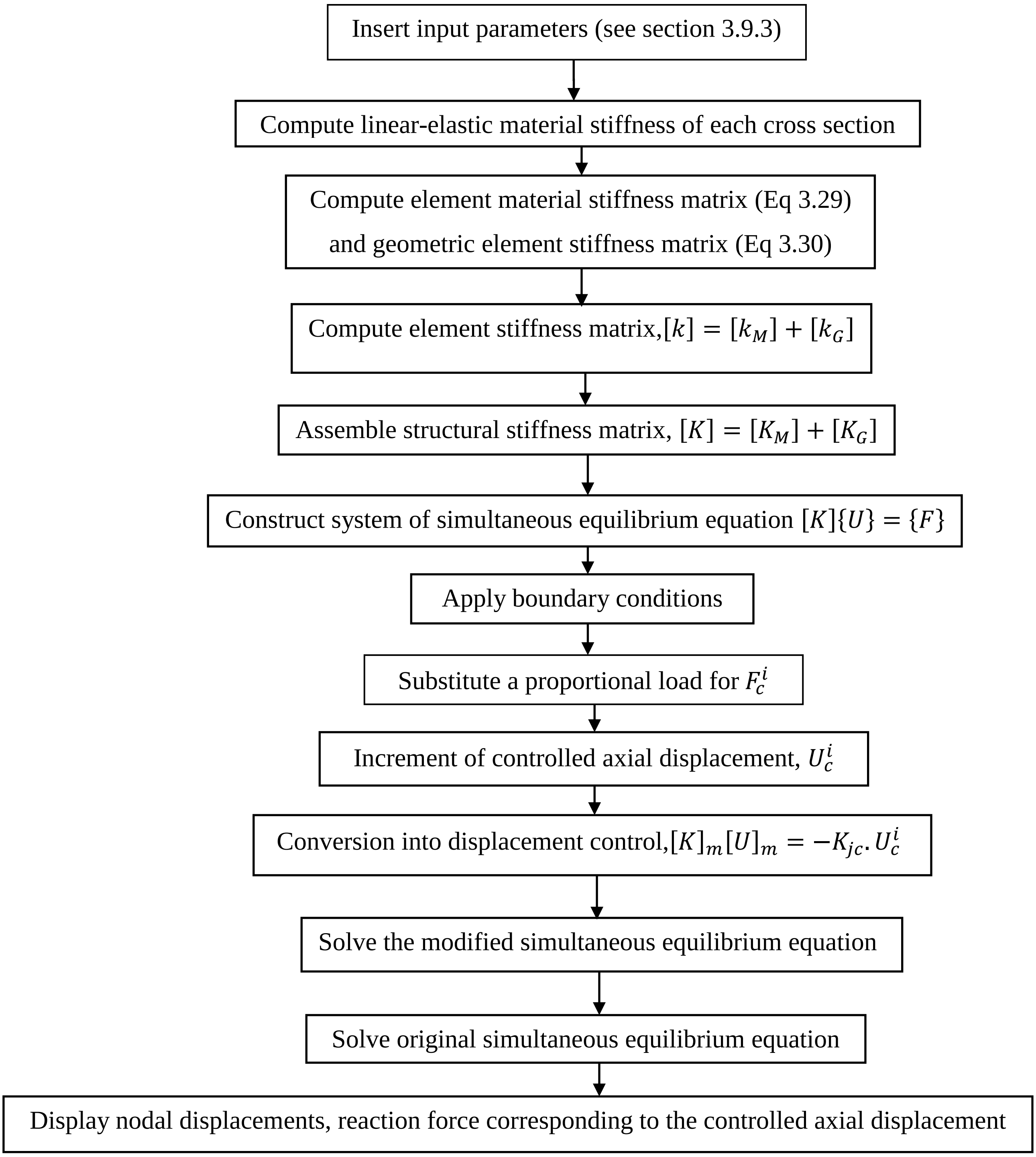

Figure 3-11: Linear-elastic analysis flow chart

3.6 Non-linear Second-Order Analysis

There are two types of second-order effects in slender reinforced concrete columns. The first is a linear second-order effect which takes into consideration the linear elastic material stiffness matrix and nonlinear geometric stiffness matrix. The second is a nonlinear second-order effect that takes into account both material and geometric nonlinearity and this type of second-order effect are studied in this paper. In modeling the nonlinear second-order analysis of the slender reinforced concrete column, the materially layered cross-section model and geometrically nonlinear finite element technique is used. This approach not only allows the nonlinear effect of the most highly stressed element to be taken into consideration but also includes the nonlinear effect of all the elements along the length of the column.

3.7 Member Stability ($\boldsymbol{P-\delta}$ Effect)

To account buckling or second-order $P-\delta$ effect of the slender column at the critical section, the additional eccentricity due to lateral deflection, δ_i obtained from the preceding iteration is added to the initial eccentricity of the applied axial load, $(e+\delta_{max})$ for the subsequent iteration. Hence, the maximum moment increases to $M=P(e+\delta_{max})$. In addition to this, the nonlinear geometric stiffness matrix was used, which ensured the inclusion of the second-order effect due to axial load-lateral deflection interaction with in the elements.

3.8 Structural Stability

The joint global coordinates are modified after each iteration to account for the current joint displaced position, that is, the previous deformed length of each column element gave to the current one. This reflects the load-displacement interaction of the structure. Since the element equilibrium matrix and the element stiffness matrix are functions of the current nodal displacements, the element stiffness matrix must be developed based on the current displaced coordinates of joints. This can be done using a while loop by giving the previous axial, transverse, and rotational nodal displacements to the current one at all nodes. Hence, the nonlinear structural stiffness matrix is repeatedly updated not only at every displacement increment but also for every cycle of iteration within the increment.

3.9 Non-linear Solution Algorithm

The objective of nonlinear finite element analysis is to trace the response of the structural model subjected to the given loading history. This is usually an incremental-iterative procedure. The load is applied in a number of steps (increments), and the structural response after each step is computed from the equilibrium equation (3.36). As these equations are nonlinear, they have to be solved by an iterative method. This means that inside the top-level loop of load incrementation, we have an iterative loop that restores equilibrium. The load control, displacement control, or various versions of the arc-length control are examples of step-size control techniques. There are four basic numerical iterative solution strategies for non-linear analysis, Owen and Hinton (1980). These are the direct iteration method (successive approximation), the Newton-Raphson method, the tangent stiffness method, and the initial stiffness method. In this study, the direct iteration method has been used and discussed briefly as follows.

3.9.1 Direct Iteration Method (Iterative Secant Stiffness Algorithm)

Among the basic nonlinear modeling approaches, the direct iteration method (iterative secant stiffness algorithm) was adopted to search for the nonlinear second-order analysis solution of the column. The displacement-controlled solution algorithm, (the increments of the load-point displacement,U_c, are prescribed and calculate the load, P, as a reaction at the point of prescribed displacement, U_c) was used to analyze the entire axial load-lateral deflection relationship including the post-peak softening behavior.

In this particular algorithm, there are two primary while loop phases are necessary. In the correcting phase (steps 2-14), the controlled displacement magnitude is kept constant and the solution iterates until convergence of the solution occurs. This while loop is referred to as iteration loop. In the advancing phase (steps 1-15), a controlled axial displacement increment is applied. That is, it utilizes a combination of incremental and iterative schemes. Here, the controlled axial displacement is applied incrementally, but after each increment successive iterations are performed. This phase is referred to displacement increment loop. In this method of nonlinear solution algorithm processes, the value of the unknown nodal displacements at all nodes and reaction at a node corresponding to the prescribed displacement determined during any iteration is the total value. Note that, nonzero reactions are obtained only for the nodal points at which the value of the unknown has been prescribed.

3.9.2 Numerical Algorithm Procedures

In order to develop the nonlinear second-order analysis program code in MatLabR2019a iterative secant stiffness algorithm has been used and the algorithm is briefly stated as follows.

Step-1: Apply incremental controlled axial displacement, U_c^i

Step-2: Calculate the total strains $\varepsilon(x, y)$ at the mid points of all layers in all nodal cross sections from the values obtained in the preceding iteration, for the subsequent iterations (from the values of element end nodal displacements at the end of the preceding displacement step for the first iteration) using strain-displacement relationship of the element.

Step-3: According to the nonlinear stress-strain relationship of the material constitutive law, calculate the total stress, σ from the strain,ε at the midpoints of all layers. The state of stress at the middle of a layer is taken as representative for the entire layer.

Step-4: Compute the secant modulus,E_{sec} using the updated strains and stresses values of each layer from the stress-strain curves. As the obtained secant modulus values for each layer of the cross-section are different then the corresponding secant stiffness are different. This allows to take variation of section stiffness not only at each layer of the cross-section but also along the length of the column which leads nonlinear material stiffness matrix.

Step-5: Determine section secant stiffness of each column element. Update the nonlinear material stiffness matrix using the latest section secant stiffness (secant axial stiffness, $E_{sec}A$, secant flexural stiffness, $E_{sec}I$ as well as secant combined axial and flexural stiffness, $E_{sec}R$) at the midpoint of each layer and sum up these gives stiffness of the section.

i. Secant axial stiffness

$$E_{sec}A = \int_A E_{sec} dA = \sum_i^n E_{seci}A_{ci} = \sum_i^{n_c} E_{seci}A_{ci} + \sum_j^{n_s} E_{secj}A_{sj} \qquad (3.66)$$

ii. Secant flexural stiffness

$$E_{sec}I = \int_A E_{sec} y^2 dA = \sum_{i=1}^{n} E_{seci}\, y_i^2 A_i + \sum_{i=1}^{n} E_{sec} I_o$$

$$= \sum_{i=1}^{n_{ci}} E_{seci} y_{ci}^2 A_{ci} + \sum_{i=1}^{n_{ci}} E_{seci} I_{ocj} + \sum_{j=1}^{n_{sj}} E_{seci} y_j^2 A_{sj} + \sum_{j=1}^{n_{sj}} E_{seci} I_{osj}$$

$$= \sum_{i=1}^{n_{ci}} E_{seci} y_{ci}^2 A_{ci} + \sum_{i=1}^{n_{ci}} E_{seci} \frac{1}{12} b_i t_i^3 + \sum_{j=1}^{n_{sj}} E_{seci} y_j^2 A_{sj} + \sum_{j=1}^{n_{sj}} E_{seci} \frac{\pi r^4}{4} \qquad (3.67)$$

iii. Secant combined axial and flexural stiffness

$$E_{sec}R = -\int_A E_{sec}ydA = -\sum_i^n E_{seci}y_iA_i$$

$$= -\sum_i^{n_c} E_{seci}y_{ci}A_{ci} - \sum_j^{n_s} E_{secj}y_{si}A_{sj} \tag{3.68}$$

Step-6: Compute element end forces (cross-sectional analysis)

Step-7: Based on current total displacements, update member geometry (update element length). The deformed length of each column element is determined as:

$$L = \sqrt{(L_0 + u_i)^2 + v_i^2} \tag{3.69}$$

Step-7: Compute nonlinear material stiffness matrix, k_{sec} of each element. In addition to this, the nonlinear geometric stiffness matrix, k_G,is updated based of the total applied axial force obtained in the previous iteration.

Step-8: Assemble the nonlinear material structural stiffness matrix and the non-linear geometric stiffness matrix.

Step-9: Construct the system of simultaneous equilibrium equations.

Step-10: Implement the boundary conditions, including the controlled displacement.

From the boundary condition of the column the prescribed displacement values are as follows:

For pin support at node-1: $(at\ x = 0) \rightarrow u_1 = 0, v_1 = 0$ and $\theta_1 \neq 0$

For roller support at node-11: $(at\ x = L) \rightarrow v_{11} = 0$ and $\theta_{11} \neq 0$

For the controlled axial displacement at the roller support (at node-11): U_c

Step-11: Substitute the proportional constants for F_c^i

In this case the proportional constant for the applied axial forces are one, initial eccentricity plus additional lateral deflection (at the i^{th} iteration, $e_i = e_o + \delta_i$) for the uniaxial bending moment, whereas the proportional constant for shear force is zero as there is no lateral force.

Step-12: Modify or adjust the assembled nonlinear structural stiffness matrix using conversion into displacement control by applying boundary conditions and incremental controlled axial displacement.

Step-13: Solve the adjusted (converted into displacement control) simultaneous equation using eq. (3.36) to obtain new total applied axial force, F_c^i as a reaction corresponding to the controlled axial displacement and new nodal displacements of each element, $U^{(i+1)}$ (axial displacement, transverse displacement and bending rotation of the nodal cross sections).

$$K_{sec}^{(i)} U^{(i+1)} = -K_{ic}^{(i)}.U_c^{(i+1)} \rightarrow U^{(i+1)} = \left[K_{sec}^{(i)}\right]^{-1} \left(-K_{ic}^{(i)} U_c^{(i+1)}\right) \tag{3.70}$$

Where, $K_{sec}^{(i)}$ is secant structural stiffness matrix and $K_{ic}^{(i)}.U_c^{(i+1)}$ is adjusted or modified nodal loads of the column. $U^{(i+1)}$ is nodal displacements corresponding to the adjusted nodal loads and the superscript $(i+1)$ indicates the $(i+1)^{th}$ iteration.

Step-14: Check convergence

It can be expensive to check the decay of displacements for every degree of freedom and therefore, some overall evaluation is performed and normally norms are used for this purpose. In this paper, a global convergence check is employed rather than such a local one. Compare the current displacements with the preceding iteration to check the specified convergence criterion. When the previous and current nodal displacements satisfy the convergence criteria, select one point on the axial force versus lateral deflection relation of the column. Repeating this procedure for successive incremental controlled axial displacement would lead the entire curve of axial force-lateral deflection relationship up to the ultimate load and post-peak behavior of the columns.

The following convergence criterion is used:

$$\left| \frac{\sum_{i=1}^{N} (U_i^r)^2}{\sum_{i=1}^{N} \left(U_i^{r-1}\right)^2} - 1 \right| * 100\% \leq t \tag{3.71}$$

Where, N denotes the total number of nodal points in the problem extends over all degrees of freedom i and r and $r-1$ denote successive iterations and t is chosen tolerance, typically 1%. Eq.(3.71) states that convergence is assumed to have occurred if the ratio in the norm of the unknowns between two successive iterations minus one is less than or equal to tolerance.

If the criterion is not met, return to step-2 and loop on iterations by keeping the magnitude of the prescribed increments of controlled axial displacement, U_c constant until converged.

Step-15: Calculate load P as the reaction at the point of prescribed displacement, U_c. Determine the internal forces (axial force and bending moment) for each finite element.

Return to step 1 and start the next incremental controlled axial displacement. If all displacement increments have been applied stop the process.

Fig.3.12 shows the algorithm for the proposed numerical analysis model.

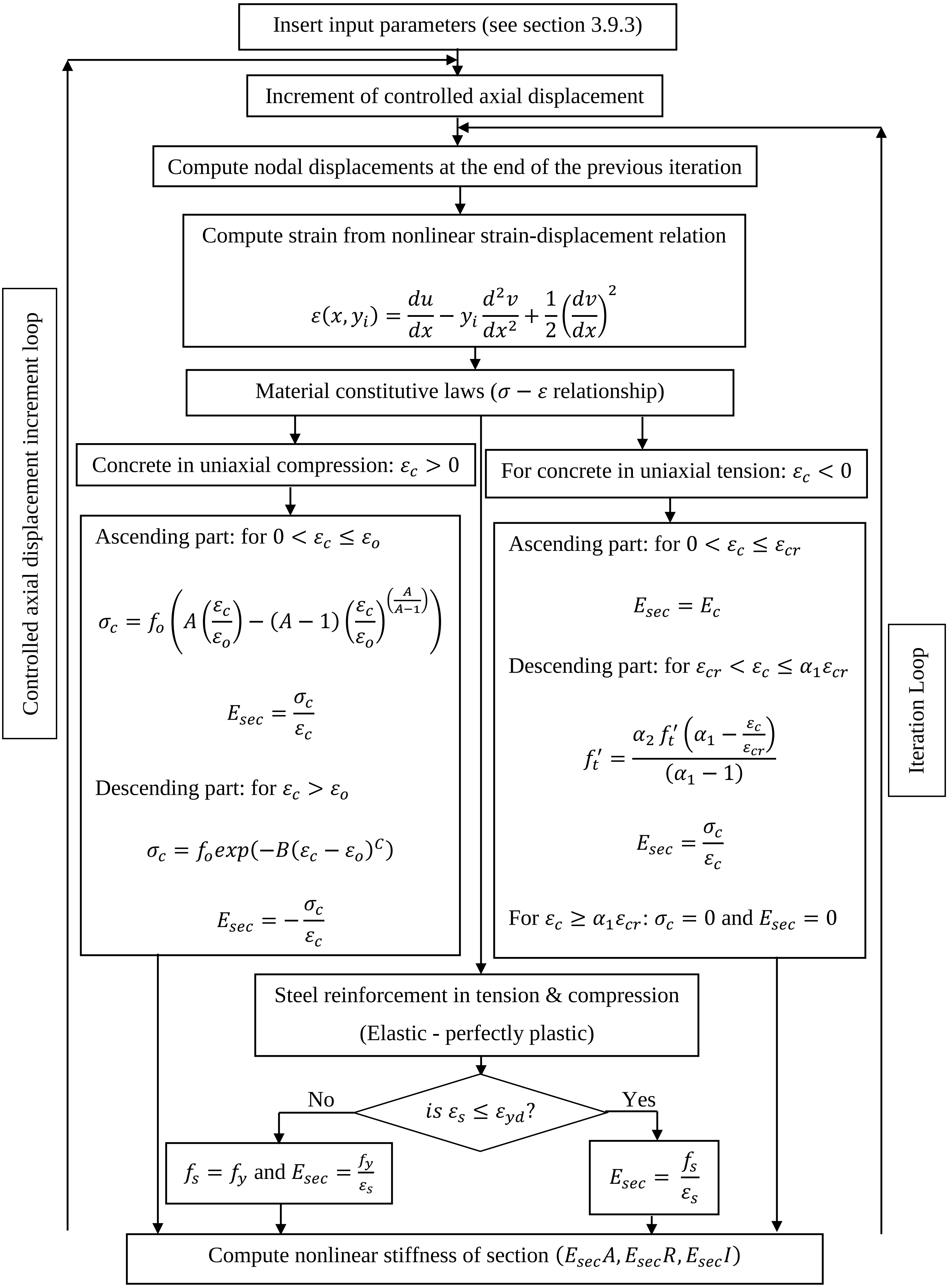
Insert input parameters (see section 3.9.3)
Increment of controlled axial displacement
Compute nodal displacements at the end of the previous iteration
Compute strain from nonlinear strain-displacement relation
$\varepsilon(x, y_i) = \frac{du}{dx} - y_i \frac{d^2v}{dx^2} + \frac{1}{2}\left(\frac{dv}{dx}\right)^2$
Material constitutive laws ($\sigma - \varepsilon$ relationship)
Concrete in uniaxial compression: $\varepsilon_c > 0$
Ascending part: for $0 < \varepsilon_c \leq \varepsilon_o$
$\sigma_c = f_o\left(A\left(\frac{\varepsilon_c}{\varepsilon_o}\right) - (A-1)\left(\frac{\varepsilon_c}{\varepsilon_o}\right)^{\left(\frac{A}{A-1}\right)}\right)$
$E_{sec} = \frac{\sigma_c}{\varepsilon_c}$
Descending part: for $\varepsilon_c > \varepsilon_o$
$\sigma_c = f_o exp(-B(\varepsilon_c - \varepsilon_o)^C)$
$E_{sec} = -\frac{\sigma_c}{\varepsilon_c}$
For concrete in uniaxial tension: $\varepsilon_c < 0$
Ascending part: for $0 < \varepsilon_c \leq \varepsilon_{cr}$
$E_{sec} = E_c$
Descending part: for $\varepsilon_{cr} < \varepsilon_c \leq \alpha_1 \varepsilon_{cr}$
$f_t' = \frac{\alpha_2 f_t'\left(\alpha_1 - \frac{\varepsilon_c}{\varepsilon_{cr}}\right)}{(\alpha_1 - 1)}$
$E_{sec} = \frac{\sigma_c}{\varepsilon_c}$
For $\varepsilon_c \geq \alpha_1 \varepsilon_{cr}$: $\sigma_c = 0$ and $E_{sec} = 0$
Steel reinforcement in tension & compression
(Elastic - perfectly plastic)
No
$is\ \varepsilon_s \leq \varepsilon_{yd}?$
Yes
$f_s = f_y$ and $E_{sec} = \frac{f_y}{\varepsilon_s}$
$E_{sec} = \frac{f_s}{\varepsilon_s}$
Compute nonlinear stiffness of section ($E_{sec}A, E_{sec}R, E_{sec}I$)
Controlled axial displacement increment loop
Iteration Loop

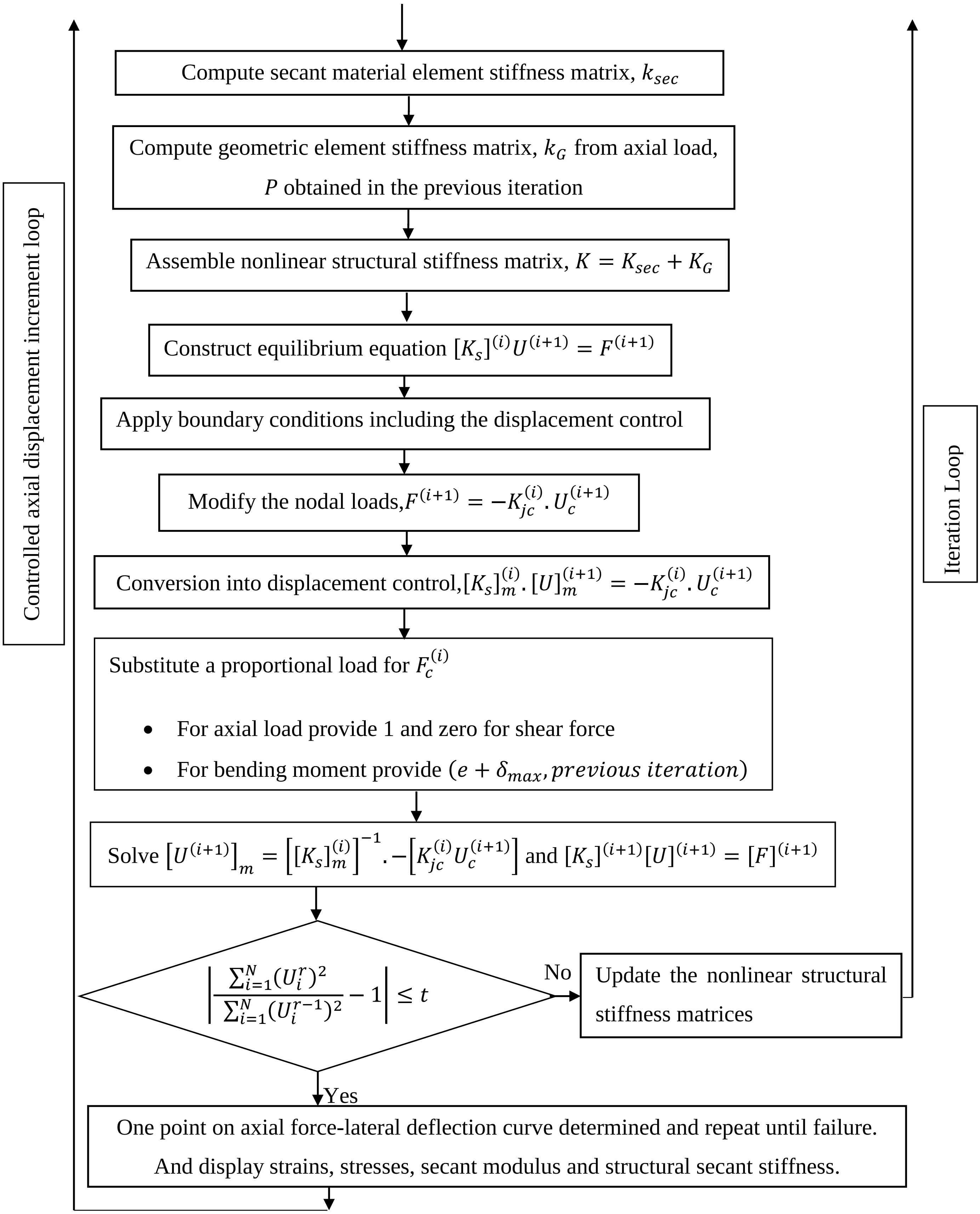

Figure 3-12: Iterative secant stiffness algorithm

In which a superscript i indicate the iteration number.

3.9.3 Input Parameters and Incremental Controlled Axial Displacement

To study the influence of numerous parameters on the structural response of the column the following input parameters were used.

Input parameters 1: Material and geometric properties

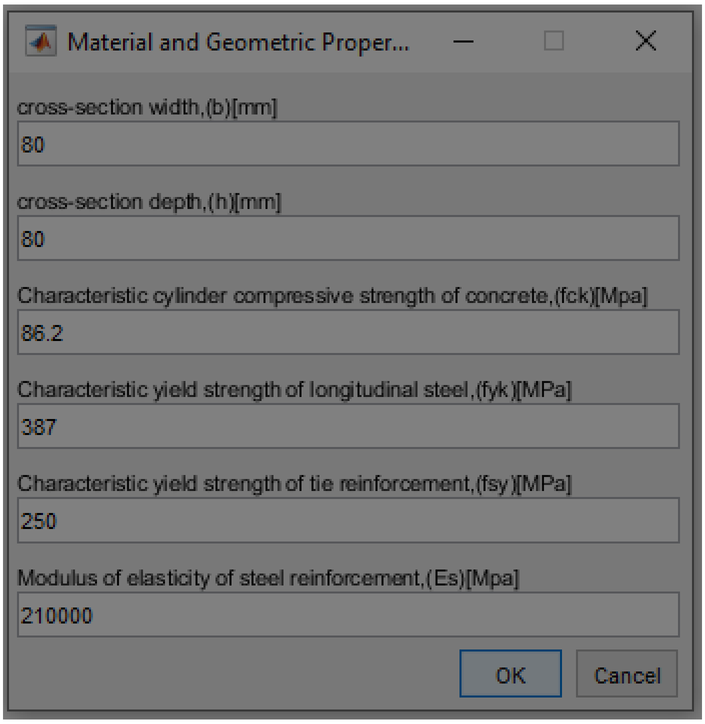

Input parameters 2: Detail of steel reinforcement

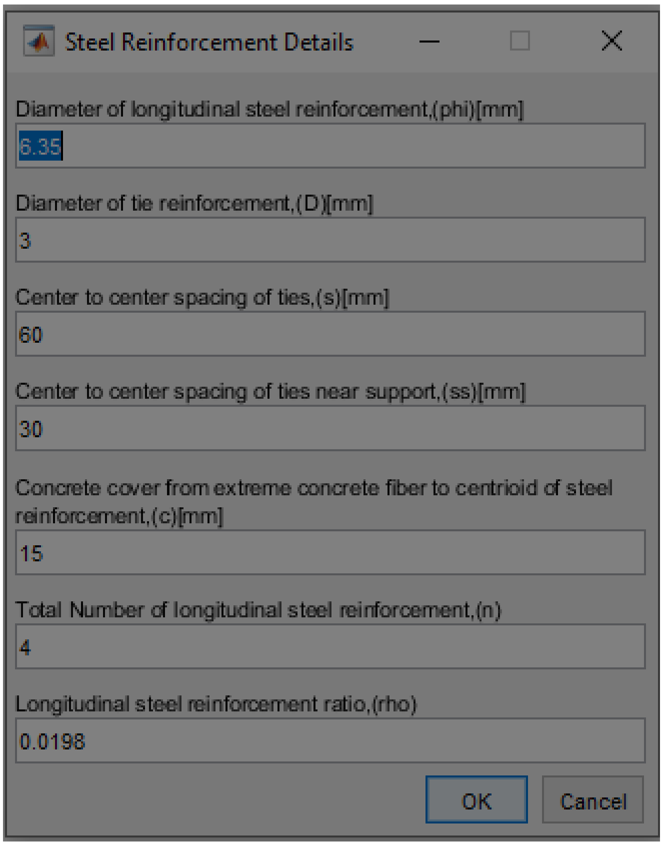

Input parameters 3: Mesh size, layer size and controlled axial displacement

This input consists of length of column, discretization of reinforced concrete column (total number of elements along the length of the column and total number of layers on the cross-section), initial eccentricity of the applied axial load, controlled axial displacement (initial incremental, incremental step-size and final incremental).

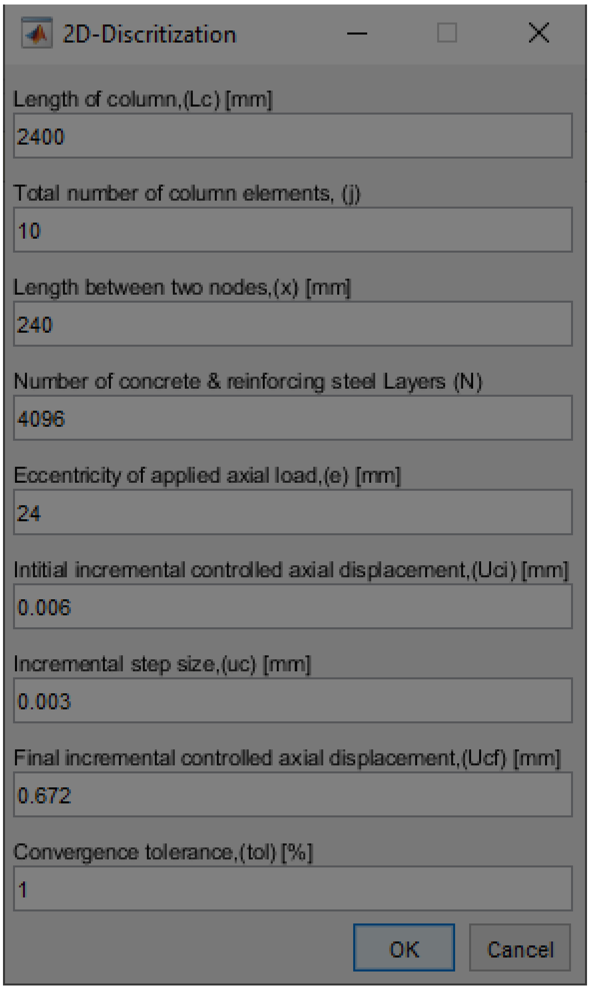

The output, which can be requested for each displacement increment and each iteration, consists of the following:

i. Element nodal displacements (axial displacement, transverse displacement and rotational displacement) and load P as the reaction at the controlled displacement.
ii. The transverse displacements are the lateral deflection of the column having maximum lateral deflection at the mid-height of the column.
iii. Strain, stress and secant stiffness of each concrete and reinforcing steel layers.
iv. The entire axial load-lateral deflection curve data points.

Table 3.1 shows the number of elements, number of layers, incremental controlled axial displacement and incremental controlled axial displacement step size of each column that have been used in this numerical analysis.

Table 3-1: Mesh size, layer size and controlled displacement step size

Specimen	$f_c'(MPa)$	λ	$\rho(\%)$	Number of Elements, j (Mesh size)	Number of Layers, N (Layer size)	Incremental axial displacement, U_{ci} (mm)	Incremental step size, u_c (mm)
For Kim and Yang (1995)							
10L2	25.5	10	1.98	10	4096	0.003 to 0.4	0.003
10L4		10	3.95	10	4096	0.003 to 0.4	0.003
60L2		60	1.98	10	4096	0.003 to 1.2	0.003
100L2		100	1.98	10	4096	0.003 to 0.927	0.003
100L4		100	3.95	10	4096	0.003 to 1.111	0.003
10M2	63.5	10	1.98	10	4096	0.003 to 0.4	0.003
10M4		10	3.95	10	4096	0.003 to 0.4	0.003
60M2		60	1.98	10	4096	0.003 to 0.927	0.003
100M2		100	1.98	10	4096	0.003 to 0.684	0.003
100M4		100	3.95	10	4096	0.003 to 0.906	0.003
10H2	86.2	10	1.98	10	4096	0.003 to 0.4	0.003
10H4		10	3.95	10	4096	0.003 to 0.4	0.003
60H2		60	1.98	10	4096	0.003 to 0.927	0.003
100H2		100	1.98	10	4096	0.003 to 0.672	0.003
100H4		100	3.95	10	4096	0.003 to 0.75	0.003
For Lloyd and Rangan (1996)							
IA	58	32	2.2	10	4096	0.03 to 4	0.03
IB			2.2	10	4096	0.03 to 2	0.03
IC			2.2	10	4096	0.03 to 2	0.03
IIIA			1.4	10	4096	0.03 to 4	0.03
IIIB			1.4	10	4096	0.03 to 2	0.03
IIIC			1.4	10	4096	0.03 to 1.7	0.03
VA	92		2.2	10	4096	0.03 to 4	0.03
VB			2.2	10	4096	0.03 to 1.8	0.03
VC			2.2	10	4096	0.03 to 1.7	0.03
VIIA			1.4	10	4096	0.03 to 4	0.03
VIIB			1.4	10	4096	0.03 to 1.8	0.03
VIIC			1.4	10	4096	0.03 to 1.5	0.03
XIA	97.2		1.4	10	4096	0.03 to 4	0.03
XIB			1.4	10	4096	0.03 to 1.8	0.03
XIAC			1.4	10	4096	0.03 to 1.5	0.03

CHAPTER 4 RESULTS AND DISCUSSIONS

In this chapter, the deflected curve, axial load-lateral deflection response, and axial load-bending moment relation of reinforced concrete columns subjected to axial load and uniaxial bending moment are discussed. To check the validity of the predicted numerical analysis result, the results obtained from the MATLAB R2019a program were qualitatively and quantitatively compared with available laboratory experimental results conducted by Kim and Yang (1995). However, due to lack of detail qualitative test data, only quantitative experimental results were compared with Lloyd and Rangan (1996).

4.1 Inelastic Deflected Curve of Reinforced Concrete Columns

There has been a lot of research for the nonlinear analysis of slender reinforced concrete columns by adopting analytical methods which assume the deflection curve of a column as a cosine wave or sine wave and then solve the governing differential equations for a column. However, as the load is increased beyond the elastic limit, the post peak deflected response of the reinforced concrete column gradually differs from the deflection curve which is assumed in the analytical method. To overcome these short comings of the analytical methods, the geometrically nonlinear finite element codes and materially layered cross-section model was adopted in this study. Figure.4.1 shows that, the curvature distribution of the reinforced concrete column subjected to axial load and equal and opposite end uniaxial bending moment. The buckled curve follows the elastic half-sine wave and has a sinusoidal deflected shape until the ultimate load is reached. Moreover, the numerical solution by finite element show that the distribution of curvature during the loading process varies and the optimum approximation of the deflection curve by a sine curve requires varying the wavelength. However, the curvature creates a more pointed, sharp deflected curve at mid-height than a sine curve from the starting or imminent point of instability i.e., at $P = P_u$. This is due to material nonlinearity as a result of quick deterioration of its material stiffness particularly the flexural stiffness at the mid-height of the column cross-section and geometric nonlinearity because of axial load-lateral deflection interaction within the elements as well as from the rapidly increasing lateral deflection slightly above the critical load. Therefore, the application of the analytical method is almost impossible when the columns are a part of a complex structure.

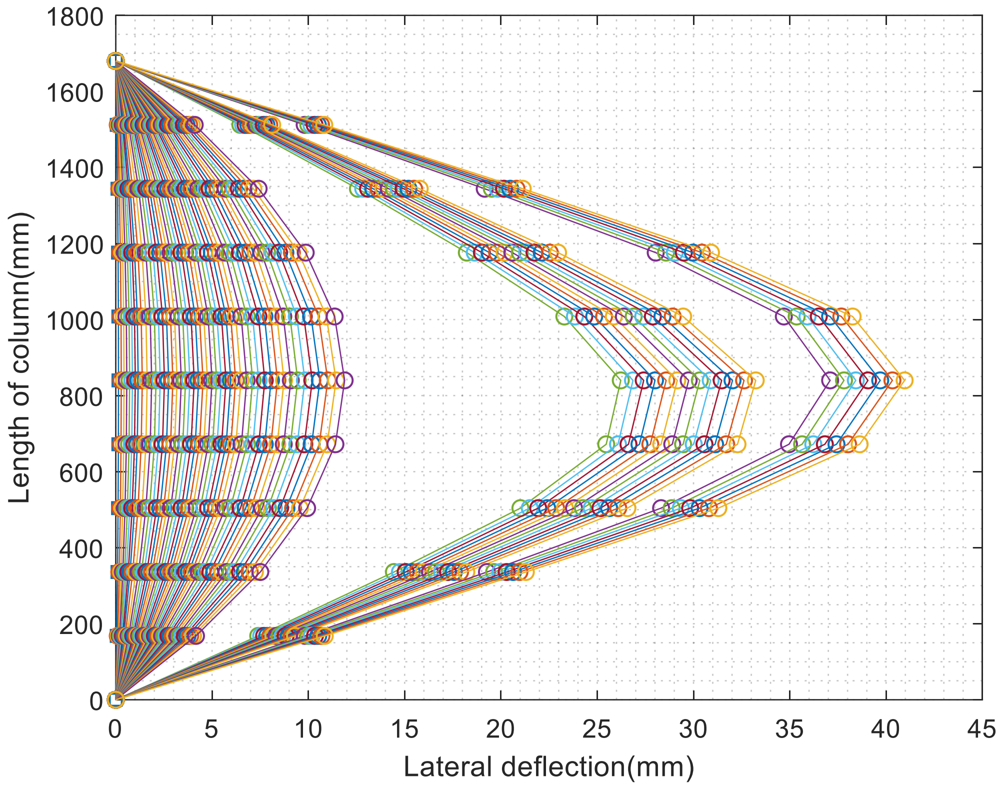

Figure 4-1: Inelastic deflected curve of short and slender reinforced concrete column

Each curve represents deflected shape of the column for each controlled axial displacement applied at the roller support of the column. The first group are elastic half sine curves for incrementally applied controlled axial displacement from 0.03mm to 1.41mm. At the end of this group the load is reached at ultimate load ($P = P_u$) and it requires 47 number of incremental controlled axial displacement and 134 number of iterations. The second and third groups are the post peak more pointed sharp deflected curves for the applied controlled axial displacement from 1.44mm to 1.8mm and from 1.83mm to 2.28mm, respectively with 0.03mm step size.

Table 4-1: Description of elastic and inelastic deflected curves

Group of curves	Incremental controlled axial displacement	Step size of the controlled displacement	Number of increments	Number of iteration
First group	0.06mm to 1.41mm	0.03mm	47	134
Second group	1.44mm to 1.8mm	0.03mm	12	49
Third group	1.83mm to 2.04mm	0.03mm	7	12
		Total	66	195

4.2 Axial Force-Lateral Deflection Responses

In this section, the results obtained in the numerical simulations using the proposed methodology are compared with the experimental test results obtained from Kim and Yang (1995) and Lloyd and Rangan (1996). The structural axial force-lateral deflection nonlinear responses of short and slender reinforced concrete columns for different compressive strength of concrete are shown from Fig. 4.2 to 4.6. Table 4.2 shows the lateral deflections at ultimate axial loads.

As shown from Fig.4.2 to 4.6, the axial load-lateral deflection curves have two ranges, stable and unstable ranges. The ascending portion of the curves are considered to be in stable equilibrium because the load-point displacement curve is rising. Whereas the descending portion of the curves is strain softening range which shows unstable equilibrium (instability of the column) because the axial force decrease with increasing lateral deflection to attain equilibrium. This post-peak strain softening behavior is due to the heterogeneity and brittleness of concrete and it is a decrease of uniaxial stress at increasing strain or a situation where the secant stiffness matrix stops to be positive definite. In addition to this, that instability mode represents strain localization into a layer of the smallest possible thickness.

Unloading takes place at points adjacent to a strain-softening zone in medium slender reinforced concrete columns, λ=60 for medium and high strength concrete. Even the column is loaded under monotonically increasing controlled displacement, the unloading typically occurs as the neutral axis moves into the previously compressed portion of the cross-section. This leads to happen snapback behavior. This effect, however, is seen to be negligible, at least up to the peak point of the column response. The reason is that the loading-unloading reversal occurs near the neutral axis where stress has little effect on bending moment. Further, it occurs at low strain levels at which the stress-strain diagram for loading is close to that for unloading. Since the unloading may occur after previous inelastic deformations within various portions of the layered cross-section, the current strain value in the centroid of each layer has to be compared with the strain value at the previous load level, and if unloading is noticed, then the proper stress-strain curve for unloading should be considered for that layer. That is, let ε_{max} be the maximum strains and ε_{min} be the minimum strains achieved in every layer and every nodal cross-section at the end of the particular incremental controlled displacement. Moreover, ε be the strains at the midpoints of all layers in all nodal cross-section from the values of nodal displacements at the end of the particular incremental controlled displacement, for the first iteration or from the values obtained in the preceding iteration, for the subsequent iterations. Thus, unloading condition occur when $\varepsilon > \varepsilon_{max}$ for tension and $\varepsilon < \varepsilon_{min}$ for compression. To overcome this, unloading-reloading stress-strain curves of concrete for compression and tension must be used.

4.2.1 Short and Slender Reinforced Concrete Columns

The numerical results have been verified against the experimental test results obtained from Kim and Yang (1995) in terms of axial force versus lateral deflection response. This section presents the result obtained in the numerical simulations of the short reinforced concrete columns, $\lambda = 10$, medium slender reinforced concrete columns, $\lambda = 60$ and high slender reinforced concrete columns, $\lambda = 100$ with normal compressive strength of concrete, f_c'=25.5MPa, medium compressive strength of concrete, f_c'= 63.5MPa, high compressive strength of concrete, f_c'=86.2MPa and reinforcement steel ratio ρ=1.98% for corner steel reinforcements with 4Ø6.35mm and ρ=3.95% with 8Ø6.35mm for uniform steel reinforcement.

The structural curves shown in Figure 4.2, show that for short reinforced concrete columns with a slenderness ratio of λ=10, as the compressive strength of concrete increases, the ultimate axial loads increase with a little increase of the corresponding lateral deflection. As lateral deflections are insignificant in these columns, small lateral deflection is presented. The experimental result of Kim and Yang (1995) reported that, specimen 10L2-1 failed during the initial stage of loading and test results were not obtained. Again, specimen 10L2-2 also failed during the experiment which explains the relatively small ultimate load. Moreover, these specimens failed at their ends by compression of the heads, which indicates an imperfect compaction at ends during casting and that is why overestimated ultimate load obtained in the present numerical analysis as compare to the test result.

The structural response of medium slender, λ = 60 and high slender, λ = 100 reinforced concrete columns as shown in Figures 4.3 and 4.4, respectively indicates as the compressive strength of concrete increases, the ultimate load increases with an increase of lateral deflection. Table 4.2 shows, the analysis slightly underestimated the latera deflections at ultimate response due to an overestimation of the tension-stiffening effect.

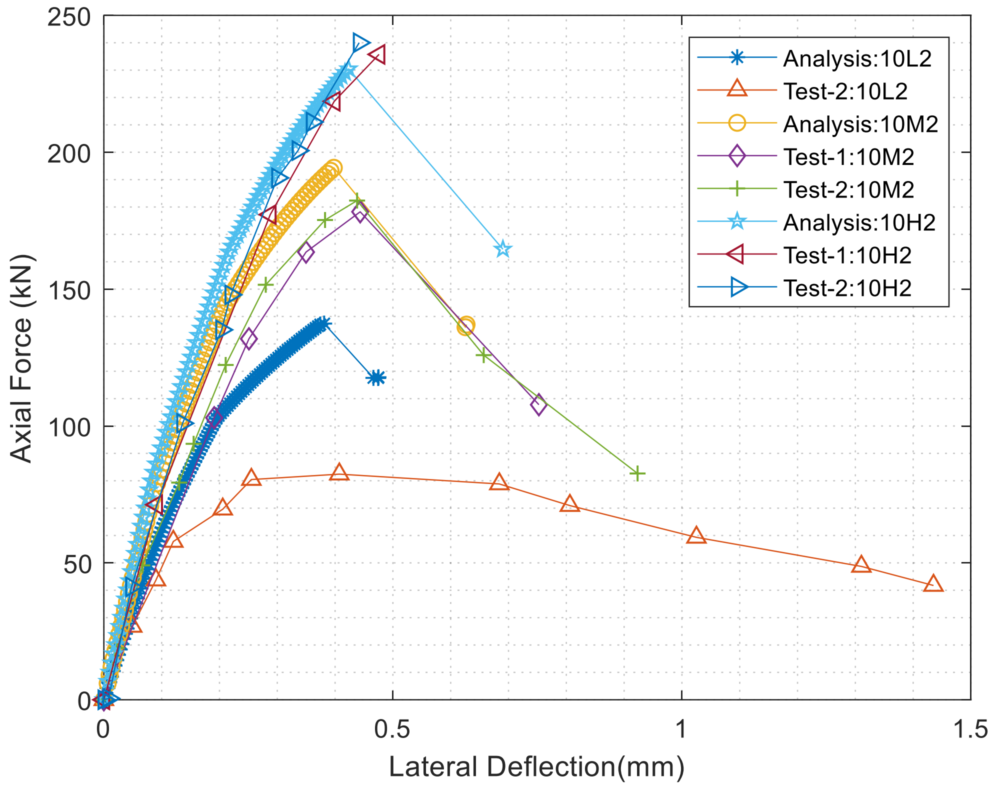

Figure 4-2: Axial force-deflection relation for λ = 10 & ρ = 1.98%

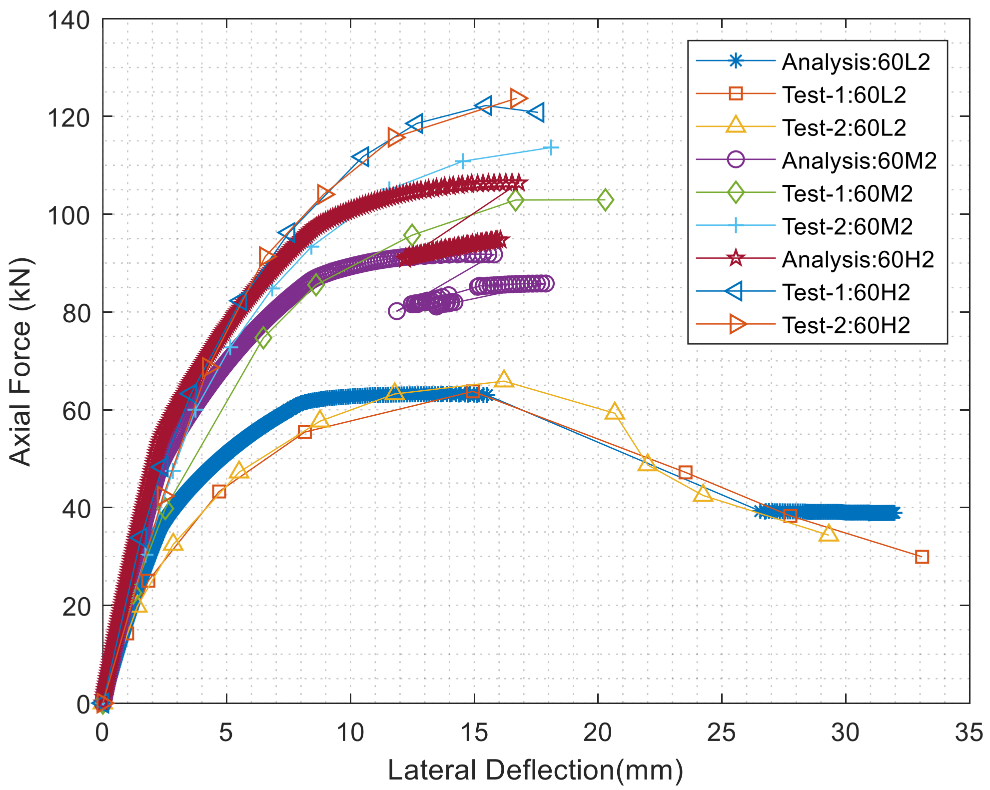

Figure 4-3: Axial force-lateral deflection relation for λ = 60 & ρ = 1.98%

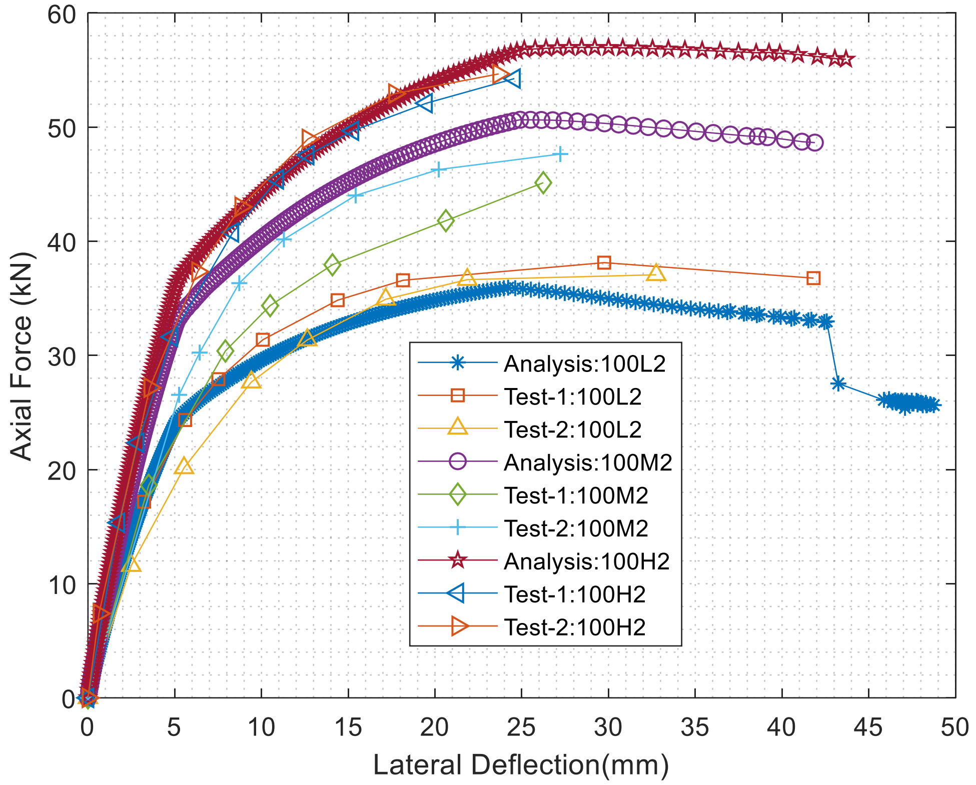

Figure 4-4: Axial force-lateral deflection relation for λ = 100 & ρ = 1.98%

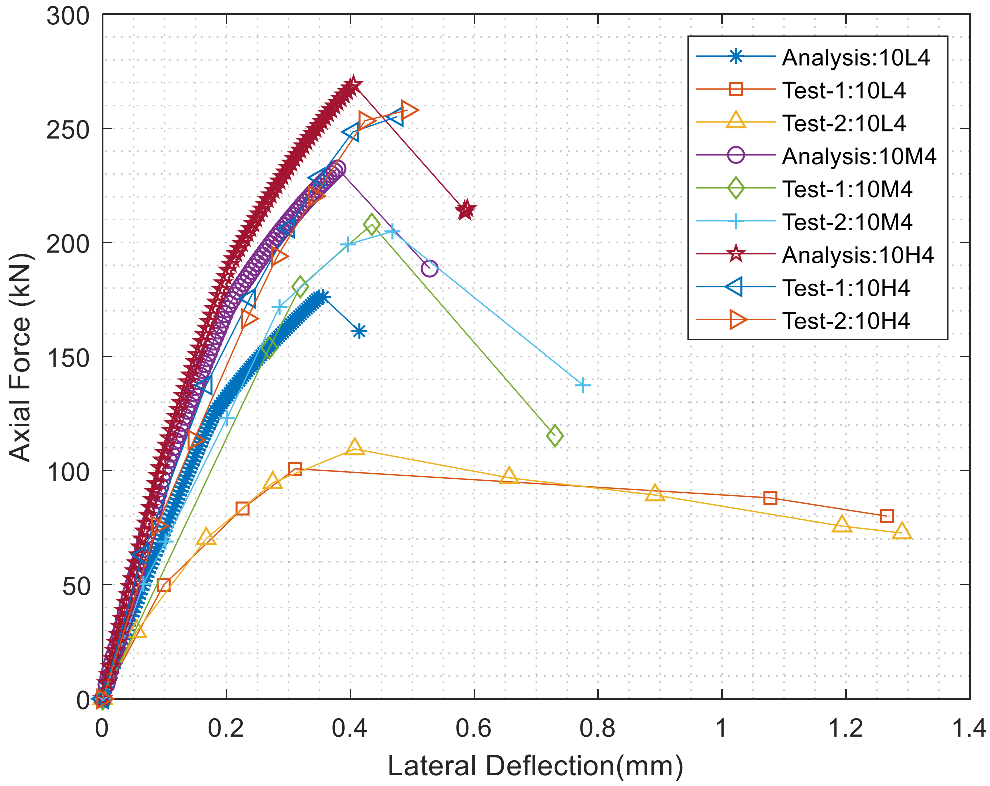

Figure 4-5: Axial force-lateral deflection relation for λ =10 and ρ=3.95%

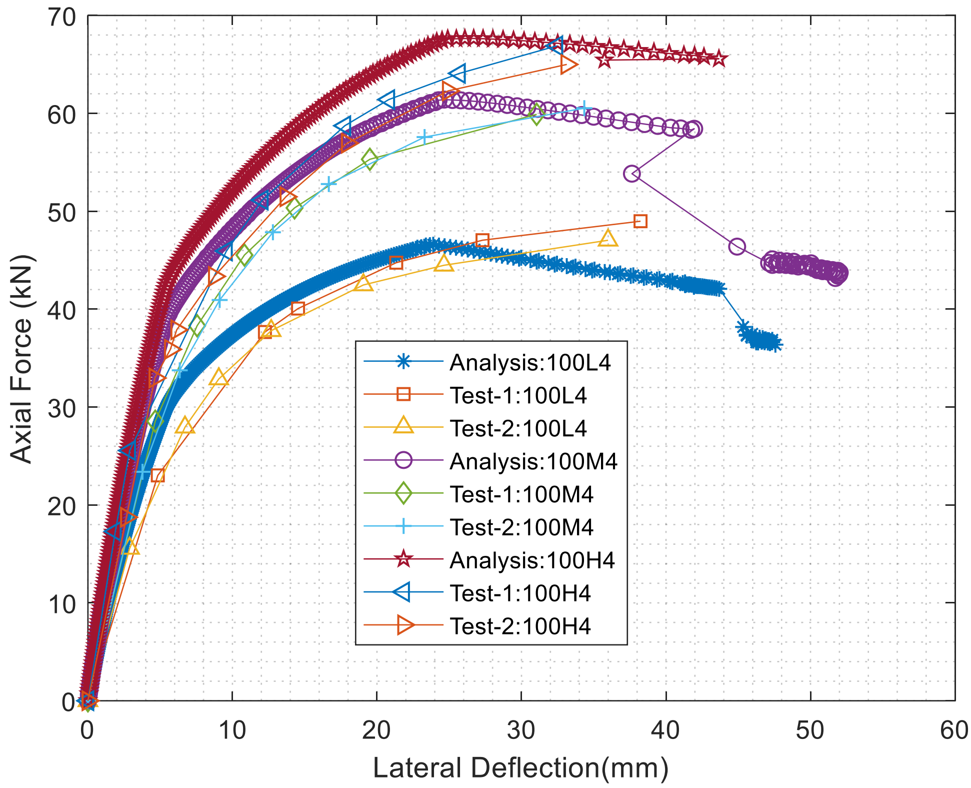

Figure 4-6: Axial force-lateral deflection relation for λ=100 and ρ=3.95%

4.3 Ultimate Axial Load

The last column of Table 4.2 shows the analytic to ultimate load ratios. Considering the percentage error in each result, the mean value and standard deviation of the whole specimens, it can be noted that the results obtained with the numerical analysis are in very good agreement with the experimental results of Kim and Yang (1995)

4.3.1 Effect of Compressive Strength of Concrete

As shown in Table 4.2, for constant longitudinal reinforcement steel ratio and slenderness ratio, the ultimate load of the column increases as the compressive strength of concrete increases. For short reinforced concrete columns, the ultimate load of high-strength concrete columns is significantly increased compared to normal-strength concrete columns. However, for very slender reinforced concrete columns, it does not increase significantly when compared to the case of the short reinforced concrete columns. In other words, when the compressive strength of concrete is increased from 25.5MPa to 86.2MPa, the ultimate load for the high strength concrete column with ρ = 1.98% is increased by 67.7% in the case of λ=10 but it is increased by 58.78% in the case of λ=100. Moreover, when the longitudinal steel reinforcement ratio is ρ=3.95% this value is 53.08% for λ=10 and 45.24% for λ=100. This indicates that the increment of the ultimate load due to the increase of concrete compressive strength is decreased with the increase in the slenderness ratio. This is because in short column, failure only occur when the stress of concrete, σ_c reaches the maximum compressive strength of concretef_c', which is by crushing of concrete (material failure) at the section of maximum moment. Whereas, in the case of a very slender column, failure occurs before reaching its compressive strength of concrete, f_c' and the strain in the compression face of concrete is not only axial strain but also strain produced by bending or curvature and nonlinear part of axial strain. In addition to this, since the stress-strain relation of concrete represents more brittle behavior as the compressive strength increases, a slender high strength concrete column has a relatively small energy absorption capacity when it is subjected to large lateral deflection accompanied by the second-order $P-\delta$ effect. That is, for slender reinforced concrete columns, the increasing of concrete strength does not provide a significant gain in terms of structural resisting capacity and it is not possible to ensure instability failure by increasing compressive strength of concrete. Therefore, the use of high-strength concrete in slender reinforced concrete columns is not as effective as in short reinforced concrete columns.

The ultimate axial loads, $P_{u,a}$ and the lateral deflections at ultimate loads, δ_a analyzed by the numerical method are presented in Table 4.2.

Table 4-2: Verification of numerical analysis with experimental results

Specimen	$f'_c (MPa)$	λ	$\rho(\%)$	δ_{test} (mm) Kim & Yang (1995)	$P_{u,test}$ (kN) Kim & Yang (1995)	δ_a at P_{max} (mm)	$P_{u,a}$(kN)	$\frac{P_{u,a}}{P_{u,t}}$
10L2-1	25.5	10	1.98	-	52.7*	0.38112	137.4087	2.61
10L2-2				0.403	83.1*			1.65
10L4-1			3.95	0.407	109.5	0.34933	175.8383	1.61
10L4-2				0.407	109.3			1.61
60L2-1		60	1.98	14.88	63.7	13.7249	63.2735	0.99
60L2-2				16.20	65.3			0.97
100L2-1		100	1.98	29.84	38.2	24.6223	35.8825	0.94
100L2-2				32.72	35.0			1.03
100L4-1			3.95	38.20	49.0	23.8940	46.5752	0.95
100L4-2				36.24	47.0			0.99
10M2-1	63.5	10	1.98	0.440	179.0	0.39783	194.3286	1.09
10M2-2				0.433	182.8			1.06
10M4-1			3.95	0.430	207.7	0.37899	232.3774	1.12
10M4-2				0.462	204.6			1.14
60M2-1		60	1.98	20.32	102.8	15.7969	91.76	0.89
60M2-2				18.08	113.5			0.81
100M2-1		100	1.98	26.24	45.2	25.5052	50.632	1.12
100M2-2				27.24	47.6			1.06
100M4-1			3.95	31.08	59.6	25.2215	61.3621	1.03
100M4-2				34.24	60.5			1.01
10H2-1	86.2	10	1.98	0.469	235.3	0.42336	230.4362	0.98
10H2-2				0.442	240.4			0.96
10H4-1			3.95	0.480	255.8	0.405	269.1852	1.05
10H4-2				0.500	257.7			1.05
60H2-1		60	1.98	15.40	122.1	16.7982	106.3818	0.87
60H2-2				16.72	123.7			0.86
100H2-1		100	1.98	24.30	54.3	28.4504	56.9756	1.05
100H2-2				23.68	54.9			1.04
100H4-1			3.95	32.44	66.6	26.6927	67.6446	1.02
100H4-2				33.32	64.7			1.05
						Average		1.12
						Standard deviation		3.5

Where, * end failure occured due to imperfect compaction of ends

$P_{u,test}$ measured ultimate load by test

$P_{u,a}$ calculated ultimate load by analysis

4.3.2 Effect of Steel Reinforcement Ratio

From figure 4.7 to 4.12 shows the effect of longitudinal steel ratio on the ultimate strength of columns. As shown in Table 4.3, for constant compressive strength of concrete and slenderness ratio, as the longitudinal steel ratio increases there is a noticeable improvement in peak axial load with a little decrease of the corresponding lateral deflection. Moreover, for constant compressive strength of concrete with increasing of slenderness ratio, the ultimate load of the column with steel ratio of 3.95% is getting higher than that of the column with steel ratio of 1.98%. Therefore, the increase of longitudinal steel ratio on the increase of ultimate load of column is more effective for slender columns than for short columns.

Table 4-3: Comparison of ultimate Loads for ρ = 1.98% and 3.95%

λ	f'_c (MPa)	ρ(%)	Lateral deflection(mm)	Ultimate axial force(kN)	% increase
λ = 10	25.5	1.98	0.46059	89.9169	20.42%
		3.95	0.44538	108.2787	
	63.5	1.98	0.39783	194.3286	19.58%
		3.95	0.37899	232.3774	
	86.2	1.98	0.42336	230.4362	16.82%
		3.95	0.40501	269.1852	
λ = 100	25.5	1.98	24.6223	35.8825	29.80%
		3.95	23.894	46.5752	
	63.5	1.98	25.5052	50.632	21.19%
		3.95	25.2215	61.3621	
	86.2	1.98	28.4504	56.9756	18.73%
		3.95	26.6927	67.6446	

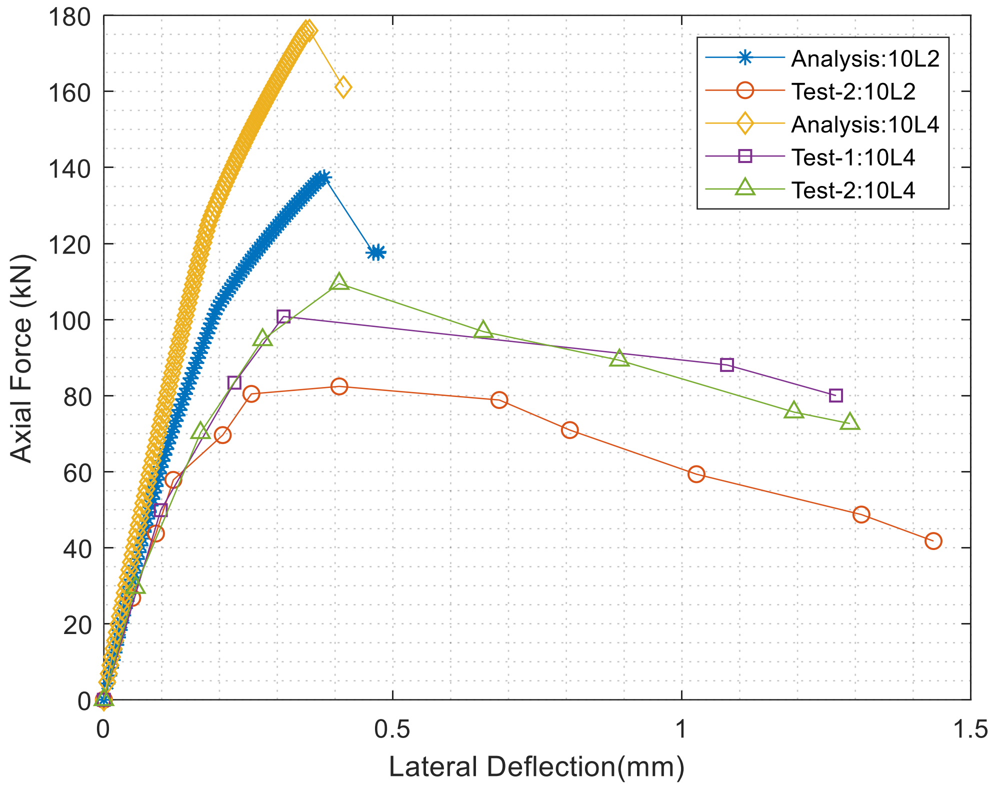

Figure 4-7: Axial force-deflection relation for λ=10 and f'_c=25.5MPa

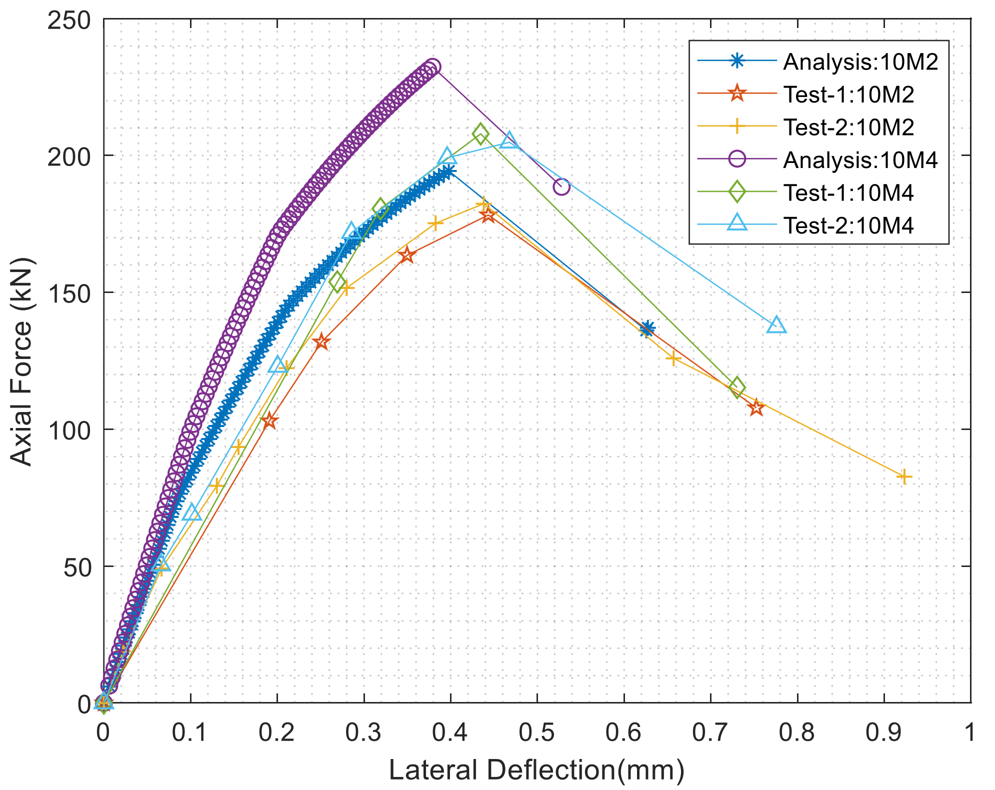

Figure 4-8 Axial force-deflection relation for λ=10 and f'_c=63.5MPa

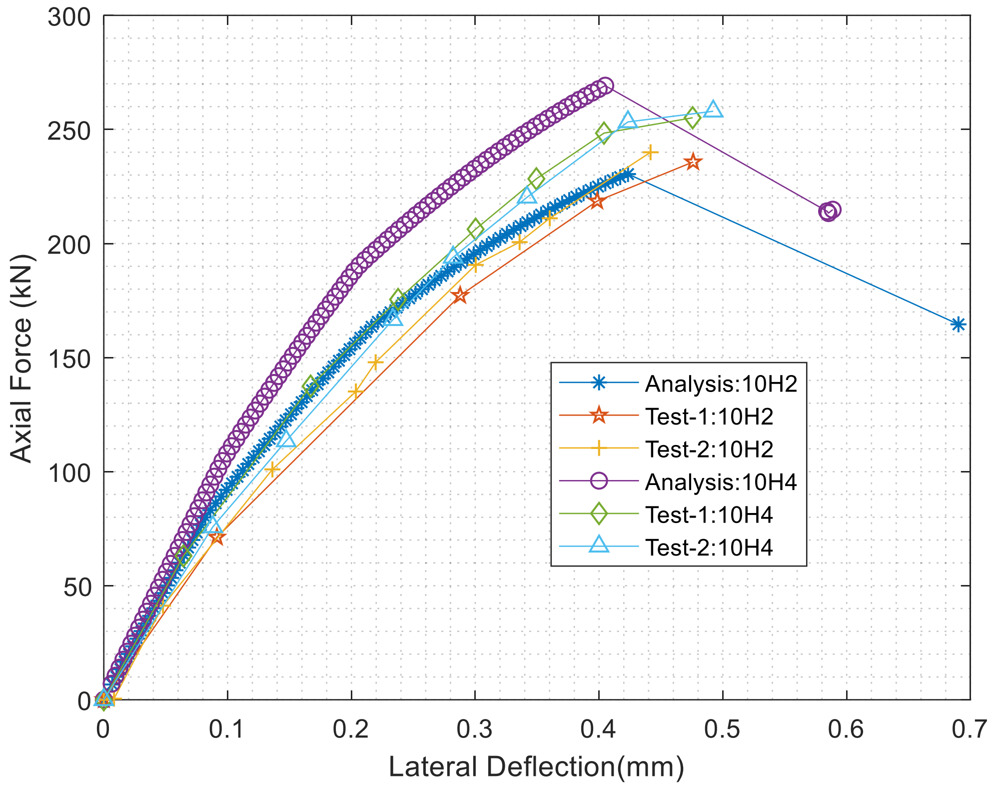

Figure 4-9 Axial force-deflection relation for λ=10 and $\boldsymbol{f'_c}$=86.2MPa

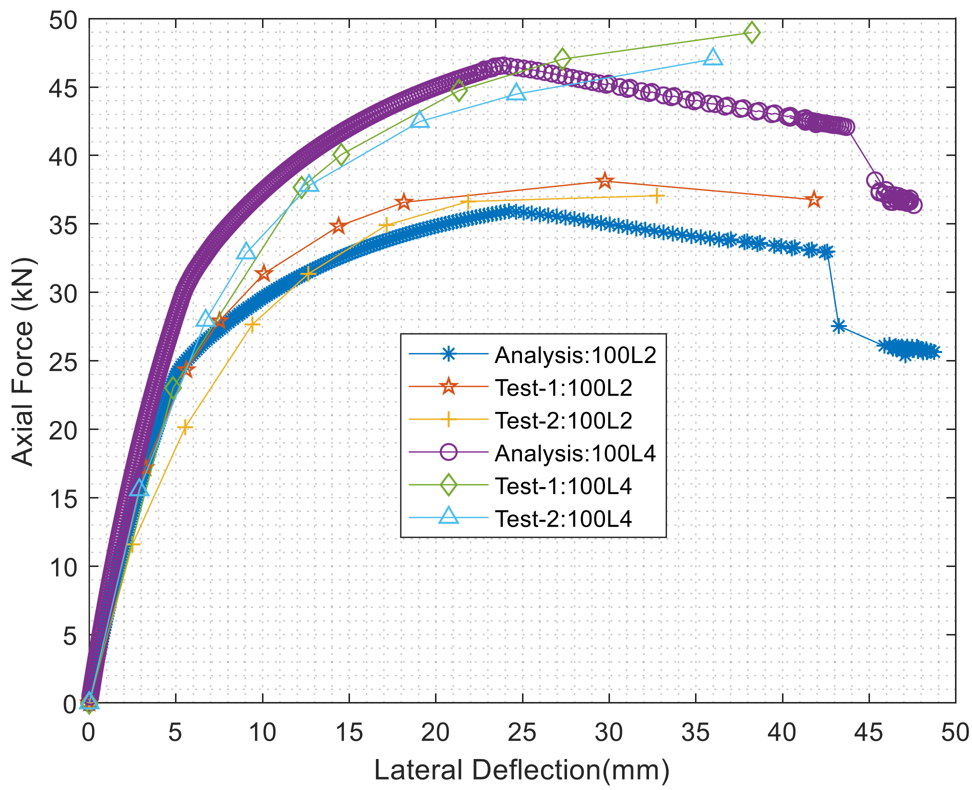

Figure 4-10 Axial force-deflection relation for λ=100 and $\boldsymbol{f'_c}$=25.5MPa

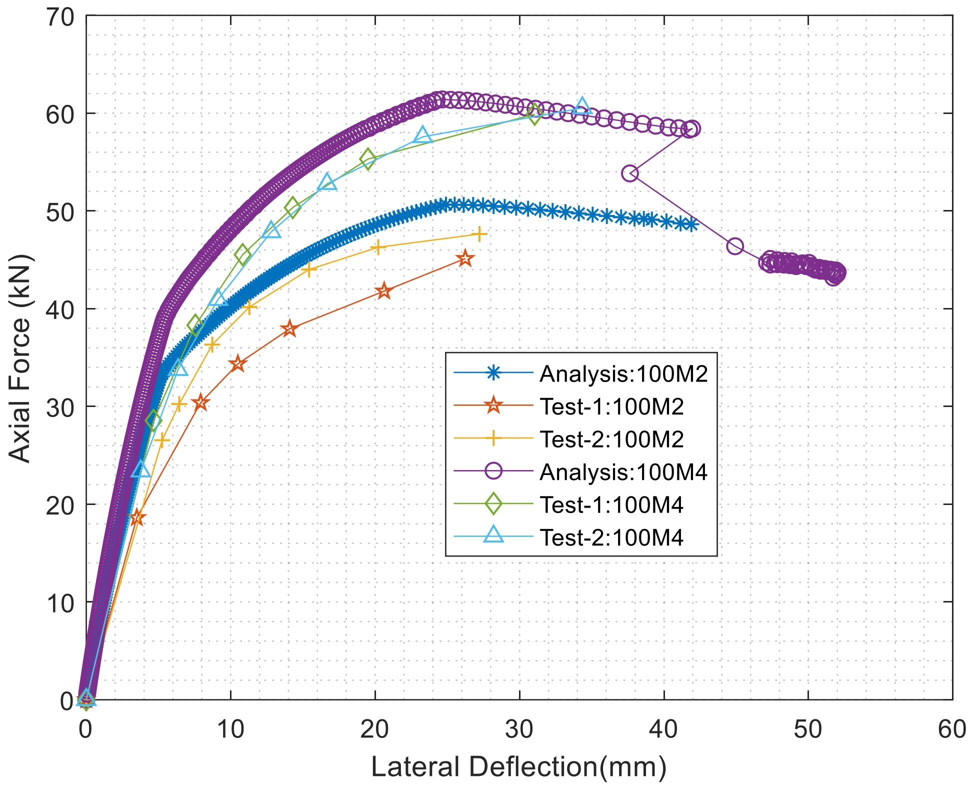

Figure 4-11 Axial force-deflection relation for λ=100 and f'_c=63.5MPa

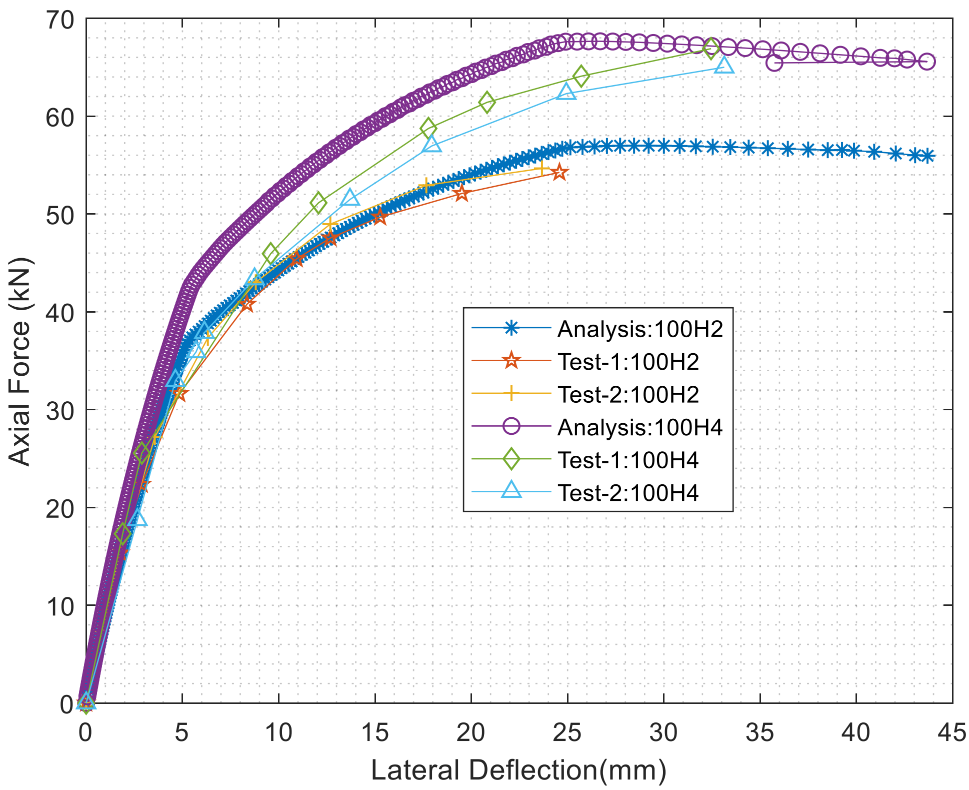

Figure 4-12 Axial force-deflection relation for λ=100 and f'_c=86.2MPa

4.3.3 Effect of Tension Stiffening

Table 4.4 shows that, when the stiffness of tension stiffening is taken in to account, the lateral deflection decreases, irrespective of slenderness ratio and compressive strength of concrete. However, the ultimate load carrying capacity of short reinforced concrete columns increased from 8 to 13% and it is increased from 2 to 6% for slender reinforced concrete columns. The same phenomenon is also observed when the longitudinal reinforcement steel ratio is increased. Thus, the role of tension stiffening on the increases of ultimate load of column is more evident for short reinforced concrete columns than slender columns.

As shown from Figure 4.2 to 4.6, the axial load-lateral deflection behavior including tension stiffening is appreciably stiffer, because of the phenomenon known as tension stiffening (consisting of the tensile resistance of concrete between the cracks). As shown on Appendix A, neglecting tension stiffening causes underestimated stiffness which results underestimated ultimate load with increased lateral deflection when compared with the experimental curves. Thus, tension stiffening has contribution on stiffness and a significant effect on the load deflection behavior of the columns.

Table 4-4: Effect of tension stiffening on lateral deflection and ultimate axial load

Specimen	$f_c'(MPa)$	λ	$\rho(\%)$	material & geometric nonlinearity with tension stiffening		material & geometric nonlinearity neglecting tension stiffening		$\frac{(P_{u,MGNT} - P_{u,MGN})}{P_{u,MGN}}$ (percentage increase)
				δ_a (mm)	$P_{u,MGNT}(kN)$	δ_a (mm)	$P_{u,MGN}(kN)$	
10L2	25.5	10	1.98	0.38112	137.4087	0.38273	121.576	13.023%
10L4			3.95	0.34933	175.8383	0.35696	156.4151	12.42%
60L2		60	1.98	13.7249	63.2735	15.8227	59.9399	5.5%
100L2		100	1.98	24.2117	35.9295	24.7286	33.7741	2.16%
100L4			3.95	23.8940	46.5752	23.5662	44.0627	5.70%
10M2	63.5	10	1.98	0.39783	194.3286	0.39969	176.8995	9.85%
10M4			3.95	0.37899	232.3774	0.38045	210.7507	10.26
60M2		60	1.98	15.9178	90.1216	16.1783	87.6905	2.77%
100M2		100	1.98	24.9059	50.6394	27.738	47.972	5.56%
100M4			3.95	24.6572	61.404	28.1892	58.2193	5.47%
10H2	86.2	10	1.98	0.42336	230.4362	0.4235	211.1667	9.13%
10M4			3.95	0.405	269.1891	0.40918	247.031	8.97%
60H2		60	1.98	16.5229	106.4244	16.8805	102.0385	4.30%
100H2		100	1.98	28.4505	56.9756	32.8334	54.3405	4.85%
100H4			3.95	26.6927	67.6446	29.996	64.4934	4.20%

Where: $P_{u,MGN}$ is the ultimate load of the column for material and geometric nonlinearity without tension stiffening and $P_{u,MGNT}$ is ultimate load for material and geometric nonlinearity including tension stiffening.

4.4 Axial Force-Bending Moment Relation

As shown in Table 4.5, the bending moment of normal strength concrete column at ultimate load is not much decreased compared with that of high strength concrete column. That is, for ρ=1.98%, the bending moment of slender normal strength concrete column is decreased by 26.31%, whereas for slender high strength concrete column, it is decreased by 91.37%. Moreover, in the case of ρ=3.95%, it is decreased by 18.93 % for normal strength concrete and by 91.95% for high strength concrete column. Therefore, possibility of buckling or stability failure for a slender high strength concrete column is greater than for a slender normal strength concrete column.

The effect of longitudinal steel ratio on the axial force-bending moment relation is also discussed. Table 4.5 exhibits the total moment values including $P - \delta$ moment at ultimate loads for columns with λ=100 and ρ=3.95% are larger than those with λ=100 and ρ=1.98%, irrespective of the concrete compressive strength.

Table 4-5: Ultimate bending moment including $\boldsymbol{P-\delta}$ moment

Specimens	$\rho(\%)$	$f_c'(MPa)$	λ	$M_{u,t}$ (kNm) Kim and Yang (1995)	$M_{u,a}$ (kNm)	$\frac{M_{u,a}}{M_{u,t}}$
10L2-1	1.98	25.5	10	-		
10L2-2				2.0339	2.1993	1.08
10L4-1	3.95			2.61042	2.6468	1.01
10L4-2				2.67401		0.99
60L2-1	1.98		60	2.47881	2.3827	0.96
60L2-2				2.63771		0.90
100L2-1			100	2.06568	1.7412	0.84
100L2-2				2.12924		0.82
100L4-1	3.95			3.05189	2.2256	0.73
100L4-2				2.82355		0.79
10M2-1	1.98	63.5	10	4.40013	4.741	1.08
10M2-2				4.49016		1.06
10M4-1	3.95			5.08978	5.6649	1.11
10M4-2				5.00995		1.13
60M2-1	1.98		60	4.25666	3.6461	0.86
60M2-2				4.26715		0.85
100M2-1			100	2.28852	2.502	1.09
100M2-2				2.45765		1.02
100M4-1	3.95			3.28045	3.015	0.92
100M4-2				3.51962		0.86
10H2-1	1.98	86.2	10	5.76424	5.6277	0.98
10H2-2				5.88212		0.96
10H4-1	3.95			6.2619	6.5693	1.05
10H4-2				6.3565		1.03
60H2-1	1.98		60	4.82122	4.3314	0.90
60H2-2				5.0334		0.86
100H2-1			100	2.29862	2.9407	1.28
100H2-2				2.60511		1.13
100H4-1	3.95			3.74901	3.4224	0.91
100H4-2				3.70164		0.92
				Average		0.97
				Standard deviation		0.43

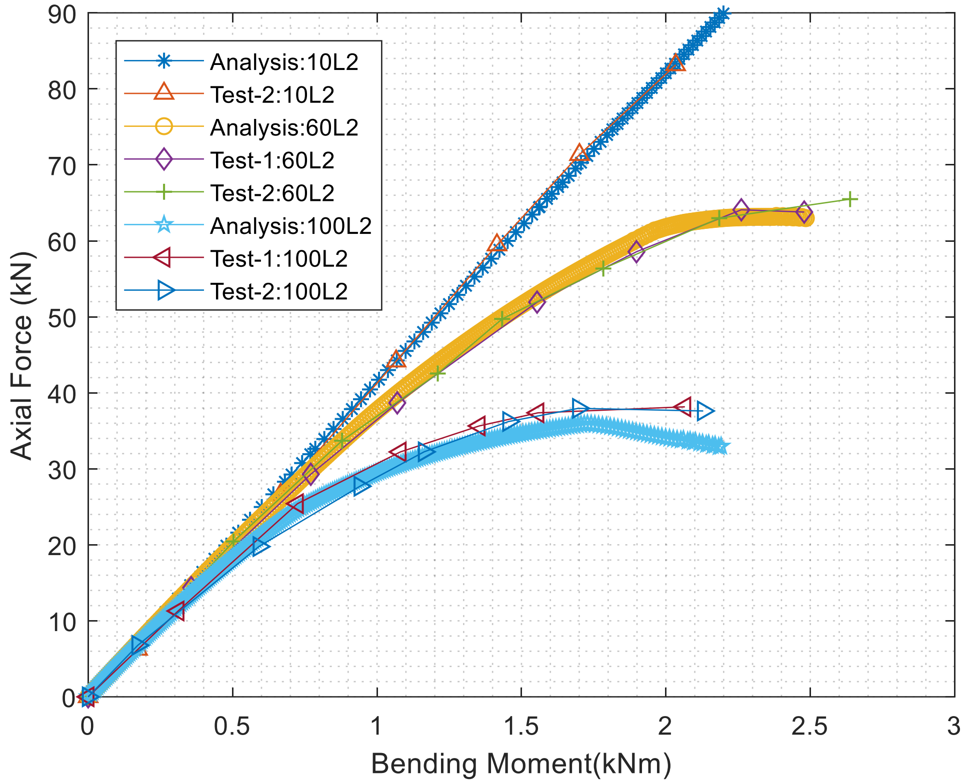

Figure 4-13:Axial force-bending moment relation for f'_c = 25.5MPa and ρ = 1.98%

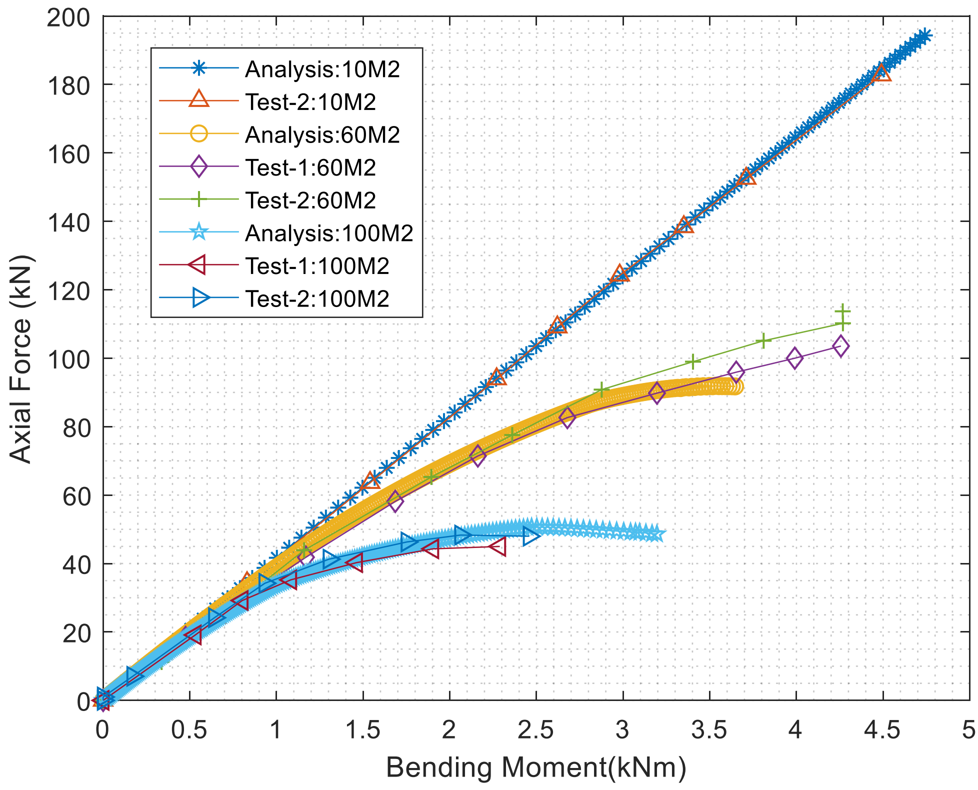

Figure 4-14: Axial force-bending moment relation for f'_c = 63.5MPa and ρ = 1.98%

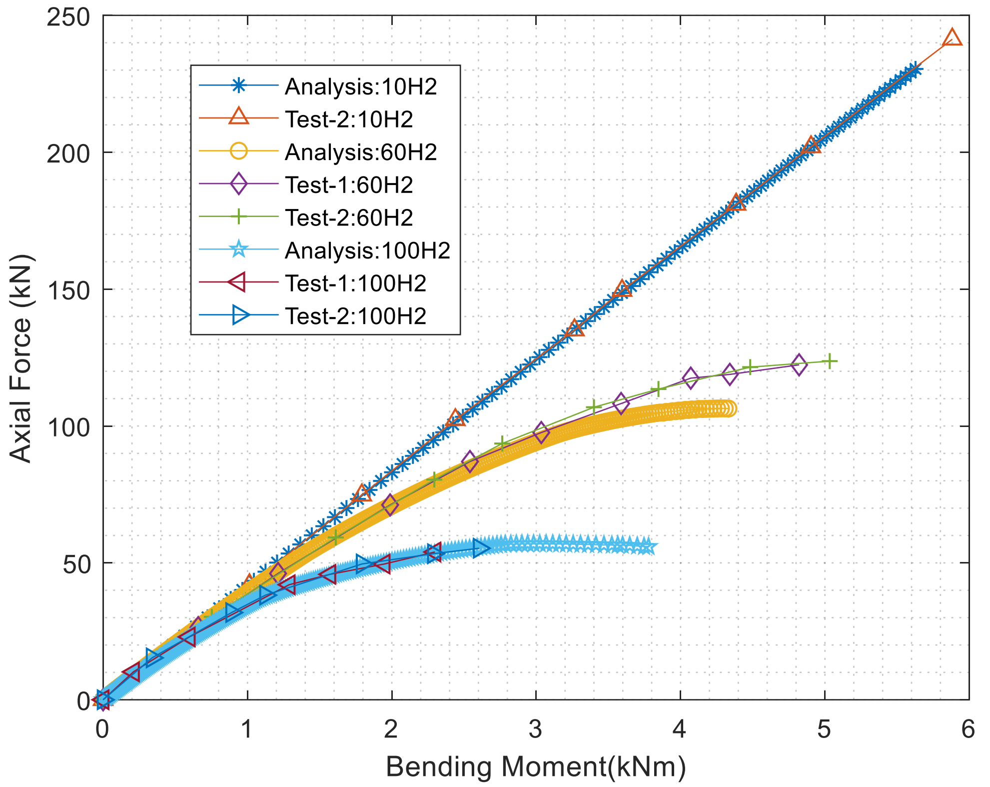

Figure 4-15: Axial force-bending moment relation for f'_c = 86.2MPa and ρ = 1.98%

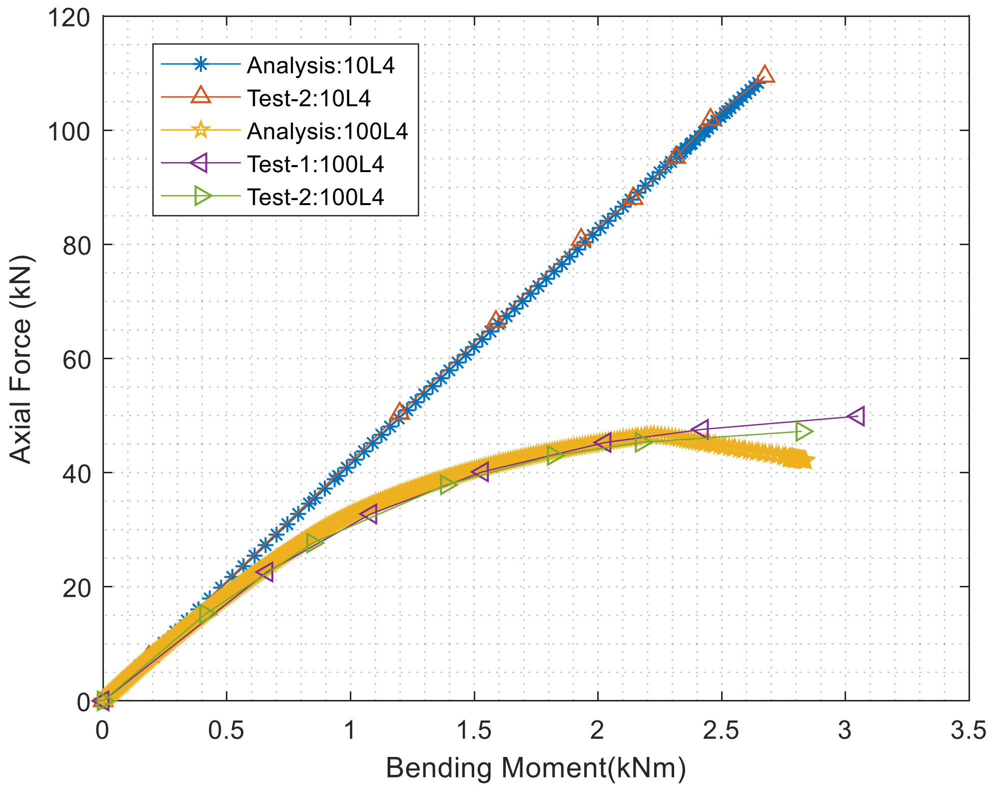

Figure 4-16: Axial force-bending moment relation for f'_c = 25.5MPa and ρ = 3.95%

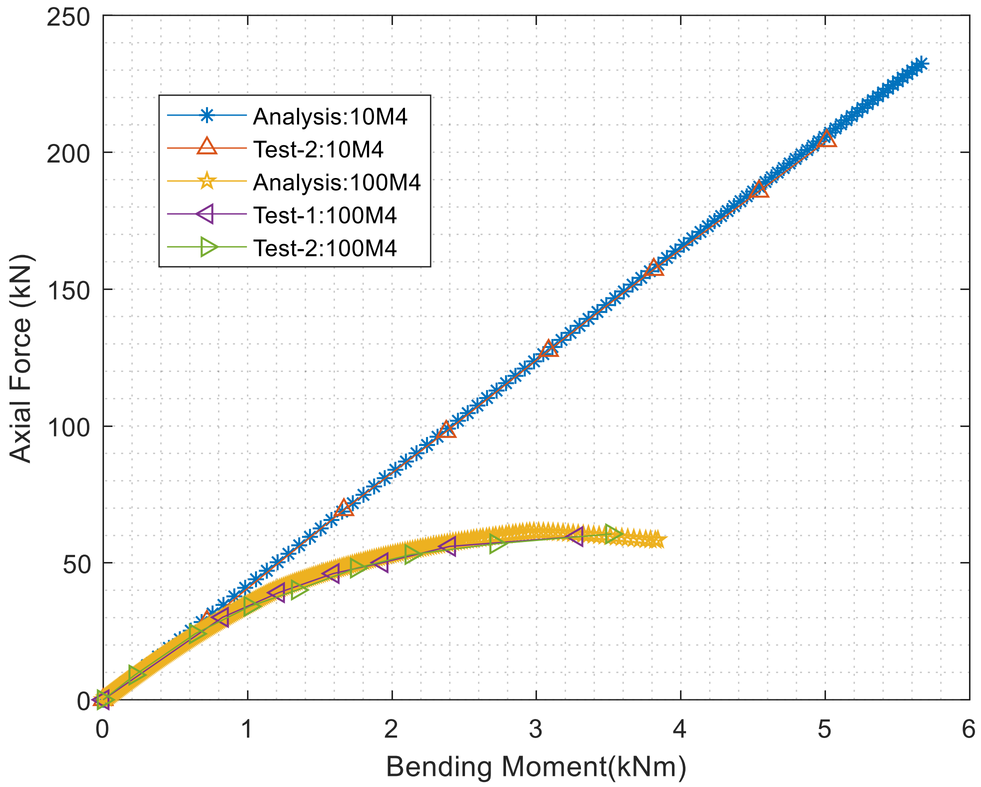

Figure 4-17: Axial force-bending moment relation for f'_c = 63.5MPa and ρ = 3.95%

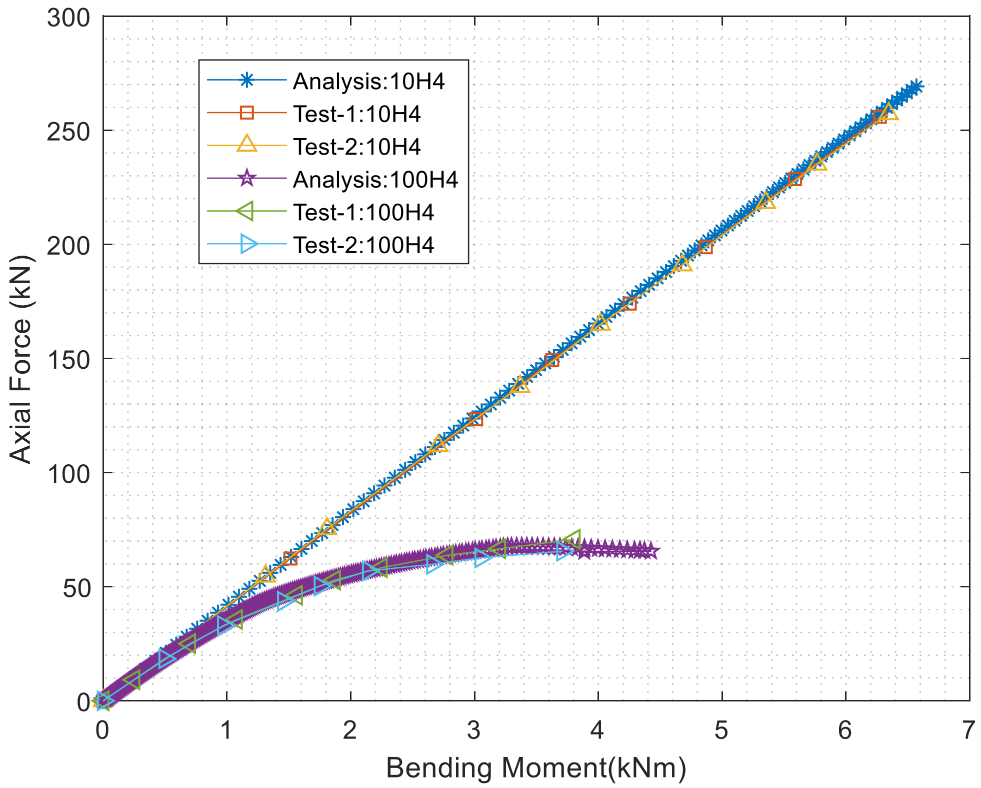

Figure 4-18: Axial force-bending moment relation for f'_c = 86.2MPa and ρ = 3.95%

4.5 Experimental Results of Columns Reported by Lloyd and Rangan (1996)

Referring to Table 4.6, good agreement was achieved between the predicted and observed ultimate responses. The analysis reflects the essence of the test results that an increase in the initial eccentricity ratio (e/h, where e is the eccentricity and h is depth of the column's cross-section) resulted in a decrease in the ultimate load and an increase in the column deflection at failure. For the same compressive strength of concrete, as the reinforcement steel ratio increases, the peak axial load increases with a little decreasing of lateral deflection. The numerical model overestimated the column capacity for specimens with initial eccentricity of 15mm.

The range of difference in the load-carrying capacity of the column is +48% to -14%, The difference between the values from tests and those obtained from the present analysis may be due to the variation between the mean test strength and the in-situ material strengths (in the present analysis, they are assumed to be the same), joint effect on the test loads and un-intentional restraining effect from the applied loads.

Table 4-6: Column specimens tested by Lloyd and Rangan (1996)

Specimen	λ	$f'_c(MPa)$	$\rho(\%)$	e(mm)	e/h	δ_t(mm)	$P_{u,t}$(kN)	δ_a(mm)	$P_{u,a}$(kN)	$P_{u,a}/P_{u,t}$
IA	32	58	2.2	15	0.09	8.3	1476	7.3488	1811.8938	1.23
IB			2.2	50	0.29	12.5	830	10.9527	769.1763	0.93
IC			2.2	65	0.37	13.2	660	11.8677	636.5094	0.96
IIIA			1.4	15	0.09	8.8	1140	7.7232	1689.0973	1.48
IIIB			1.4	50	0.29	12.9	723	11.5307	647.7492	0.90
IIIC			1.4	65	0.37	11.7	511	12.1404	535.3582	1.05
VA		92	2.2	15	0.09	6.2	1704	7.4466	2384.1611	1.40
VB			2.2	50	0.29	9.7	1018	11.0235	954.738	0.94
VC			2.2	65	0.37	12.3	795	11.7783	791.4502	0.99
VIIA			1.4	15	0.09	7.6	1745	7.7331	2247.0335	1.30
VIIB			1.4	50	0.29	11.1	905	11.3805	833.7557	0.92
VIIC			1.4	65	0.37	15.4	663	11.8840	689.4556	1.04
XIA		97.2	1.4	15	0.09	6.4	1975	7.8309	2328.5622	1.18
XIB			1.4	50	0.29	10.9	1002	11.3932	860.6532	0.86
XIAC			1.4	65	0.37	14.2	746	12.3783	718.522	0.96
								Average		1.08
								Standard deviation		0.53

CHAPTER 5 CONCLUSIONS AND RECOMMENDATIONS

5.1 Conclusions

In this study, a nonlinear two-dimensional second-order analysis program was developed to predict the behavior of reinforced concrete columns by applying materially layered cross-section model and geometrically nonlinear finite element method. The proposed method accounted the stiffness of tension stiffening and the coupling effect between axial force and bending moment. If the stiffness of tension stiffening was not considered, the ultimate load could be underestimated and the lateral deflections could be overestimated. The developed model was verified to relevant test data from the literature to determine its level of accuracy in dealing with any combination of column parameters. The comparison of the results involved the column capacity and the load-deflection characteristics. The results obtained through this limited investigation can be summarized as follows:

1) The numerical finite element analysis shows that, the reinforced concrete columns subjected to axial load and uniaxial bending moment under nonlinear material and geometric stiffness, the curvature distribution follows the elastic half sine wave curve and has a sinusoidal deflected shape until the ultimate axial load reached. However, as the load is increased beyond the elastic limit which is from the starting or imminent point of instability (at $P = P_u$), the curvature at the mid-height of the column creates a more pointed, sharp post peak deflected curve. Therefore, the application of analytical method is almost impossible when the columns exist as a part of complex structure.
2) The increment of the ultimate load due to the increase of concrete compressive strength is decreased with the increase in the slenderness ratio. Therefore, the use of high-strength concrete in slender reinforced concrete columns is not as effective as in short reinforced concrete columns.
3) The bending moment of normal strength concrete slender column at ultimate load was not much decreased compared with that of high strength concrete slender column. Therefore, the possibility of buckling for the slender column is increased with increasing concrete strength.
4) The increase of longitudinal steel ratio on the increase of ultimate load of column is more effective for slender columns than for short columns.

5) The role of tension stiffening on the increases of ultimate load of column is more evident for short columns than slender reinforced concrete columns.
6) An increase in the initial eccentricity ratio resulted in a decrease in the ultimate axial load and an increase in the column deflection at failure under the same compressive strength of concrete.

5.2 Recommendations for Future Study

In this study, even using displacement control method, the post-peak strain softening behavior is not well captured due to highly nonlinear behavior of the reinforced concrete column. At the critical state with ${dP}/{du} \to -\infty$, and beyond, the present iterative secant stiffness algorithm does not converge and sudden drop of loads is existed beyond the ultimate load specially for the short reinforced concrete columns. To overcome this, additional numerical strategies such as Crisfied arc-length method (1980, 1981, 1983 and 1986) could then be used.

In addition to this, unloading was takes place at points adjacent to a strain softening zone for monotonically increasing displacement. Therefore, the study can be extended to use the existing layered cross-section model with the stress-strain relationship of materials including unloading-reloading curves to account for unloading loading history.

Moreover, the present rigorous numerical analysis can be extended to reinforced concrete columns subjected not only to uniaxial bending moment but also to biaxial bending moment including the long term time dependent deformation effect such as creep to trace the post-peak nonlinear softening behavior. Along with this, interaction chart of slender reinforced concrete columns including second-order effect should be developed using stress-strain material constitutive law applying layered cross-section model. Again, a deep analysis about the complex interface behavior between the steel and concrete, crack patter should be made.

REFERENCES

AL-Manaseer, A.A. (1983). "A nonlinear finite element study of reinforced concrete beams." Ph.D. Thesis, Department of Civil Engineering, University of Glasgow.

ACI Committee 363," State of the art report on high-strength concrete." ACI 363R-92 (Reapproved 1997).

Bazant, Z.P., Pan, J.Y. and Cabot, G.P. (1987). "Softening in reinforced concrete beams and frames." Journal of Structural Engineering, ASCE, Vol. 113, No.12, Page 2333-2347.

Bazant, Z.P. and Xiang, Y. (1997). "Inelastic buckling of concrete column in braced frame." Journal of Structural Engineering, ASCE, Vol. 123, No.5.

Bazant, Z.P. Cedolin, L. and Tabbara, M.R. (1991). "New method of analysis for slender column." Journal of Structural Engineering, ACI, Vol.88, no.4, Page 391-401.

Chajes, A. and Churchill, J.E (1987), "Non-linear frame analysis by finite element methods." Journal of Structural Engineering, ASCE, Vol. 113, No.6, Page 1221-1235.

Chuang P.H. and Kong, S.K. (1998). "Strength of slender reinforced concrete columns. "Journal of Structural Engineering, ASCE, Vol. 124, No.9, Page 992–998.

Cope, R.J., Rao, P.V., and Clark, L.A., (1979). "Nonlinear design of concrete bridge slabs using finite element procedures". CSCE-ASCE-ACI-CEB International Symposium, University of Waterloo, Waterloo, Ont., Page 379-407.

Crisfield, M.A. (1980). "The automatic non-linear analysis of stiffened plates and shallow shells using finite elements." Proc. Instn Civil Engineering (London), Vol.69, Part 2, Page 891-909.

Crisfield, M.A. (1981)." A fast incremental/iterative solution procedure that handles' snap through." Computers and Structures, Vol.13, Page 55-62.

Crisfield, M.A. (1983). "An arc-length method including line searches and accelerations." International Journal for Numerical Methods in Engineering, Vol.19, Page 1269-1289.

Crisfield, M.A (1986). “Snap-through and snap-back response in concrete structures and the dangers of under-integration” International Journal for Numerical Methods in Engineering, Vol.22, Page 751-767.

El-Metwally, S. E. and Chen, W.F. (1989). “Non-linear behavior of reinforced concrete frames.” Computers and Structures, Vol. 32, No. 6, Page 1203-1209.

Fafitis, A. and Shah, S.P. (1985). “Predictions of ultimate behavior of confined columns subjected to large deformations.” ACI Journal, Page 423-433.

Gilbert, R.I. and Warner, R.F. (1987b). “Tension stiffening in reinforced concrete slabs” Journal Structural Engineering, ASCE, Vol. 104, NoST12, Page 1885-1900.

Goto, Y. and Chen, W.F. (1987). “Second-order elastic analysis for frame design.” Journal Structural Engineering, ASCE, Vol. 113, No. 7, Page 1501-1519.

Hahn, B.H. and Valentine, D.T. (2013). Essential MATLAB for Engineers and Scientists, 5th edition. Linacre House, Jordan Hill, Oxford OX2 8DP, UK.

Hognestad, E. (1951). “A study of combined bending and axial loads in reinforced concrete members”. University of Illinois, Engineering Experimental Station, Bulletin Series No. 399, Vol.49.

Kenyon, J.M. (1993). “Non-linear analysis of reinforced concrete plane frames.” Ph.D. Thesis, Department of Civil Engineering, University of Adelaide, Australia.

Kim, J. K.., and Lee, T. G. (1992). “Nonlinear analysis of reinforced concrete beams with softening.” Computers and Structures, Vol. 44, No. 3, Page 567-573.

Kim, J.K. and Lee, T.G. (1993). “Failure behavior of reinforced concrete frames by the combined layered and non-layered method.” Computers and Structures, Vol. 48, No.5, Page 819-825.

Kim, J. K.., and Lee, T. G. (2000). “The behavior of reinforced concrete columns subjected to axial force and biaxial bending.” Engineering Structure, Vol. 22, No. 11, Page 1518-1528.

Kim, J. K. and Yang, J.K. (1995). “Buckling behavior of slender high strength concrete columns.” Engineering Structure, Vol. 17, No.1, Page 39-51.

Kwak, H.G., and Filippou, F.C. (1997). “Nonlinear finite element analysis of reinforced concrete structures under monotonic loads.” Computers and Structures, Vol. 65, No. 1, Page 1-16.

Kwak, H. G. and Kim, J. K. (2006). “Nonlinear behavior of slender reinforced concrete columns.” Construction and building materials. Vol. 20, Page 527-537.

Lin, C.S. and Scordelis, A.C. (1975). “Nonlinear analysis of reinforced concrete shells of general form.” Journal of Structural Division, ASCE, ST3, Page 523-538.

Lloyd, N.A. and Rangan, B.V. (1996). “Studies oh high-strength concrete columns under eccentric compression.” ACI Structural Journal, Vol.93, No.6, Page 631-638.

MacGregor, J.G. and Wight, J.K. (2009). Reinforced Concrete: Mechanics and Design, 6th edition. Pearson Prentice Hall, Upper Saddle River, New Jersey.

Owen, D.R.J., and Hinton, E. (1980). “Finite elements in plasticity: Theory and practice.” Pineridge Press Ltd, Swansea, England.

Scanlon, A. and Murray, D.W. (1974). “Time dependent reinforced concrete slab deflections.” Journal of Structural Division, ASCE, ST9, Vol. 100, Page 1911-1924.

Vebo, A. and Ghali, A. (1977). “Moment-curvature relationship of reinforced concrete slabs.” Journal of Structural Division, ASCE, Vol. 113, Page 515-531.

Wong, K.W. (1989). “Non-linear behavior of reinforced concrete frames.” Ph.D. Thesis, Department of Civil Engineering, University of Adelaide, Australia.

APPENDIX A

In this appendix axial load-lateral deflection response of reinforced concrete columns neglecting stiffness of tension stiffening is presented.

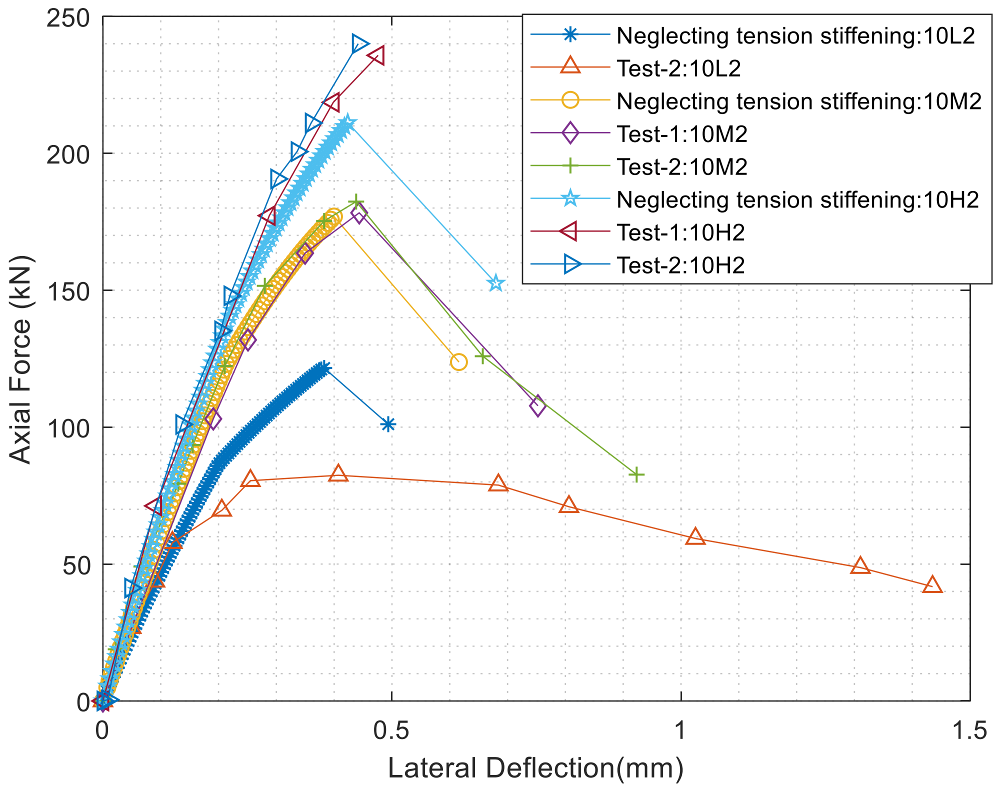

Figure A-1: short reinforced concrete columns (λ=10) with ρ = 1.98%

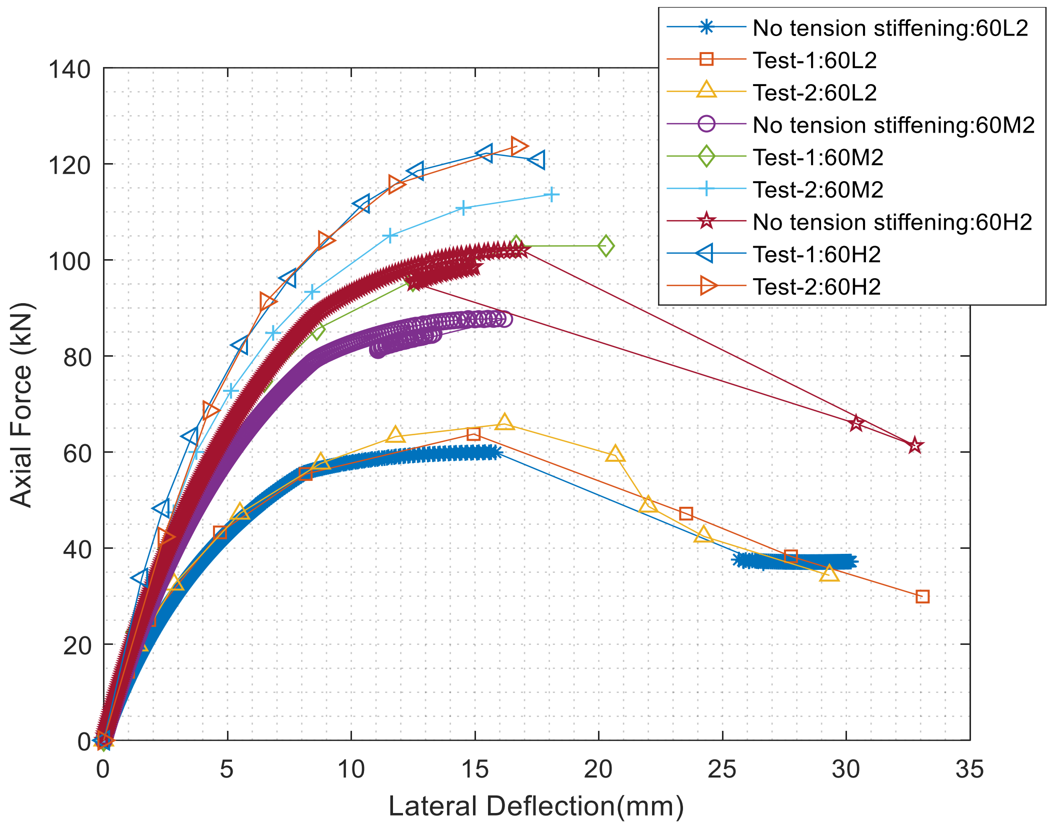

Figure A-2: Medium slender reinforced concrete columns (λ=60) with ρ = 1.98%

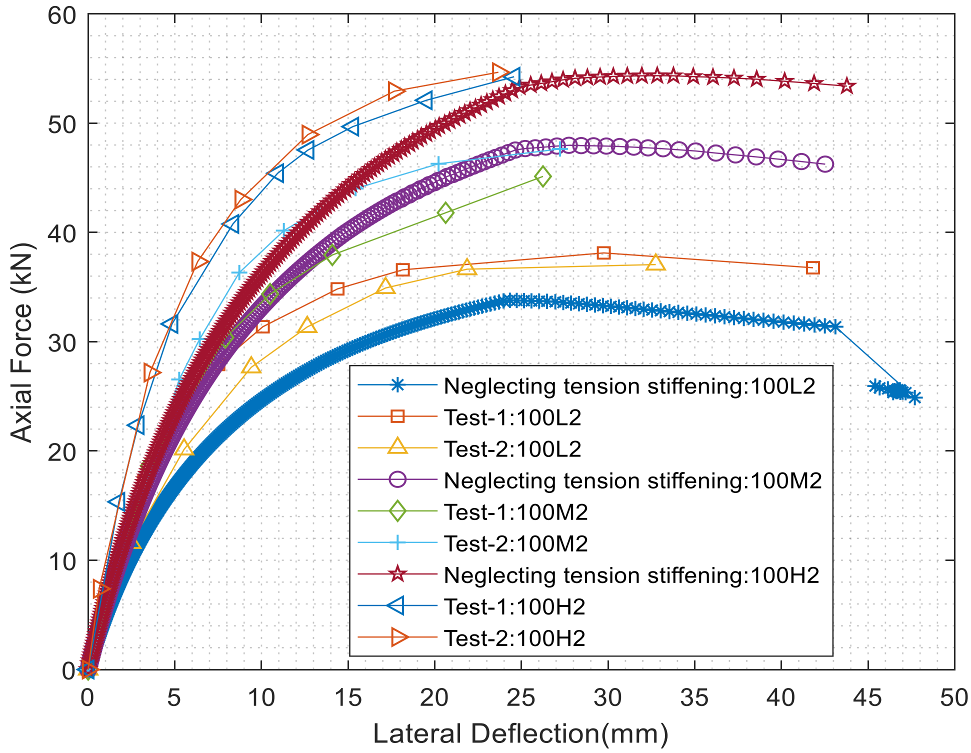

Figure A-3: High slender reinforced concrete columns (λ=100) with ρ = 1.98%

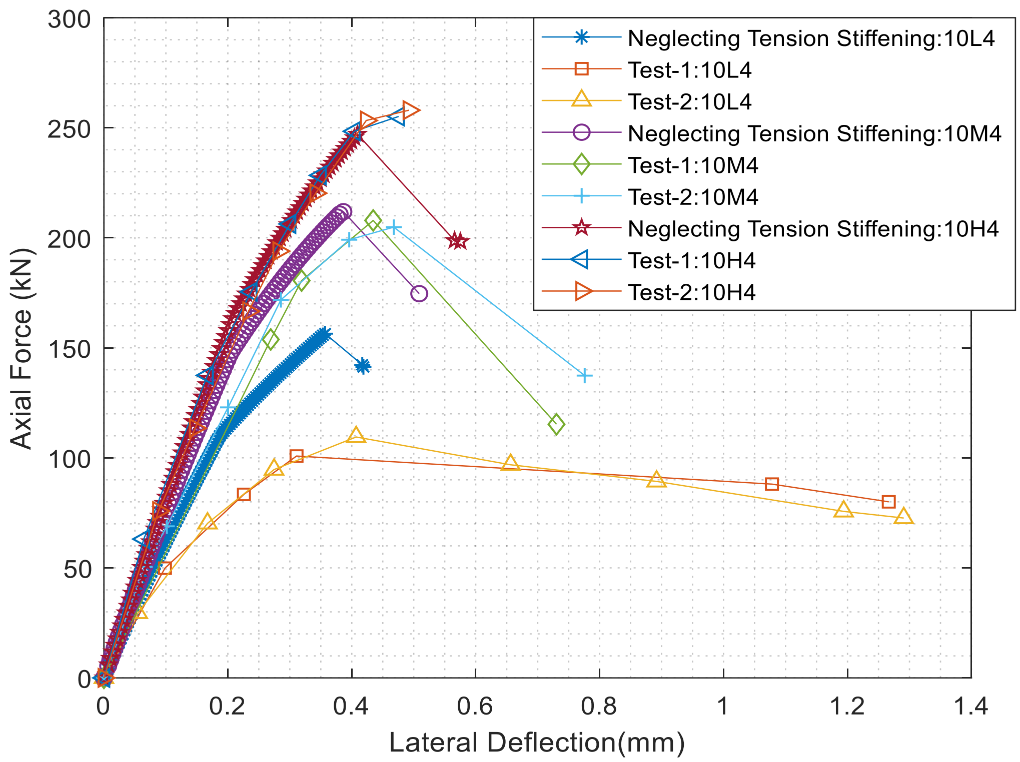

Figure A-4: Short reinforced concrete columns (λ=10) with ρ = 3.95%

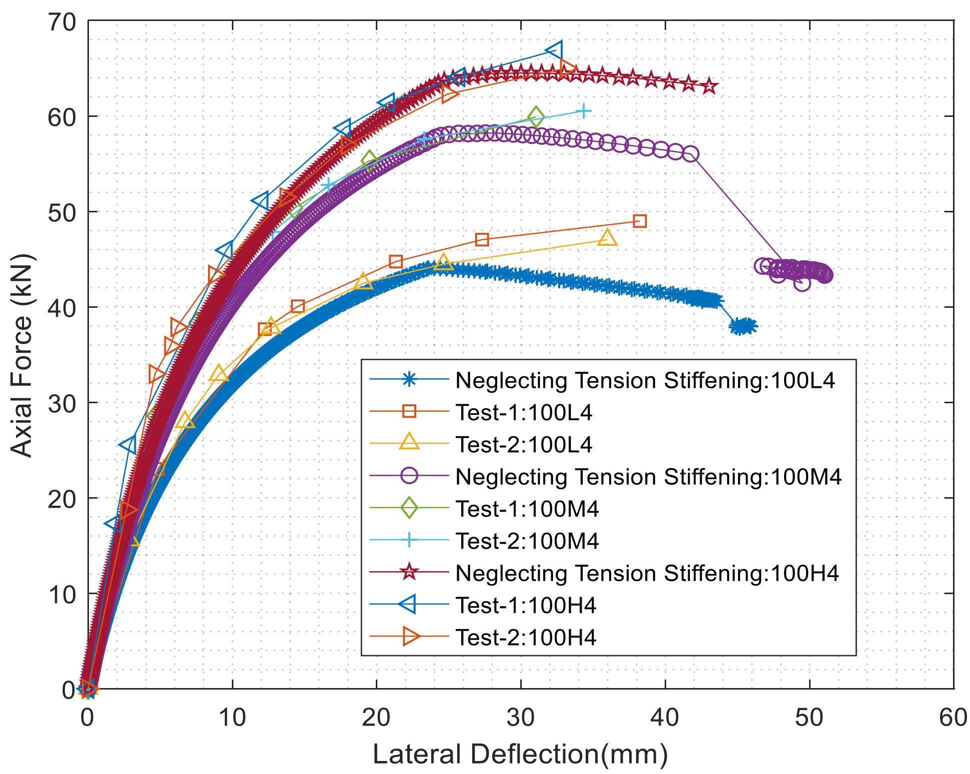

Figure A-4: High slender reinforced concrete columns (λ=100) with ρ = 3.95%